Addis Ababa University

Faculty of Natural Sciences, Physics Department

School of Graduate Studies

Ultraviolet (UV) Radiation and its physical Modulating Factors in Africa Based on TOMS and NOAA Polar Orbiting Satellites

Presented by

Gemechu Fanta Garuma

A Thesis Submitted to Addis Ababa University, Faculty of Science, Physics Department for the partial fulfillment of Master of Science degree for physics

Advisor: Abebe Yeshanew (PhD)

Co-Advisor: Gizaw Mengistu (PhD)

July 2007

Ultraviolet, aerosol and ozone space and time-series data from 1978 -2003 for this research are obtained from this

Abstract

Ultraviolet radiation is the main source of energy for the photochemical reaction and dynamics in the stratosphere and ionosphere. It is also one of the main sources of energy required for the evolution of animals and plants.

The method used to make people aware the risks related to UV is using a calculation of the amount of daily irradiance, which is called dose rate. This dose rate then is changed to UV index (UVI). Erythermal UV radiation (UVery) is the integrated solar spectrum over the effective biological response to UV wavelengths on the ground between 295-400 nm. This effective biological response is called action spectrum. The action spectrum is the normalized UV amount, which affects the health of animals and plants or biosphere in general. The value of UVI in Africa is 4 to 9, moderate to high overall. This is due to the tropical nature of most parts of Africa. The trend of UV radiation in Africa shows significant decrease in the year from 1980 to 1992 and a slight increase in recent years from 1997 to 2002. The ozone amount on the other hand is increasing in Africa. The variability of ozone in tropical Africa is relatively stable. The aerosol index in Africa is generally decreasing. UV, aerosols and ozone do not show high seasonal variability in this part of the continent.

The study and understanding of UV and its determining factors in Africa hardly exists. Here attempts are made to associate UV with these determining factors. UV and ozone established 41% of the total variability in the surface UV in Africa. Clouds show 31% variability in the surface UV and aerosols established only 7% total surface UV determination.

Acknowledgements

I would like to thank those people abroad and around me who have given me encouragement and help during this thesis work. My special thanks go to my Advisor Dr. Abebe Yeshanew who have accepted me and guided me throughout the year. His friendly manner, his critical remarks, corrections and his pleasant manner is too big an input to the fruition of this work.

Second, I would like to thank my co-advisor Dr. Gizaw Mengistu who is routinely helpful, understanding, and helped me focus on the scientific work at hand.

My particular thanks go to Eric Beach at the National Oceanic and Atmospheric Administration (NOAA) for helping me get the SBUV version 8 data. His timely response and dedication for the use of data made me to appreciate him.

Michael Bell at the International Research Institute (IRI) has also been advising me for how to use the IRI dataset and software and shown the way to get data from the NOAA. I would like to thank him for the all patience and cooperation he has shown me.

I do not forget my sister who has always been with me since undergraduate. My friends, my family and my uncle's family, who are always positive and helpful about my work, I say, thank you very much!

Table of Contents

Title **Pages**

List of Figures

List of Tables

Abbreviations and Symbols

DNA	Deoxyribonucleic Acid
DU	Dobson Unit
IRI	International Research Institute
NOAA	National Oceanic and Atmospheric Administration
SBUV	Solar Backscatter Ultraviolet
SZA	Solar Zenith Angle
TOMS	Total Ozone Mapping Spectrometer
TOA	Top of the Atmosphere
UV	Ultraviolet
UVI	Ultraviolet Index
UVR	Ultraviolet Radiation
UVery	Erythemal UV

Chapter One

Introduction

1.1 General Overview

The thesis in point is about the UV radiation and its association with physical variables like aerosols, ozone and clouds in Africa. It presents the UV radiation phenomena, and the UV relationships with other factors like ozone, aerosols, scattering albedo and others, which have direct and indirect effect on UV irradiance at the surface. The results are exposed spatially and temporally in space-time.

There has been a growing interest in the UV radiation study along with other parameters like aerosol, ozone, clouds and many others partly because of the impact of UV on ecosystem and in the study of atmospheric radiative forcing (photolysis dissociation). The thesis in point is initiated as UV affects human immune system, eye disease (cataracts), early ageing of skin, biosphere, infrastructures and climate system. The ozone amount both in column and in vertical distribution is emphasized in an effort to contribute to the air quality attributable to ozone. Understanding the characteristics and unraveling the mechanisms of UV irradiance leads to its predictability towards minimizing its influence on human, material and biotic systems.

In the first part, the theoretical background and literatures reviewed will be presented. It incorporates the discussion of the characteristics of UV radiation reaching the Earth's surface through radiative transfer equations, the absorption mechanisms of molecules, and the UV action-spectra. In the second part the determining factors of UV radiation at the surface of the Earth will be discussed. The influential factors are ozone, which has a big influence in the role played to absorb the harmful UV radiation, aerosols (scattering and absorption), and scattering albedo. The fate of ozone in the atmosphere has three distinct parts: ozone production, ozone depletion and ozone transport. These are discussed briefly. The third part is the data types and methods of data analysis adopt to obtain the results. The final part deals with the results obtained which quantify the UV level in Africa, the ozone-mixing ratio in parts per millionth of a volume (ppmv) of air,

the aerosol characteristics and the correlation of UV with other variables. Special attention is given to the vertical distribution of ozone and its relevance both in air quality study and its effect on UV radiation level at the surface of the Earth. The discussions and conclusions are also made based on the results obtained and the previous studies. Literatures are referred in each part of the above for clarity and comparison of this work with the previous ones.

1.2 Gaps in understanding UV and the determining factors

The research thesis is first of its own kind to establish the understanding of UV and its interrelationship with ozone, aerosols, and clouds in Africa. But, scientific gaps exist in the understanding of UV and its variance shown below:

a) Very few scientific studies are done in Africa on isolated cases (in space and time) and not in an integrated approach. For instance, UV indices are developed in South Africa to categorize the UV index (Human and Bajic, 1999).
b) The total column ozone in tropical areas reveals intact (no depletion) (Bais A. F., and D. Lubin, 2006). But, further studies are needed to show the variability and trend of tropical ozone.
c) UV interaction with clouds is a complex myriad. So far no research has addressed quantitatively its interplay with cloud properties.

In this research, attempts have made to address these issues. Towards that end, the general characteristics of UV and its associations with other variable are laid down. It has unraveled UV irradiance vulnerable areas of Africa. The modulation of ozone, aerosol and clouds and its variants on UV irradiance are addressed and quantified. Furthermore, contributions of each physical factor to UV variability are investigated to bridge the scientific gaps in these areas.

1.2 Problem statement and contribution

The problems to be investigated in this paper are:

a) Estimation of the dose of UV in Africa using the UV index (UVI),

b) Quantification of the relationship of UV with ozone, aerosols, and clouds,

c) Investigation of the vertical distribution of ozone in Africa and comparison with the higher latitudes.

Most of Africa is situated in both desert areas and tropical latitudes. This means the amount of UV radiation reaching the surface of Africa is high. The reasons are: 1) the overhead sun all the year round in most parts of tropical Africa, 2) due to the cloud nature (broken) or less in some arid and semi-arid regions in Africa, 3) the UV absorbing and scattering characteristics of aerosols (dust, and sulfates among good UV absorbers; salt, sand, and playas among efficient UV scatterers) found dispersed in most parts of the northern, north western, and eastern parts of Africa.

The effects of UV radiation reaching the surface are suppression of the human immune system by killing the white blood cells, affecting the general balance of ecosystem, making optimum breading environment for viruses, bacteria, and many other disease causing organisms. Most to be mentioned in the effects category is the effect of UV on infrastructure. It highly reduces the age of infrastructure by breaking the molecular bond of pigments, rubber, paints and the likes.

Gaps in this area of research exist over tropical Africa.
But, little study has been found in Africa in this field. UV indices greater than 10 are common, in SA and Australia (Human and Bajic, 1999).

Looking the effects of the UV, one can be motivated to know the amount (Dose Rate) and action spectrum of UV radiation in Africa. This study hence addresses this issue at initial ground level.

The other problem at hand is the dependence of UV radiation on many other physical variables that makes it too cumbersome and hence this study attempts to relate the variables at ground level. This is done using singular value decompositions, correlation-regression statistics, variance analysis and physical explanations.

The contributions of this paper are to foster an understanding of UV irradiance and its characteristic with other variables, seasonal variability of UV and all the modulating variables, and examining stratospheric and tropospheric ozone-mixing ratio in Africa. This understanding further helps for the study of photolysis reaction in Africa, the contribution of UV in atmospheric dynamics, help for the investigation of pollutants that

are related to the UV amount, aid for infrastructure designers, assist to take protective measures against health problems to animals and plants associated with UV.

1.3 Objectives

1.3.1 General Objectives

The research's central objective is towards development and understanding modes of variability for UV radiation in Africa and establishment of its interplay with ozone, aerosols, and cloud parameters. In so doing, the detailed analyses of ozone both its horizontal total amount and vertical allotment (ozone mixing ratio) is shown. The aerosol characteristics both spatially and temporally got attention and relations are established with UV irradiance.

1.3.2 Specific Objectives

Towards achieving the core objectives, the following specific objectives are outlined:

a) To identify and explain the mode of variability of UV radiation in Africa in space and time,

b) To illustrate the seasonal variability of UV, Ozone, and aerosols in Africa,

c) Understand how UV are modulated by various physical processes and factors

d) To establish the physical mechanisms of the variation of UV in space and time, and

e) To develop the relationship between UV and cloud parameters in Africa.

1.4 Chapter Summary

Of the total energy of the sun, UV radiation is about 8%, which could possibly play an important role in the radiation budget of the planet. However, it is in the shortest wavelength region and is the most energetic part of the solar spectrum. Importantly, the knowledge of UV radiation can help one; take actions to avoid damage caused due to

overdose of the ultraviolet radiation and hazardous in the sun. Establishing the mode of variability of UV radiation, characterizing ozone amount both vertical distribution and thickness, and the spatial and temporal variability of aerosols will be the main theme of the thesis at hand.

Chapter Two

Theoretical Background and Literature Review

Radiation is the key component of the Earth-Atmosphere system. Solar radiation derives atmospheric circulation and hence weather and climate. The radiation emitted by the sun is approximately equivalent to the emission of a blackbody of 5700K and thus, more than 99% of the solar energy received at the top of the Earth's atmosphere (TOA) is in the wavelength range of $0.25 - 4\ \mu$m. Radiation in this wavelength range is called solar radiation or shortwave radiation. Tropospheric and stratospheric chemistry are controlled by photochemical reactions and hence by shortwave radiation.

Combined measurements of UV radiation, aerosols and ozone provide useful information on radiation balance, air quality, and effects on biosphere and material. Accurate knowledge about solar and terrestrial radiation and their interaction with clouds, aerosols particles, and trace gases are therefore required for a variety of purposes.

The short history of UV radiation is its study started positively in the pretext of its cure for tuberculosis and its importance for necessity for vitamin D production, which makes our bodies strong during childhood. It was later that the negative effects of UV discovered.

This chapter incorporates the theoretical background about UV Radiation and review of literatures on UV Radiation in Africa. First, the definition of UV radiation is presented then absorption in the UV is discussed followed by the UV spectral measurement using the radiative transfer equations based on Liou (1983). The biologically active UV radiation (UVery) is cited. In all of the above discussions, selected literatures on this particular issue are reviewed.

2.1 UV Light Spectrum and Solar Radiation

Ultraviolet radiation is part of the solar electromagnetic radiation spectrum from about 400 nm to 100 nm (where the visible ray range ends). Ultraviolet radiation is invisible to the human eye, but its effects can be demonstrated.

It is randomly divided into three bands width of different wavelength (Athas, Hunt, and Key, 2003). The divisions first anticipated by the Second International Congress on Light in 1932 were UVA (400-315 nm), (UVB 315-280 nm) and (UVC 280-100 nm). The classification is made by WHO (Lucas, McMichael, Smith, and Armstrong, 2006).

In discussing UV radiation, it should be noted that it represents a very small portion of the solar radiation spectrum from the sun that reaches the Earth's surface. The atmosphere filters much out. Table 1 lists the various regions of the solar spectrum, indicating the percentage of total solar energy in each region. UV radiation (UV-A, UV-B, and UV-C) make up only a little over 8% of the total. At the surface the amount of UV – A is 94%, UV – B is 6% and UV – C is 0%. Most of the solar radiation is in the visible and infrared. The integrated solar radiation over the whole spectrum is called solar constant or total solar irradiance (TSI) which amounts to 1366 Wm^{-2}. Most scientists made this study and its value is relatively similar. The value is referred to TOA at the mean Sun-Earth distance, which is defined as one astronomical unit.

Spectral Region	Wavelength	% of total energy
Infrared	>700 nm	49.4
Visible	400-700 nm	42.3
UV-A	400-315 nm	6.3
UV-B	315-280 nm	1.5
UV-C	<280 nm	0.5

Table 2.1: Distribution of wavelength ranges infrared, visible, UV-A, UV-B, UV-C and percentage of each of the total solar irradiance energy.

The ultraviolet (UV) has the highest radiant energy and has paramount negative effects on the all components of the environment (Atmosphere, biosphere, vegetation,

cryosphere, and hydrosphere) and human immune system, skin cancer, eye cataract (Midgley et al. 1998). UV radiation as well influences climate change through ozone (indirect) and directly through physical variables such as clouds, aerosols, and snow cover (Kerr and Seckmeyer, 2006).

It is therefore, vital to give special attention to understand and predict UV variability in time and space. The amount of ultraviolet radiation reaching the surface of the Earth is dependent on a variety of atmospheric factors, of which stratospheric ozone is the most important. Apart the significance of the ozone layer, other atmospheric conditions such as boundary layer aerosol, clouds, and boundary layer ozone can also have a significant role (Zerefos, 1995).

In this thesis project, we will contribute in understanding the UV irradiance over Africa and uncovering the physical causes of its modulation in space and time making use of satellite data from NASA TOMS (Total Ozone Mapping Spectrometer), and NASA Nimbus7.

2.2 Absorption in the UV

UV radiation strongly interacts with the terrestrial atmosphere through scattering and absorption processes. The intensity of UV irradiance on the Earth's surface is strongly influenced by ozone absorption whereas the spectral distribution of the radiation is determined by scattering on air molecules and aerosols.

There are ways in which a molecule can store various energies. Any moving particle has kinetic energy because of its motion in space. This is known as translational energy. The average translational kinetic energy of a single molecule in the x, y, and z direction is found to be equal to $KT/2$, where K is the Boltzman's constant and T is the absolute temperature.

The molecule, which is composed of atoms can rotate, or revolve, about an axis through its center of gravity and, therefore, has rotational energy. The atoms of the molecule are bounded by certain forces in which the individual atoms can vibrate about

their equilibrium positions relative to one another. The molecule therefore will have vibrational energy.

These three molecular energy types are based on a rather mechanical model of the molecule that ignores the detailed structure of the molecule in terms of nuclei and electrons. It is possible, however, for the energy of a molecule to change due to a change in the energy state of the electrons of which it is composed. Thus, the molecule has electronic energy. The last three energy types are quantized and hence take discrete values only. Absorption and emission of radiation takes place when the atoms or molecules undergo transitions from one energy state to another. In general, these transitions are governed by selection rules. Atoms can exhibit line spectra associated with electronic energy.

For a gas, the absorption spectrum is concentrated in a complex array of lines that correspond to transitions between the discrete electronic, vibrational and rotational energy levels of molecules. Electronic transitions are stimulated by radiation in the UV and visible wavelengths, whereas vibrational transitions occur in the IR range.

Solar radiation is mainly absorbed in the atmosphere by $O_2, O_3, N_{2,} CO_2, H_2O, O,$ and N, although NO, N_2O, CO, and CH_4, which occur in very small quantities, also exhibit absorption spectra. Absorption spectra due to electronic transitions of molecular and atomic oxygen and nitrogen, and ozone occur chiefly in the ultraviolet (UV) region. While those due to the vibrational and rotational transitions of the triatomic molecule such as H_2O, O_3, and CO_2 lie in the infrared region. There is very little absorption in the visible region of the solar spectrum. Most of the UV radiation is absorbed in the upper atmosphere by oxygen and nitrogen species (see Figure 2.1).

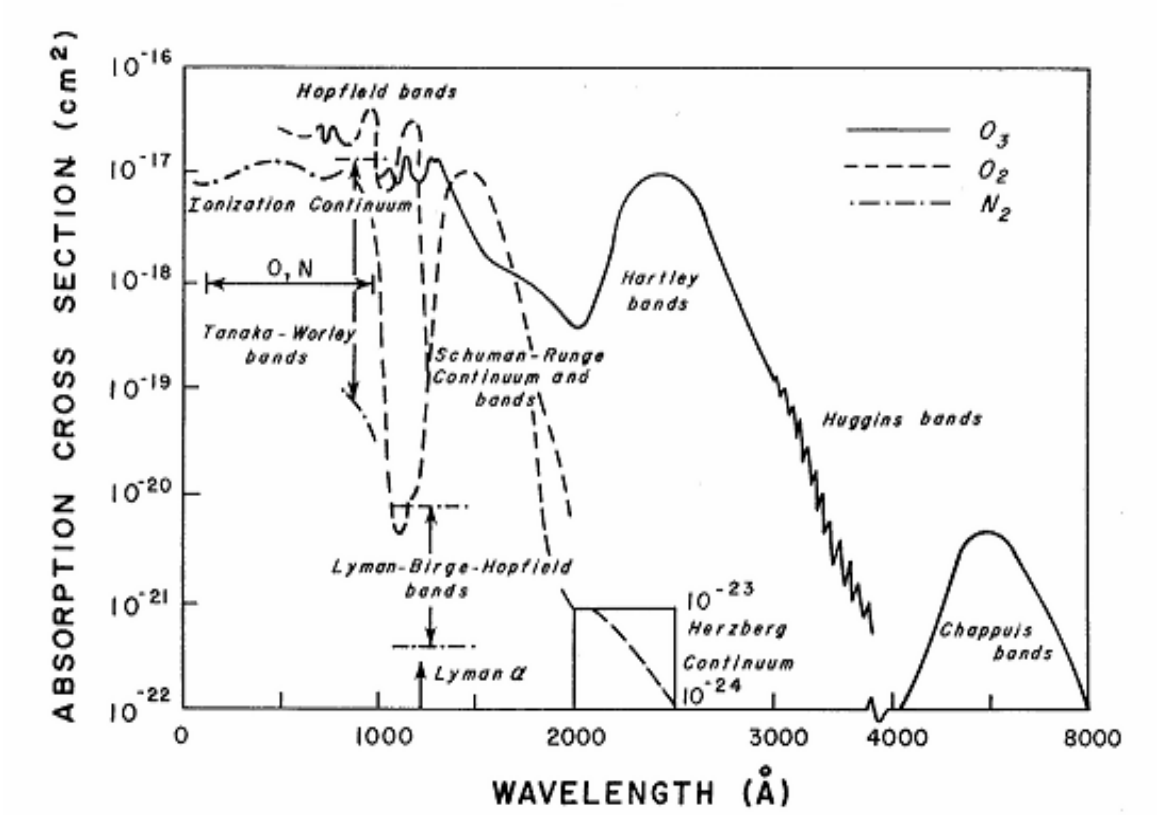

Figure 2.1: Absorption Cross sections σ in [Cm^2] ozone, molecular oxygen and molecular nitrogen in the ultraviolet spectral region. Absorption regions for atomic nitrogen and oxygen are also shown (according to Liou 1983).

The nitrogen molecule N_2 displays no obvious absorption features except in the far UV at wavelengths shorter than 100 nm (Tanaka-Worley bands). Due to the large quantity of nitrogen in the atmosphere, even very weak bands become observable. The N_2 molecule is symmetric and would be expected to have no electric dipole transitions, but a quadrupole band is found at the fundamental vibrational frequency. In addition, incident energy is absorbed by N_2 molecules and stored as rotational energy. The UV absorption spectrum of the molecular oxygen begins at about 2600 A^0 and continues down to shorter wavelengths (see table 2). See also Figure 2. 2.

S.No		Wavelength absorbed (A^0)	Characteristics
1	Hertzberg bands	2600 – 2000	- V. weak and little importance in the absorption of solar radiation due to overlap with ozone bands - significant for the formation of ozone
2	Schumann – Runge band	2000 – 1250	Strong and important
3	Several bands e.g. Lyman α line	1250 – 1000 1216	V. strong O_2 absorption spectrum
4	Hopfield bands	<1000	V. strong O_2 bands

Table 2.1: Absorption bands in the UV wavelength region for oxygen species.

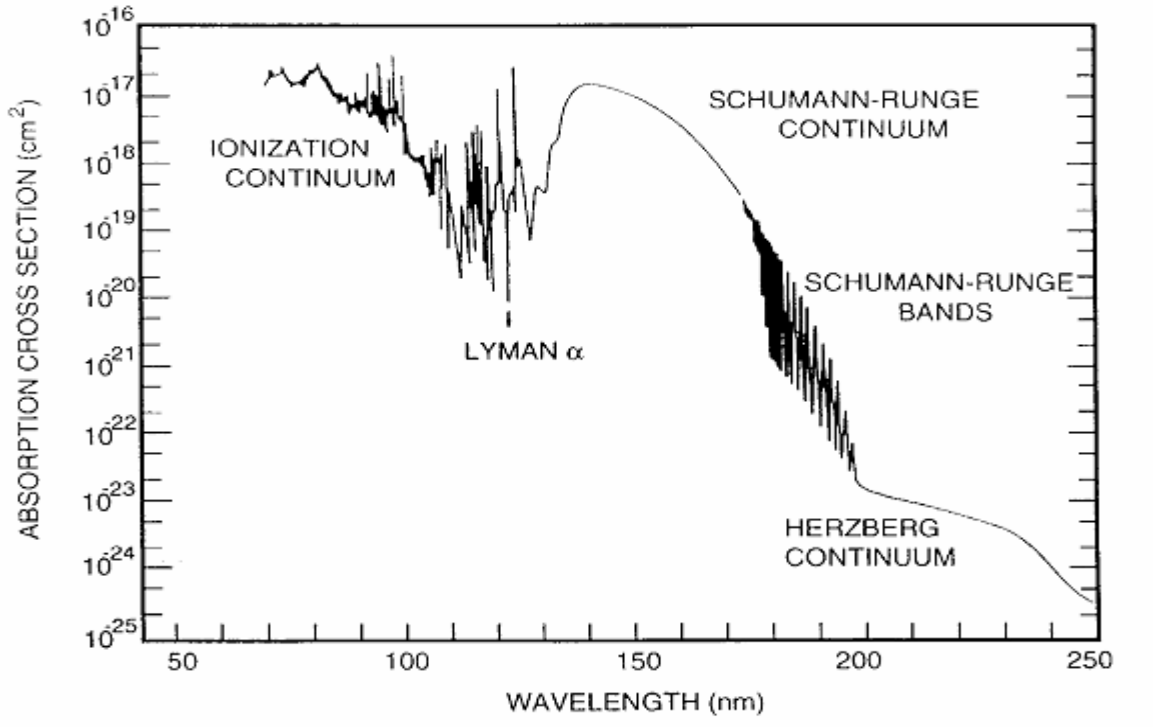

Figure 2.2: Absorption cross section as a function of wavelength for molecular oxygen (according to Liou (1983)

In the ionization process, the atom or molecule may absorb more than the minimum energy required to remove the electron. This additional energy is not quantized. As a result, the absorption is not selective but is continuous. The ionization continuum occurs on the high frequency (shorter wavelength) side of the ionization frequency. Because of the absorption of solar UV radiation, some of the oxygen and nitrogen molecules in the upper atmosphere undergo photochemical dissociation and are dissociated in to atomic oxygen and nitrogen.

Atomic nitrogen exhibits absorption spectrum from about 10 A^0 to about 1000 A^0. Although atomic nitrogen probably is not abundant enough to be a significant absorber in the upper atmosphere, it may play an important role in the absorption of UV radiation in the atmosphere. Atomic oxygen also shows absorption continuum in the region of 10 to 1000$A^{0.}$ The absorption spectrum of molecular nitrogen begins at 1450 A^0 and continues down to short wavelengths (see table 3).

S.No	Bands	Wavelength absorbed (nm)	Characteristics/ importance level
1	Lyman – Birge – Hopfield	1450 – 1000	Narrow and sharp lines
2	Tanaka – Worley bands	1000 – 800	Very complicated and absorption coefficient are highly variable.
3	Ionization continuum	<800	Ionization is a process in which an electron is removed from its orbit.

Table 2.1: Absorption in the UV wavelength by nitrogen species.

The ionized layers in the upper atmosphere are formed mainly as a result of the absorption of solar UV radiation – where by portions of the molecular and atomic oxygen and nitrogen becomes ionized. O_2 weakly absorbs between 2000 to 3000 A^0. The ozone in the upper stratosphere and mesosphere primarily absorbs this part of the solar

spectrum. The region that consists of the strongest absorption bands of O_3 is called Hartley bands. The bands between 3000 and 3600 A^0 are called Huggins bands, which are not as strong as Hartley bands. O_3 also shows weak absorption bands in the visible and near infrared regions from about 4400 to 11,800 A^0, called Chappius bands.

Note that the absorption cross-section α (in units of cm^2) is related to the absorption coefficient k (in units of $(cm\text{-}atm)^{-1}$ through the Loschmidt's number N_0 (2.687×10^{19} particles cm^{-3} at the standard temperature and pressure 1013mb); i.e., $K=\sigma N_0$. Both σ and K frequently are used in the field of upper atmosphere.

The absorption of solar UV radiation represents the prime source for the energetics and dynamics of the upper atmosphere. The upper atmosphere is composed of ions and some elements like oxygen, and nitrogen. The motion in the upper atmosphere is due to temperature difference. Molecules like oxygen, nitrogen, ozone, and other trace gases absorb UV radiation and emit infrared (IR) which increases the temperature of part of the atmosphere.

2.3 The Equations for Radiative Transfer

Radiative transfer models are used to determine the backscattered radiance. At the heart of any radiative transfer models is a procedure to calculate the radiation field for a given distribution of optical properties. This procedure ranges from a variety of parameterizations and approximations to sophisticated and accurate solutions of the full three-dimensional transfer equation.

A pencil of radiation traversing a medium will be weekend by interaction with matter. If the intensity of radiation I_λ becomes $I_\lambda + dI_\lambda$ after traversing a thickness ds in the direction of its propagation, then

$$dI_\lambda = -K_\lambda \rho I_\lambda ds \qquad (2.1)$$

where the subscript λ stands for the wavelength dependence of the irradiance, ρ is the density of the material, and K_λ is the mass extinction cross-section. Thus, the reduction

in intensity is caused by absorption in the material as well as scattering of radiation by the material. On the other hand, the intensity may be strengthened by emission of the material plus multiple scattering from all other directions in to the pencil under consideration at the same wavelength. (See Figure 2.3)

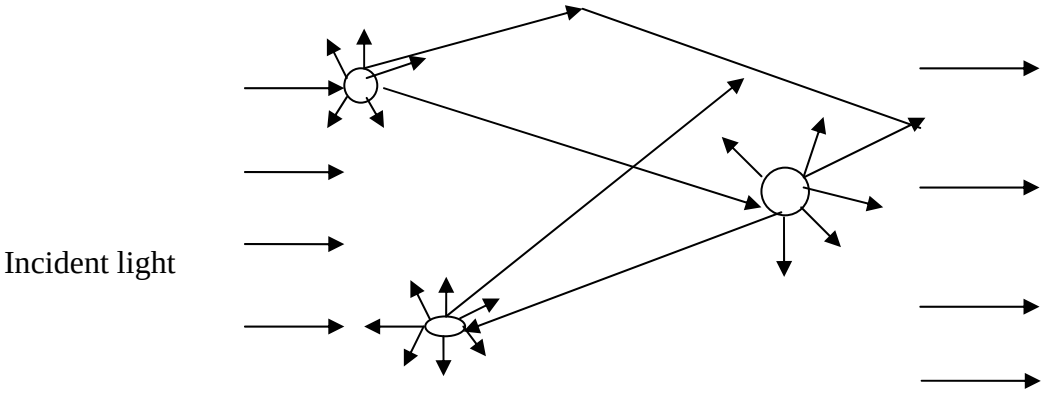

Figure 2.3: Multiple Scattering (Liou, 1983)

We define the source function j_λ such that the increase of intensity due to emission and multiple scattering is given by

$$dI_\lambda = j_\lambda \rho \, ds \qquad (2.2)$$

Here j_λ has the same meaning as the mass extinction coefficient.

$$dI_\lambda = -K_\lambda \rho I_\lambda ds + j_\lambda \rho \, ds \qquad (2.3)$$

Moreover, it is convenient to define the source function J_λ such that

$$J_\lambda = \frac{j_\lambda}{K_\lambda}$$

Rearranging,

$$\frac{dI_{\lambda}}{K_{\lambda}\rho\, ds} = -I_{\lambda} + J_{\lambda} \qquad (2.1)$$

where the source function J is defined as

$$J_{\lambda} = \frac{\omega}{4\pi}\sqrt{P(\Omega,\Omega')I(\Omega')d\Omega' + (1-\omega)B(T)} \qquad (2.2)$$

Here I is the radiance at location (x,y,z),B the volume extinction coefficient, ω is the single scattering albedo, $P(\Omega,\Omega')$ is the phase function giving the likelihood of a scattering event redistributing radiation from direction Ω' to Ω, and $B(T)=\sigma T^4$ is the Planck function (σ is the Stefan-Boltzman constant, and T is temperature). The later can usually be neglected for wavelengths below about $4\,\mu m$.

2.4 The Equation of Transfer for Plane parallel Atmosphere

Most of the solvers are plane parallel (pp) that is; they neglect the earth's curvature and assume an atmosphere of parallel homogeneous layers. This is generally a good assumption for solar and observation zenith angles (SZA) smaller than about 70^0 (Dahlback and Stamnes, 1991).

In problems of radiative transfer in plane parallel atmospheres it is convenient to measure, linear distances normal to the plane of stratification. The geometry for plane parallel atmospheres is as shown below (Figure 2.4).

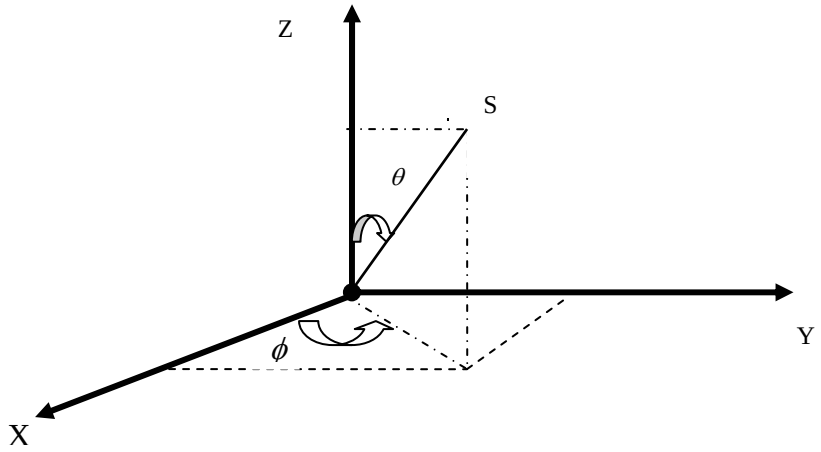

Figure 2.4 Geometry for plane parallel Atmosphere (Liou, 1983)

If Z denotes this distance, then the general equation of transfer

$$\frac{dI_{\lambda}}{K_{\lambda}\,\rho\,ds} = -I_{\lambda} + J_{\lambda} \qquad (2.6)$$

Becomes,

$$\cos\theta\,\frac{dI(z;\theta,\phi)}{k\,\rho\,dz} = -I(z;\theta,\phi) + J(z;\theta,\phi) \qquad (2.7)$$

where θ denotes the inclination to the upward normal, and ϕ the azimuthal angle in reference to the X-axis. Here, we omit the subscript λ on various radiative quantities.

Introducing the normal optical thickness,

$$\tau = \exp\left(-\int_{z}^{\infty} K\,\rho\,dz\right), \qquad (2.8)$$

One may note that the weighting function,

$$w = \frac{d\tau}{ds} = \frac{k\rho}{\cos\theta}\tau \qquad (2.9)$$

Measured from the outer boundary downward, we have

$$\mu \frac{dI(\tau;\mu,\phi)}{d\tau} = I(\tau;\mu,\phi) - J(\tau;\mu,\phi) \qquad (2.10)$$

where $\mu = \cos\theta$.

This is the basic equation for the problem of multiple scattering in plane parallel atmospheres. For the upward and downward intensities for a finite atmosphere which is bounded on two sides at $\tau = 0$ and $\tau = \tau_1$ as shown in Figure 2.5.

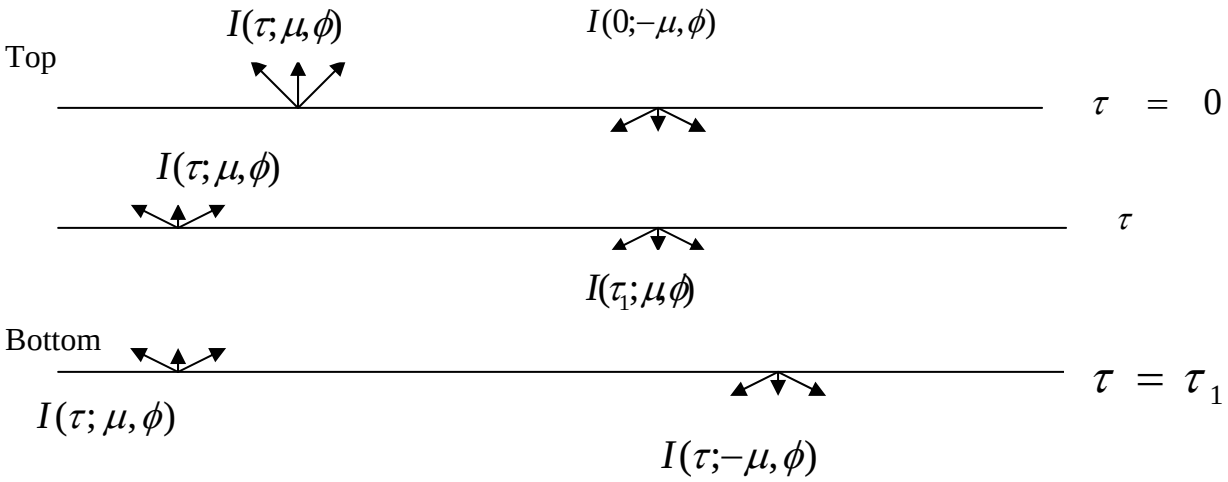

Figure 2.5: The upward and downward intensities (Liou, 1983).

To obtain the upward intensity ($\mu \geq 0$) at level τ, we multiply the equation (2.10) by a factor of $e^{\frac{-\tau}{\mu}}$ and perform integration from $\tau = 0$ to $\tau = \tau_1$. This leads to

$$I(\tau;\mu,\phi) = I(\tau_1;\mu,\phi)e^{\frac{-(\tau_1-\tau)}{\mu}} + \int_{\tau}^{\tau_1} J(\tau';\mu,\phi)e^{-(\tau'-\tau)/\mu}\frac{d\tau'}{\mu} \quad , (1 \geq \mu \succ 0)$$

(2.11)

To get the downward intensity $((\mu < 0)$ at level τ, a factor $e^{\tau/\mu}$ is used in equation (2.10) and μ is replaced by $-\mu$. After carrying out integration from $\tau = 0$ to τ, we obtain the expression,

$$I(\tau;-\mu,\phi) = I(0;-\mu,\phi)e^{\frac{-\tau}{\mu}} + \int_{0}^{\tau} J(\tau';-\mu,\phi)e^{-(\tau_1-\tau')/\mu}\frac{d\tau'}{\mu} \quad , (1 \geq \mu \succ 0)$$

(2.12)

Here, I $(\tau_1;\mu,\phi)$, and $I(0;-\mu,\phi)$ represent respectively, the inward source intensities at the bottom and top surfaces.

For planetary applications, it is desirable to measure the emergent outward intensities at the top and bottom of the atmosphere in conjunction with remote sensing of atmospheric compositions, and radiative balance studies.

Up on setting $\tau = 0$, in equation (2.11), we find

$$I(0;\mu,\phi) = I(\tau_1;\mu,\phi)e^{\frac{-\tau}{\mu}} + \int_{0}^{\tau_1} J(\tau';\mu,\phi)e^{-\tau'/\mu}\frac{d\tau'}{\mu} \quad , (1 \geq \mu \succ 0)$$

(2.13)

where the first and second terms represent, respectively, the bottom surface contribution (attenuated to the top) and the internal atmospheric contribution.

Moreover, up on setting $\tau = \tau_1$ in to equation (2.12), we get

$$I(\tau;-\mu,\phi) = I(0;-\mu,\phi)e^{\frac{-\tau_1}{\mu}} + \int_{0}^{\tau_1} J(\tau';-\mu,\phi)e^{-(\tau_1-\tau')/\mu}\frac{d\tau'}{\mu} \quad , \quad (1 \geq \mu \succ 0)$$

(2.14)

Where again the first and second terms represent, respectively, the top surface contribution (attenuated to the bottom) and the internal atmospheric contribution.

Once the radiative transfer equation is solved, a number of radiative quantities can be calculated. These include the downward direct and diffuse $E_{\downarrow}$ irradiances and the upward $E_{\uparrow}$ irradiances:

$$E_{\downarrow} = \int_{2\pi} L(\Omega) \cos\theta \, d\Omega = \int_{0}^{2\pi} \int_{\frac{\pi}{2}}^{\pi} L(\theta, \phi) \cos\theta \sin\theta \, d\theta \, d\phi \tag{2.15}$$

$$E_{\uparrow} = \int_{0}^{2\pi} \int_{0}^{\frac{\pi}{2}} L(\theta, \phi) \cos\theta \cos\phi \, d\theta \, d\phi \tag{2.16}$$

In addition, the corresponding actinic fluxes are

$$F_{\downarrow} = \int_{2\pi} L(\Omega) \, d\Omega$$

$$= \int_{0}^{2\pi} \int_{\frac{\pi}{2}}^{\pi} L(\theta, \phi) \sin\theta \, d\theta \, d\phi \tag{2.17}$$

$$F_{\uparrow} = \int_{0}^{2\pi} \int_{0}^{\frac{\pi}{2}} L(\theta, \phi) \sin\theta \, d\theta \, d\phi \tag{2.18}$$

Here θ and ϕ are the polar and azimuthal angles, respectively.

2.5 Biologically Active UV Radiation

The sensitivity of organisms to UV radiation is strongly dependent on wavelength. The action spectra have been calculated by different people to represent different responses;

an example is shown in Figures 2.6 and 2.7. DNA action spectrum decreases as the wavelength increases.

The product of the biological action spectrum B (λ) and the surface spectral irradiance is the spectral dose rate. The peak response is usually between 300 and 310 nm, which are demonstrated in Figure 2.7. for the DNA damage spectrum at three different solar zenith angles. The integration of the spectral dose rate over wavelength yields the dose rate:

$$\text{Dose Rate} = \int B(\lambda)E(\lambda)d\lambda \qquad (2.19)$$

The dose rate is an instantaneous measure of the biologically weighted UV irradiance; its units are W/m^2. The dose rates reach a maximum at solar noon at any given latitude. This can be seen from Figure 2.9. Integration of the dose rate over a full day gives the daily dose, and over a full year the yearly dose, in units of Jm^{-2},

$$\text{Dose Rate} = \iint B(\lambda)F(\lambda)d\lambda dt \qquad (2.20)$$

where t is time. The seasonal and latitudinal dependence of daily DNA-damaging dose rates is shown in Figure 2.10. The latitudinal variation is illustrated in Figure 2.10, where the spectral exposure of UV is greater in the tropical region.

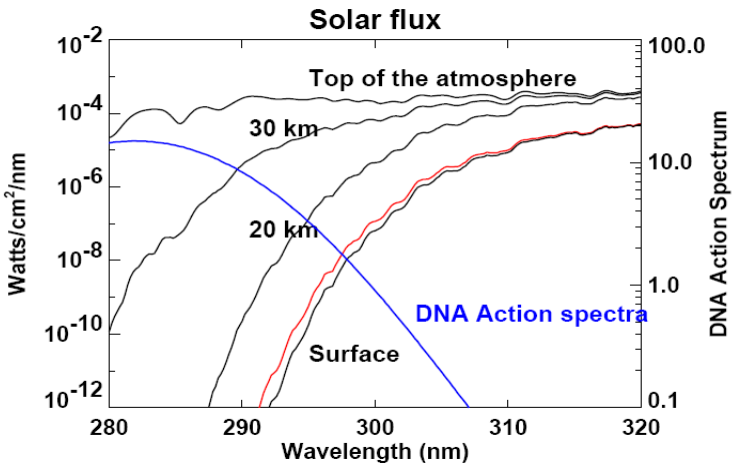

Figure 2.6 Solar Flux for different altitudes

(http:// see.gsfc.nasa.gov/edu/SEES/strat/class/S_class.html).

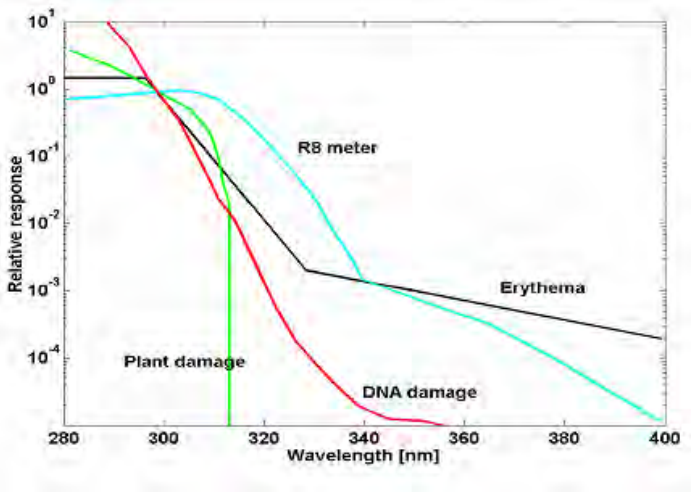

Figure 2.7 Action spectra for DNA damage (Setlow 1974), the Robertson-Berger UV radiometer (Urbach et al. 1974) and the generalized plant damage (Caldwell et al. 1986). The spectra all are normalized to unity at 300 nm and show relative response per energy unit (Madronich 19 93a).

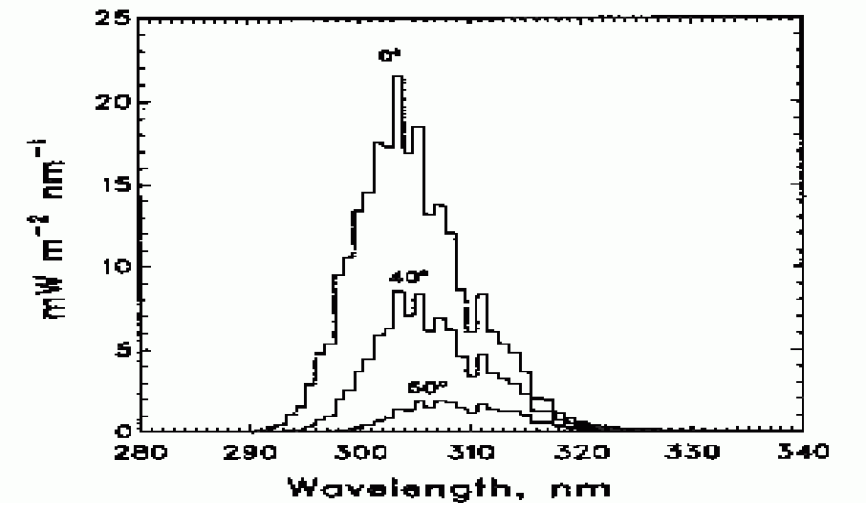

Figure 2.8 Spectral dose rates weighted for the DNA damage at three different solar zenith angles, for clear skies and an ozone column of 300 DU (Madronich 1993b).

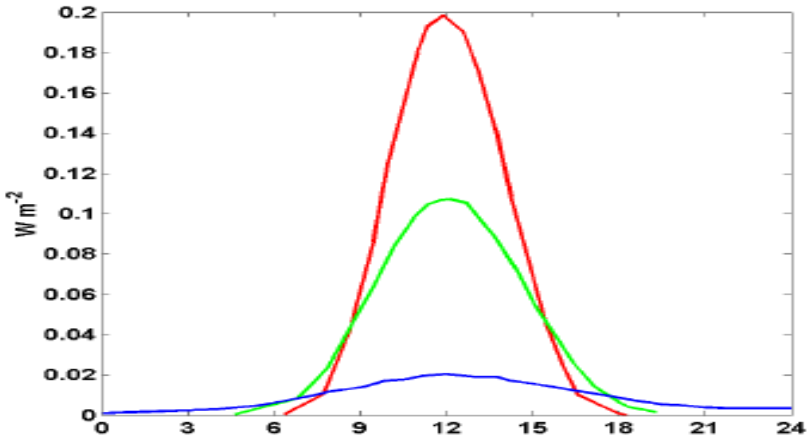

Figure 2.9 Diurnal dependence of DNA-damaging dose rate on 21 June at three different latitudes (Madronich 1993a).

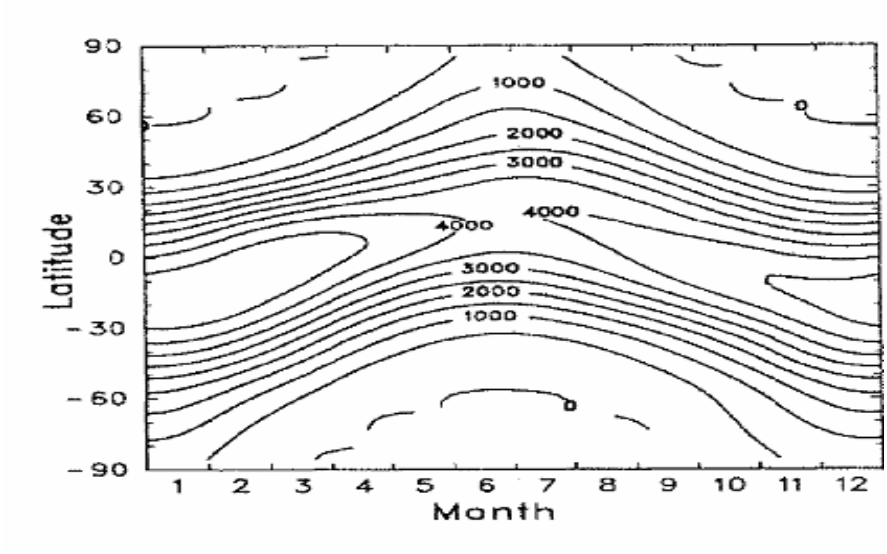

Figure 2.10 Season and latitudinal dependence of the daily dose (Jm^{-2} day^{-1}) for DNA damage, calculated for clear skies, using ozone column averages over 1979-1989 (Madronich 1992).

2.6 Chapter Summary

Ultraviolet radiation is that range of the solar spectrum, which is found at the end of the visible and is the most energetic part of the solar spectrum. It is divided in to three distinct UV ranges. The first is UV-A (315 nm to 400 nm) and is almost unabsorbed in the atmosphere. In small dose, it is required for the vitamin D synthesis in our body; in long time exposure, it causes ageing (our skin look aged than we are!) and it is believed to cause skin cancer called melanoma. The second part of UV is called the skin burning UV called erythemal UV (UVery) or UV-B (280 nm – 315 nm). This is absorbed partially by ozone and is not required at surface. The reason is it causes problems of which skin cancer (melanoma), eye disease (cataract), human immune suppression and material degradation like plastics, asphalt etc are some of them. Then this part of UV has shown increase in recent years in middle latitudes and Polar Regions due to the decrease of stratospheric ozone. UV-C is the third category of and is totally absorbed by ozone.

Radiative transfer equations are modified accordingly to get the exact amount of spectral bands, which could help get the amount of erythemal (sun burning) dosage (UVery) of the UV radiation, the total amount of ozone, the UV absorbing aerosols, the total cloud cover of an area and the vertical distribution of ozone. Modifications are made accordingly to obtain the required measurement mentioned in the data types part in chapter 4. The dosage per day during the noontime could also be calculated using the dose rate formula.

Chapter Three

UV Reliance on Other Variables

Many complicated scattering and absorption processes in the atmosphere and at the Earth's surface influence solar UV radiation, which reaches the ground. These processes must be understood in order to describe fully the characteristics of the current climatology of the surface UV radiation on a global Scale and to project it to the past and future.

Results of the studies show that there have been past changes in UV (caused by changes in ozone as well as changes in other variables such as clouds, aerosols, and snow cover). Before considering the dependence of UV on the geophysical variables, it is better to understand: 1) The stability of the extraterrestrial radiation, since the increase or decrease of the extraterrestrial solar radiation affects the amount of ozone formed in the atmosphere and hence, UV irradiance; 2) How particles absorb and scatter radiation coming from the sun. The absorption is discussed briefly in section 2.2 above. The scattering by gaseous molecules (Rayleigh scattering) which is the major theory that affects UV radiation and scattering by aerosols (Mie scattering) are considered below.

3.1. The Extraterrestrial Solar Spectrum

Accurate knowledge of the solar spectrum is important for studying surface UV, since it is used in radiative transfer (RT) models that are ultimately compared with measurements. Knowledge of the stability of solar irradiance at UV wavelengths is important because it drives many geophysical processes, including the formation of stratospheric ozone. It could also be used as a reference standard for UV measurements. Changes in solar irradiance from 1700 to present were determined by Flaggie and Solanki (2000). Their model assumes that solar irradiance variations on time scales from days to centuries are due only to the changing distribution of solar surface magnetic features. The study determined an increase of solar spectral irradiance at the 11-year solar activity cycle minimum since the Maunder minimum (year 1700) of 3.0% for wavelengths less than 300 nm and 1.3% for the band 300-400 nm. The total (all wavelengths) and the

visible irradiance showed an increase of about 0.3% Rozema et al. (2000). Note that a past long-term increase on solar UV-C radiation would lead to an increase in the production of stratospheric ozone that would reduce surface UV-B irradiance.

3.2 Scattering by Gaseous Molecules (Rayleigh Scattering)

Rayleigh Theory

Scattering by air molecules is based on the assumption that the scattering particles are less than 0.2λ in diameter and that the particles scatter independently of each other.

Consider a small, homogeneous, isotropic, spherical particle with radius much smaller than the wavelength of the incident radiation. The incident radiation produces homogeneous electric field, which generates a dipole configuration on the particle. The electric field of the particle, caused by the electric dipole, modifies the applied field inside and near the particle. The intensity of radiation is proportional to the average of E^2. Incident sunlight of intensity I_0 is then scattered in to the scattering angle θ with intensity

$$I(\theta, r) = I_o K^4 \frac{\alpha^2 (1 + \cos^2 \theta)}{r^2 2}, \qquad (3.1)$$

where r is the distance from the dipole, α the polarizability and k the scattering coefficient. In terms of the phase function and wavelength $\lambda / 2\pi k$, Equation (3.1) may be cast into the canonical form

$$I(\theta, r) = I_o \frac{\alpha^2 32\pi^4}{r^2 3\lambda^4} P_{Ray} \qquad (3.2)$$

with the Rayleigh phase function

$$P_{Ray} = \frac{3}{4}(1 + \cos^2 \theta) \ . \qquad (3.3)$$

The scattered intensity has maxima in the forward ($\theta = 0^0$) and backward ($\theta = 180^0$) directions, with equal energy directed into each half-space. The scattered flux follows as in Equation 3.3, but with the incident flux F_o in place of I_o. Integrating the scattered flux over a sphere of radius r results in the scattered power

$$\psi = F_o \alpha^2 \frac{128\pi^5}{3\lambda^4}, \tag{3.4}$$

this has dimensions of energy/time. In this context α is the polarizability of the scatterer. Then the scattered cross section for and individual molecule is

$$\sigma_s = \frac{\psi}{F_o} = \alpha^{2-} \frac{128\pi^5}{3\lambda^4}. \tag{3.5}$$

Finally, the scattered intensity at distance r can be expressed as

$$I(\theta, r) = I_o \frac{\sigma_s}{4\pi r^2} P(\theta). \tag{3.6}$$

Electromagnetic field theory relates the polarizability α to the dimensionless refractive index $m = m_r - m_i$. The real and imaginary parts of m refer to the phase speed and absorption of electromagnetic radiation in a medium relative to those in a vacuum. An ensemble of scatterers with number density n has polarizability

$$\alpha = \frac{3}{4\pi n} \frac{m^2 - 1}{m^2 + 2}. \tag{3.7}$$

At wavelengths of visible radiation for example, absorption by air molecules is small enough for m_i to be ignored, while m_r is close to unity. Then Equation 3.7 reduces to

$$\alpha \approx \frac{m_r - 1}{2\pi n}, \tag{3.8}$$

So the scattering cross section for and individual molecule is given by

$$\sigma_s = \frac{32\pi^3 (m_r - 1)^2}{3n^2 \lambda^4}. \qquad (3.9)$$

This solution was derived late in the 19th century by Lord Rayleigh and therefore it is called Rayleigh's theory. The Rayleigh scattering explains why the sky appears blue. The λ^{-4} dependence of σ_s implies that shorter wavelengths are scattered by air molecules much more effectively than longer wavelengths. Blue light ($\lambda \sim 0.4\mu m$) is scattered five times more than red light ($\lambda \sim 0.65\mu m$), therefore it arrives at the Earth's surface as diffuse radiation emanating from all directions. On average, about 40% of the shortwave flux is scattered out of the incident beam in the near UV region, whereas less than 1% is removed in the near IR region. Overall, about 10% of shortwave radiation incident on the atmosphere is scattered by atoms and molecules. Most of that scattering takes place in the lowest 10Km, where n (Z) is large. Therefore, Rayleigh scattering also influences ozone photochemistry and stratospheric heating, for example by enhancing the shortwave flux available to the Chappius bands of O_3.

The Rayleigh scattering cross section and total volume scattering coefficients have been tabulated and formulas are given for various model atmospheres. They give results as a function of the wavelength, with incorporation of the variation of the depolarization factor with wavelength. For example the Rayleigh scattering cross section $\sigma_s(\lambda)$ equals to 5.59 *10^{-26}cm^2 at 300 nm and 1.67 * 10^{-26} cm^2 at 400 nm (WMO 1985). The volume scattering coefficient β_λ is given by

$$\beta_\lambda(z) = n(z)\sigma_s(\lambda), \qquad (3.10)$$

where n(z) is the molecular number density at altitude z at given pressure and temperature.

3.3 Scattering by Aerosols (Mie Scattering)

Mie Theory

Scattering from spherical particles of arbitrary dimension was first treated by Mie (1908). The Mie scattering theory applies to the interaction of radiation with aerosols and cloud droplets. If the particle dimensions are comparable with the wavelength of the incident light, the proper radiation field of the particle cannot be regarded as a dipole.

Depending on the relation between the dimensions of particles and the incident light, it is necessary to take into account fields of higher orders, such as quadrupole or octopole.

Application of Mie scattering to atmospheric aerosol relies on particles being sufficiently separated for their interactions with the radiation field to be treated independently. Mie's theory solves Maxwell's equations for the electromagnetic field about a dielectric sphere of radius r in terms of and expression in spherical harmonics and Bessel functions (Liou 1983).

Mie has developed a theory assuming particles to be uniform spheres with a given complex refraction index and radius. The Mie theory gives the dimensionless extinction coefficient Q_{ext}, the scattering efficiency $Q_{sca.}$ See Equations 11 and 12.

$$Q_{ext} = \sigma_e(\lambda) \Big/ \pi r^2 , \qquad (3.11)$$

$$Q_{sca} = \sigma_s(\lambda) \Big/ \pi r^2 , \qquad (3.12)$$

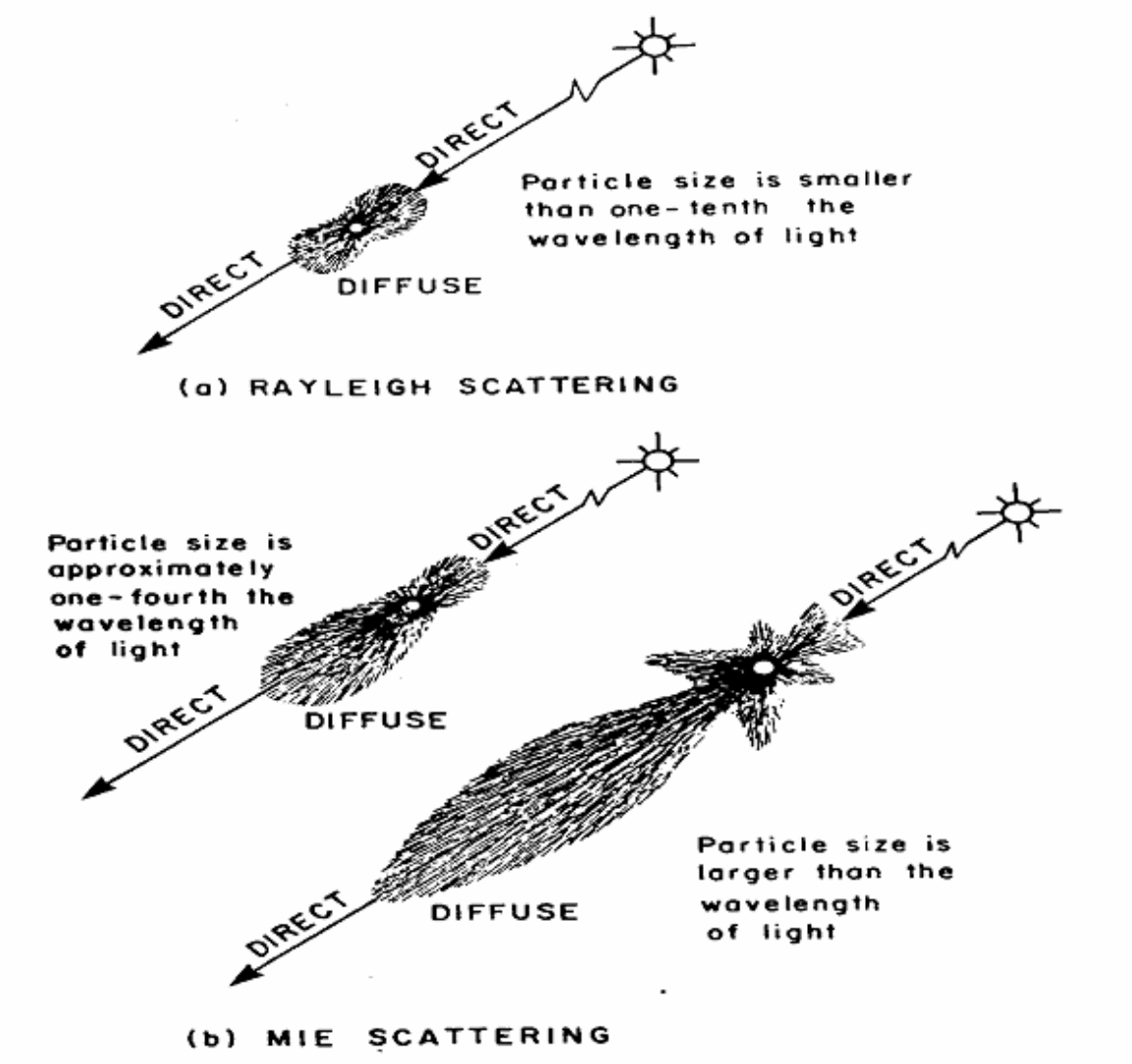

Figure 3.1 Scattering cross sections by Rayleigh (top) and Mie (bottom) scattering of electromagnetic radiation (according to Iqbal 1983)

The most notable feature of Mie scattering is the forward peak for all but the smallest particles (see Figure 3.2). In the case of a tiny scatterer ($2\pi r \leq \lambda$), the scattering diagram would be symmetric, equal amounts scattered in backward and forward directions (Rayleigh scattering). If the particle size were increased, an asymmetry would begin to develop, implying more forward than backward scattering. Holding the particle size constant, the forward peak is not greatly affected by an increase of the imaginary part of the refractive index m_i. The backward hemisphere is most affected. However, when the

absorption becomes very large (m_i>1), the backward scattered radiation goes through a minimum and thereafter increases again.

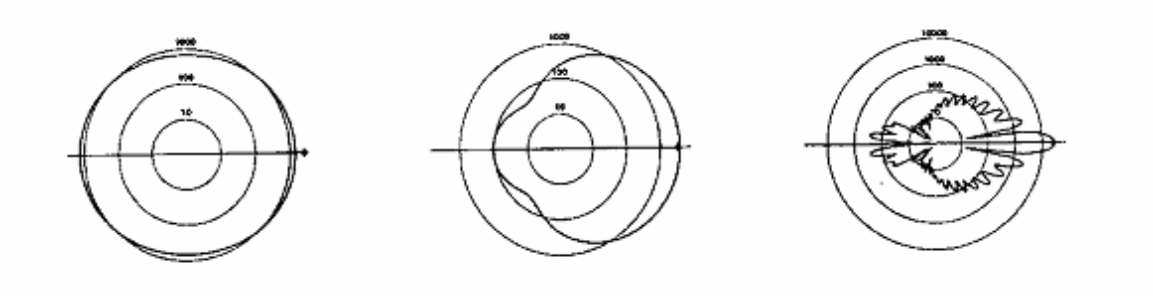

Figure 3.2 Scattering polar diagrams for $\lambda = 0.32 \mu m$. Radius = 0.01 m (left, x = 0.19), radius = 0.1 m (middle, x = 1.9) and radius = 1m (right, x = 19).

Propagation of radiation through the atmosphere is affected by absorption and scattering by particulates (e.g. haze, dust, fog and clouds) suspended in the air. Scattering and absorption by aerosol particles becomes an important factor in the boundary layer. The weak dependence on wavelength and the fact that droplet size spectra span several oscillations in Q_{sca} explain why clouds appear white.

An aerosol is a small solid or liquid particle that remains suspended in the air. Precipitation is usually excluded. In contrast to molecules of the atmospheric gases, suspended particles within the atmosphere display considerable diversity in volume, size, distribution, form and material composition. These particles are either of terrestrial (e.g. smoke, mineral dust, volcanic ash or forest burning), marine (e.g. from salt crystals or ocean spray) or biological origin. Aerosols are transported from their source regions in to the atmosphere, or may be formed within the atmosphere by gas through chemical or photochemical processes.

3.4 Dependence of UV on Geophysical variables

One of the main objectives for making good quality measurements of surface UV radiation is to understand the dependencies of UV on absorption and scattering processes that occur in the atmosphere and at the Earth's surface. In principle, if the spatial distribution of all absorbers and scatterers within the atmosphere and at the Earth's surface were fully known, it would be possible to determine the wavelength dependence and angular distribution of surface UV radiation by model calculations. In practice, the complicated distribution of the predominant variables (clouds, ozone, aerosols, and surface albedo) and their interactive impact on UV irradiance makes detailed calculations on a global scale an extremely difficult task.

3.4.1 Dependence of UV on ozone and other trace gases

The variation of the vertical distribution and temperature of ozone affects UV radiation. These effects could influence surface UV should there be a long-term change in the vertical profile or effective column temperature of ozone; however, the effects are relatively small compared to past or expected future long-term changes in total ozone.
The effects of sulfur dioxide on surface UV were shown to be negligible on a global scale but could be significant at sites near local pollution sources or continuous volcanic activity (Fioletov et al., 1998), or over wider areas in the aftermath of major volcanic eruptions.

Other gases that absorb in the UV (e.g., nitrogen dioxide, nitric acid, and formaldehyde) are not significant under natural conditions, but could be significant under heavy pollution situations.

The ozone in any given location is a balance between three processes: in situ creation, in situ destruction, and transport into or out of the location. Creation of ozone occurs mainly in the stratosphere where there is enough of the necessary ultraviolet (UV) light from the sun. Thus, most ozone molecules are found in the stratosphere. Closer to Earth's surface, less ultraviolet (UV) light penetrates to break apart the regular oxygen molecules that are necessary to create ozone. The shielding of the lower atmosphere from

UV light is actually provided by the layer of ozone molecules above. This reflects the fact that ozone creation at a given spot depends on the amount of ozone already in a column above the spot. Thus, we may say that ozone formation in the stratosphere inhibits the formation of ozone lower down in the troposphere. (The troposphere is the lowest level of the atmosphere where dynamical instability creates most of the observed weather.) This keeps ozone concentrations small at low altitudes. Ozone concentrations do not rise indefinitely, but instead fall above a certain height. This is because, the atmosphere thins rapidly (indeed, exponentially) with height. The amount of available oxygen for ozone creation drops off quickly. Less ozone is able to form even though the UV light is available. The result of these two contrasting effects: less UV light with decreasing height and less oxygen with increasing height produce the observed ozone profiles. Ozone concentrations are observed to peak between 20 and 40 kilometers with a steady decrease above and below the peak.

If we want to understand how ozone is distributed vertically, we examine profile measurements of ozone concentration. These measurements are usually reported in mixing ratio, number density, or partial pressure. Mixing ration in ppmv relates the fractional concentration of ozone as the number of ozone molecules per cubic centimeter. Partial pressure refers to the fraction of the atmospheric pressure at a given altitude for which ozone is responsible.

Partial pressure and number density profiles are very similar. This similarity is because the partial pressure of ozone can be expressed as a function of the number density.

$$P_{ozone}=nKT \qquad (3.13)$$

where n is the number density, k is Boltzman's constant (1.38×10^{23} J/K) and T is temperature measured in degrees Kelvin. While all three profiles peak between 20 and 40 km and fall off rapidly above and below this peak, in the case of the mixing ration profile, the peak is significantly higher in altitudes than for the number density and partial pressure profiles between 8 and 10 km vanish in the mixing ratio profile. The basis for

these differences can be derived from the vertical air distribution (rapidly thins with height). Clearly, number density declines with altitude.

Mixing ratio, however, accounts for this fact that there are fewer molecules higher up, and reports the fractional composition of the air molecules everywhere. In addition to profile measurements, there is a third way to measure ozone. It is called a Dobson Unit. Instead of measuring the amount of ozone at a particular height, the Dobson Unit is a measurement of the total amount of ozone in a column extending vertically from Earth's surface to the top of the atmosphere. This measurement of ozone is directly related to the amount of UV light reaching the surface. It is therefore a measure of UV exposure received at the surface: the less total ozone in the column, the more UV light penetrates, the faster you are sunburned.

The Dobson Unit is a measure of the height of our stack of ozone molecules: 1 DU = 10^{-5}m. A typical mid latitude air column contains about 300 DU of ozone, which is equivalent to a stack of ozone molecules about 3 millimeters high, about the thickness of two stacked pennies.

3.4.1.1 Ozone Formation

Ozone is created in the middle to upper stratosphere of the tropics. It is here that the Sun provides enough of the necessary extreme ultraviolet (EUV) light (see Figure 3.3). The EUV breaks down diatomic oxygen molecules, O_2, into free oxygen atoms, which then recombine with other oxygen molecules to form ozone, O_3. As can be seen from its vertical profiles at different latitudes, ozone has an elevated peak somewhere in the lower to mid stratosphere, roughly 20 to 40 km in altitude. It is at these altitudes where the creation of ozone is maximized owing to two effects: a sufficient supply of oxygen and a sufficient amount of incoming UV light. Above and below these heights, these two effects work against each other. An additional characteristic of ozone arising from its vertical distribution and the amount of penetrating UV light involves the length of time an ozone molecule exists between its creation and destruction. Both processes involve UV light. The so-called "lifetime" of an existing ozone molecule residing at some level is determined by how long it takes a UV photon to penetrate into the atmosphere to that level and to break apart the molecule in a process known as photolysis.

The two most important photodissociaton reactions in the troposphere are firstly:

$$O_3 + h\nu \rightarrow O_2 + O^1D \; \lambda < 320 \text{ nm} \qquad (3.14)$$

which generates an excited oxygen atom which can go on to react with water to give the hydroxyl radical:

$$O^1D + H_2O \rightarrow 2OH \qquad (3.15)$$

The hydroxyl radical is central to atmospheric chemistry as it initiates the oxidation of hydrocarbons in the atmosphere and so acts like a detergent.

Secondly the reaction:

$$NO_2 + h\nu \rightarrow NO + O \qquad (3.15)$$

is a key reaction in the formation of tropospheric ozone.

The formation of ozone layer is also caused by photo-dissociation. Ozone in the earth's stratosphere is created by ultraviolet light striking oxygen molecules containing two oxygen atoms (O_2) splitting them into individual oxygen atoms (atomic oxygen); the atomic oxygen then combines with unbroken O_2 to create ozone, O_3. Ozone can also be produced at the surface in two ways, both of which are related to human activates. One way is in the form of photochemical smog that arises from industrial pollution reacting with sunlight. Another is in so-called "biomass burning". This refers to burning of jungle, savannah, and existing farmland. It is primarily due to human agricultural needs, though lightening can also trigger wild fires that result in biomass burning-related ozone creation. These forms of ozone are unhealthy, while stratospheric ozone, by blocking dangerous UV light, is essential for life on Earth's surface. Our focus here is on this beneficial ozone created by energetic UV light, principally in the stratosphere.

In addition, photolysis is the process by which CFCs are broken down in the upper atmosphere to form ozone-destroying chlorine free radicals. Figure 3.4 shows the summary of the production of ozone by the extremely energetic ultraviolet radiation.

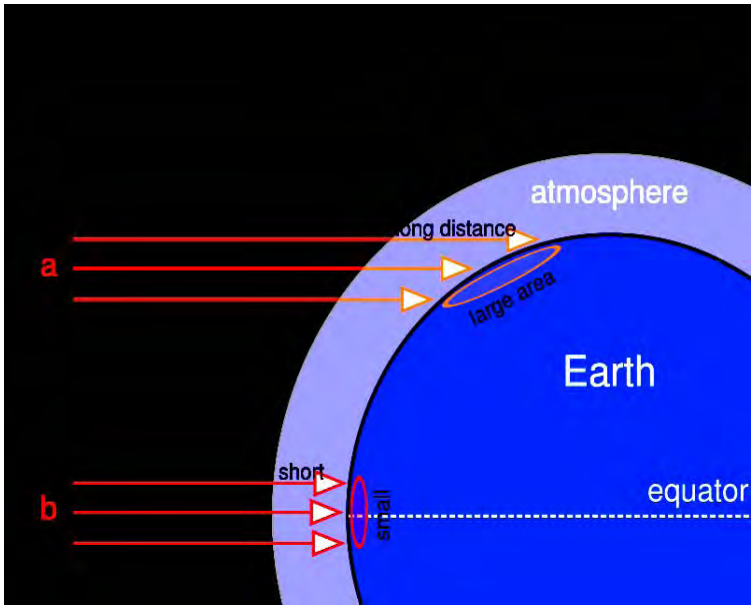

Figure 3.3: The amount of solar energy reaching the surface of the Earth varies according to latitude. In the polar region the rays cover large areas hence the amount of radiation received at a point is very small. On the other hand at the tropics the rays cover small area and the energy is sufficient to break the oxygen molecule to oxygen ions.

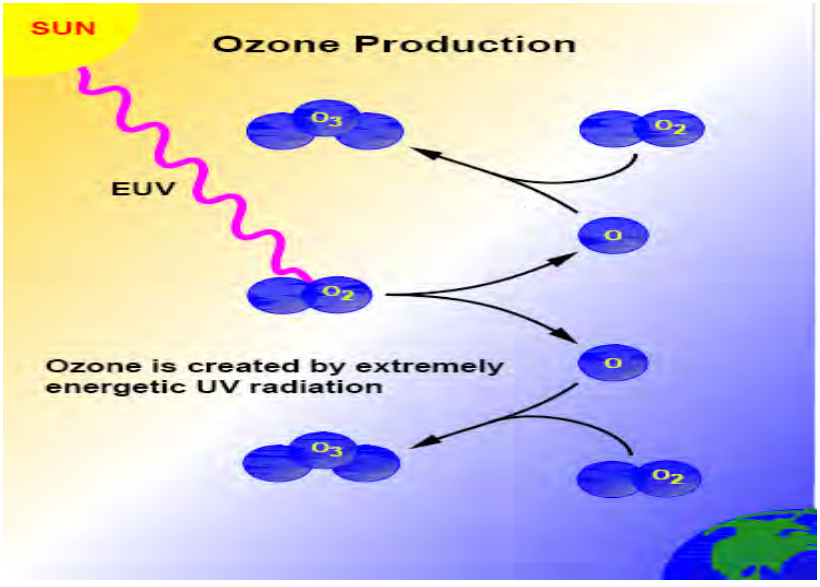

Figure 3.4: Schematic Diagram of the ozone production.
(http:// see.gsfc.nasa.gov/edu/SEES/strat/class/S_class.html).

3.4.1.2 Ozone Depletion

The chemical loss of ozone occurs primarily by two gas-phase catalytic cycles that involve chlorine oxide radicals (Molina and Molina, 1987) and bromine and chlorine oxides during the winter in the polar region (McElroy et al., 1986):

Cycle 1:

$$ClO + ClO + M \longrightarrow ClOOCl + M \quad (3.16a)$$

$$ClOOCl + h\nu \longrightarrow 2Cl + O_2 \quad (3.16b)$$

$$2\,[Cl + O_3 \longrightarrow ClO + O_2\,] \quad (3.16c)$$

Net : $2O_3 \longrightarrow 3O_2$

Cycle 2:

$$BrO + ClO + h\nu \longrightarrow Br + Cl + O_2 \quad (3.17a)$$

$$Br + O3 \longrightarrow BrO + O2 \quad (3.17b)$$

$$Cl + O3 \longrightarrow ClO + O2 \quad (3.17c)$$

Net: $2O_3 \longrightarrow 3O_2$

If loss of ClOOCl occurs by thermal decomposition:

$$ClOOCl + M \longrightarrow ClO + ClO + M \quad (3.18)$$

Rather than photolysis (1b), a null cycle that results in recycles ClO but leads to no change in ozone. Small contributions to polar ozone loss also occur due to cycles limited by the reactions ClO + O and ClO + HO_2.

Ozone molecules existing below the ozone peak can “live” for weeks to months without being destroyed by a stray UV photon. This is because the layer of ozone molecules above it are absorbing most of the UV photons. In the process of destroying (photolysing) an ozone molecule, a photon loses enough energy that it is no longer biologically harmful

UV radiation. This is precisely how the ozone layer shields Earth. The lower into the atmosphere you go; the longer an ozone molecule lives with lifetimes for molecules below the peak layer approximately weeks to months.

3.4.1.3 Ozone Circulation

As discussed in section 3.4.1.1, most ozone production occurs in the tropical stratosphere as the overhead sun breaks apart oxygen molecules (O_2) into oxygen atoms (O), which quickly react with other O_2 molecules to form ozone (O_3). The problem with this simplified picture is that most ozone is found outside the tropics in the higher latitudes rather than in the tropics. That is, most of the ozone is found outside of its natural tropical stratospheric source region. This higher latitude ozone results from the slow atmospheric circulation that moves ozone from the tropics where it is produced into the middle and polar latitudes. This slow circulation is known as the Brewer-Dobson circulation, named after Brewer and Dobson.

The simple circulation model suggested by Brewer (1949) and Dobson (1956) consists of three basic parts. The first part is rising tropical motion from the troposphere into the stratosphere. The second part is pole ward transport in the stratosphere. The third part is descending motion in both the stratospheric middle and polar latitudes, though there are important differences. The middle latitude descending air is transported back into the troposphere, while the polar latitude descending air is transported into the polar lower stratosphere, where it accumulates. This model explains why tropical air is lower in ozone than polar air, even though the source region of ozone is in the tropics. However, we are getting a bit ahead of ourselves, and it is necessary to look at the big picture in more detail.

In the stratosphere, the Brewer-Dobson circulation carries air from the equator to the poles. Pole ward of about 30°N and 30°S, the circulation becomes downward as well as pole ward. This pole ward and downward circulation tends to increase ozone concentrations in the lower stratosphere of the middle and high (i.e. extra tropical)

latitudes. In Figure 3.5, we see this increase of ozone at lower altitudes in the higher latitudes as a direct result of this circulation.

The mechanism behind the Brewer-Dobson circulation is both complex and quite interesting. At first glance, we might expect that the circulation results from solar heating in the tropics, and cooling in the polar region, causing a large equator to pole (meridional) overturning of air as warm (tropical) air rises and cold (polar) air sinks. While this heating and cooling does indeed occur, and while such a meridional overturning exists in the form of the so-called Hadley circulation, it is not the specific reason for the existence of the Brewer-Dobson circulation. Rather, the Brewer-Dobson circulation results from wave motions in the extra tropical stratosphere.

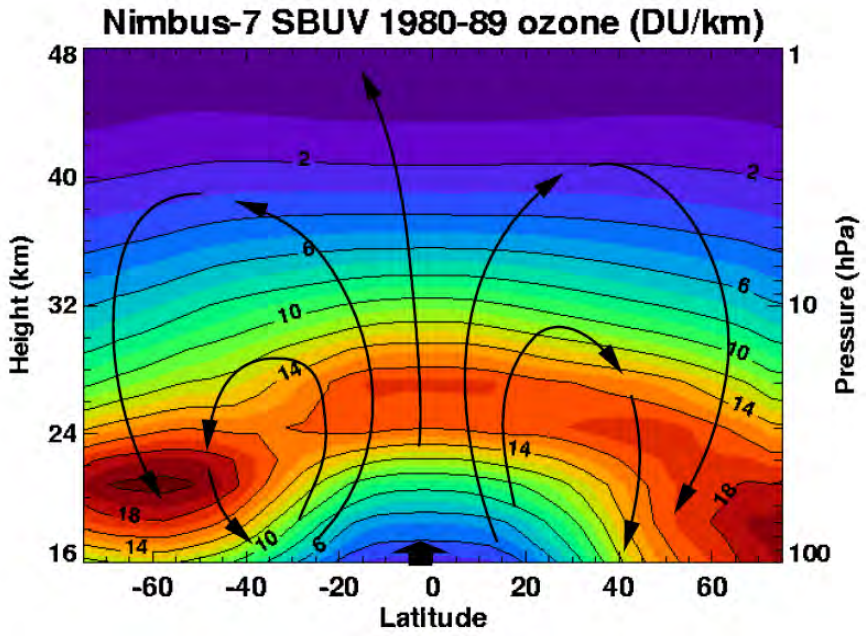

Figure 3.5 Average number density of ozone (DU per km) as measured by the Nimbus-7 Solar Backscatter ultraviolet Instrument (SBUV) plotted versus latitude and altitude, dataset from 1980-1989. The black arrows show the stratospheric Brewer – Dobson circulation. It is responsible for the observed equator-to-pole ozone distribution. The circulation varies by season and by hemisphere.
(http:// see.gsfc.nasa.gov/edu/SEES/strat/class/S_class.html).

3.4.3. Dependence of UV on Clouds

Clouds have more influence on surface UV irradiance than any other atmospheric variable. Although important, cloud effects on UV irradiance are difficult to quantify. The effect of clouds on UV is understood in principle. However, in practice the necessary parameters used to calculate the local cloud effects are rarely available, and if they were, the complexities of the cloud geometry need to be specified in sufficient detail and require the use of three-dimensional (3-D) model calculations.

Atmosphere is a dynamic system, and the local condition of turbulence, uplift and other parameters give rise to many types of clouds. Various types of clouds occur frequently enough to have acquired a name of their own; often these are further specified with additional descriptive name. Furthermore, some atmospheric processes can make the clouds organize in distinct pattern such as ‘wave cloud’ or ‘actino form cloud’, these are large-scale structures and not always readily identifiable from single point of view.

There are clouds whose horizontal dimensions are orders of magnitude greater than their vertical dimensions. These include Stratus (St), Stratocumulus (Sc), Nimbostratus (Ns), Altocumulus (Ac), Altostratus (As), and Cirrostratus (Cs), as well as Ns-As, As-Cs, and Ns-As-Cs frontal cloud systems. These types of clouds are called Stratiform Clouds. In contrast, there are clouds of vertical extent. These are clouds whose vertical dimension is greater than their horizontal dimension. Some of them include convective clouds of various depths: Cumulonimbus (Cb).

Under overcast conditions, clouds decrease the irradiance measured at the surface (Josefsson and Landelius, 2000; Renaud et al., 2000). However, enhancements of up to 25% can occur under broken cloud conditions (Sabburg and Wong, 2000), or if there are reflections from cloud decks below high-altitude observation sites such as Mauna Loa Observatory (Mckenzie et al., 2001b). Even for large cloud fractions, the reduction in irradiance can be small if the clouds do not obscure the direct beam. Thus, one of the most important parameters is whether the sun is obscured (Kerr et al., 2006). For individual sites, this poses difficulties for satellites products. Since the sun can be un-obscured even for large cloud fractions, or even obscured for small cloud fractions, the quantification of cloud effects can become problematic. The presence of scattered or broken clouds poses difficulties for comparisons between ground based measurements

and satellite estimates of surface UV irradiance. In this situation, direct solar radiation is either obscured or not obscured by a cloud at the ground-based measurement site, whereas the satellite measures an average cloud amount over its footprint.

Although in some cases high thin clouds may not be distinguishable in all-sky images, these continuous records of the spatial distribution of clouds used in parallel with UV irradiance measurements offer the potential to understand and quantify cloud effects more accurately.

3.4.4. Dependence of UV on Aerosol Scattering and Absorption

Aerosols are highly variable over space and time. They attenuate UV flux through the atmosphere to an extent that is mostly described by the aerosol optical depth (AOD) and the average column value of the single scattering albedo (ω_o), which is the ratio of scattering to extinction (where extinction = scattering + absorption). The wavelength dependence of the AOD is generally assumed proportional to λ-α, where λ is wavelength, and α is the Angstrom coefficient. The AOD in the UV was shown to be approximately inversely proportional to wavelength (i.e., $\alpha = 1.0 \pm 0.5$), and values of ω_0 between 0.84 and 0.98 were determined by comparing model results with the measurements (Kerr et al., 2006). Comparisons between satellite-derived and ground-based spectral measurements have revealed inconsistencies in satellite-derived UV that are probably related to the inability of the satellite sensors to correct for boundary layer extinctions. Ground based estimates of regional UV irradiances suffer from a similar inability to correct for horizontal inhomogenities in boundary layer extinction as well as inhomogenities in the troposphere and stratosphere. Only at the cleaner sites is there good agreement within the experimental errors. At continental sites in the Northern Hemisphere, the satellite-derived UV estimates are too large.

The radiative effect of aerosols is measured in terms of an aerosol index (AI) (Herman et al. and Torres et al) as presented by Joseph et al:

$$AI = -100 \log_{10}[(I_{\lambda 1} / I_{\lambda 2})_{meas.} - (I_{\lambda 1} / I_{\lambda 2})_{clac.}] \qquad (3.19)$$

where $I_{meas.}$ is the measured radiance at given wavelengths and $I_{calc.}$ is the calculated radiance at the wavelength using the radiative transfer model that assumes a pure gaseous atmosphere. The difference between the measured and calculated radiances is attributed to aerosols. Non-absorbing aerosols (e.g., sulfate aerosols and sea-salt particles) yield negative AI values. UV-absorbing aerosols (e.g., dust and smoke) yield positive AI values. Clouds yield near –zero values.

The vertical distribution of the aerosol particles is highly variable. The concentration generally decreases with altitude. Stratospheric aerosols, present in the lower stratosphere, are largely sulfuric acid solution droplets which are produced through photochemical reactions involving carbonyl sulfide (COS), sulfur dioxide (SO) and other gases. The stratospheric aerosols are perturbed by major volcanic eruptions which can inject significant amounts of SO and volcanic ash. The larger volcanic ash particles will settle out in a short period. However, the sulfuric acid aerosols, produced from the SO will persist for several years. Stratospheric aerosols have a small effect on the surface UV radiation. The influence may increase after a huge volcanic eruption like the eruption of Krakatau (1883), El Chichon (1982) or Mt. Pinatubo (1991).

3.4.5. Dependence of UV on Surface Albedo

The presence of snow cover surrounding an observing site increases UV irradiances. Information regarding the average albedo in the satellite field of view is important for space-based estimates of surface UV (Kerr et al., 2006). When snow depth information is used as input to estimate regional albedo, better agreement between ground-based measurements and satellite estimates is achieved, particularly under cloudy conditions (Kerr et al., 2006). However, day-to-day knowledge of regional albedo on a global scale remains a challenge combining measurements with RT model results can be used to derive estimates for unknown input parameters by statistical fitting procedures. When aerosol optical depth is relatively low (and thus the effect of inaccurately known optical characteristics of aerosols is small), regional albedo of partly snow covered terrain can be derived. Values of regional surface albedo in the range of 0.3 to 0.9 were determined, depending on local conditions of topography and snow coverage.

3.4.6. Dependence of UV on Altitude

In practice, the altitude dependence of UV irradiance is itself dependent on differences in surface albedo, boundary layer extinctions by aerosols, and tropospheric ozone concentrations. Even when these effects are ignored, it has been found that at higher altitude the dependence of UV irradiance on solar zenith angle (SZA) and wavelength changes. In general, for erythermally weighted UV, irradiances in clean conditions increase between % and 10% per kilometer (Kerr et al., 2006), with the greatest increase occurring at SZA $\sim 60^0 - 70^0$ is inevitable. In mountainous regions the vertical gradient in some instances can be larger (up to 50% per kilometer) because of local effects such as increasing albedo with altitude and high concentrations of ozone or aerosols in the lower troposphere (Kerr et al., 2006).

3.4.7. Angular Dependence of UV

Ground-based measurements of UV irradiance are generally made with a horizontal diffuse surface that would ideally follow a response proportional to the cosine of the angle from normal (vertical) incidence. In many cases the collection efficiency of the diffuser falls below the cosine function for large SZA, and calculations are made to adjust (usually increase) the measured irradiance (Kerr et al., 2006). The adjustments depend on the angular distribution of incident radiation and are complex functions of SZA, wavelength, total ozone, ozone distribution, aerosol and cloud amounts. The relationships of measured to adjusted values are corrected by use of RT models. For many biological and photochemical processes, actinic fluxes rather than cosine-weighted irradiances are more appropriate.

3.3.8. Dependence of UV under Water

The under water UV environment is an important consideration for studies of the sensitivities of aquatic (both fresh water and salt-water) species to UV radiation (de Mora et al., 2000).

Measurements show that there is wavelength-dependent absorption by water in the UV that increases with decreasing wavelength. The underwater absorption has strong dependence on the abundance of dissolved organic matter that has wide temporal and spatial variability. A sensitivity study conducted by RT modeling has shown that the main parameters controlling levels of the most harmful UV-B radiation under water for clear sky conditions are the SZA.

Attenuation of UV-B irradiance and DNA dose rate with water depth is primarily controlled by the total seawater absorption coefficient and its spectral dependence.
Absorption and scattering processes that occur within and on top of the ice reduce the transmission of UV radiation through sea ice. UV radiation is strongly absorbed by both colored dissolved organic matter and particulate organic matter, including ice algae.

3.5 Chapter Summary

An increase of solar spectral irradiance at the 11-year solar cycle activity since the year 1700 is recorded. 3.0% for wavelengths less than 300 nm and 1.3% for the band 300-400 nm. This past long term increase on solar UV-C radiation would lead to an increase in the production of stratospheric ozone that would reduce surface UV-B irradiance.
As radiation traverses the atmosphere, it encounters many complex scattering and absorption processes. For gaseous molecules, the scattering is for particle size 0.2λ in diameter. This is called Rayleigh scattering. UV radiation is scattered by such particles in the atmosphere. The scattering by aerosols in the atmosphere is due to Mie scattering in which unlike the Rayleigh scattering the particle size is greater than the wavelength of the incident radiation. Rayleigh scattering explains why the sky appears blue while the Mie scattering defines why clouds look white.

The fate of UV radiation depends on many determining factors like ozone, clouds, aerosols and climate change. The larger the amount of ozone in the atmosphere, the less the UV irradiance at the surface of the Earth. Due to the decrease in the amount of ozone in some parts of the world especially the high latitudes causes the increase in UV irradiance at the surface. Hence change in the life of people, animals and plants in such away as to adapt to the change in surface UVery. Clouds affect in such away that the

absorption and scattering by clouds depend on the cloud geometry. At overcast times clouds absorb and reflect back most part of incident radiation. Hence, the amount at the surface is reduced significantly. But at broken cloud times, it is studied that the amount of radiation at the surface increases. This geometry characteristic of clouds makes the UV study extremely difficult. But knowing the relation between clouds and types of clouds with surface erythemal UV could be important.

Aerosols affect the amount of surface radiation by absorbing and scattering. The absorbing aerosols reduce the amount of radiation at surface. The behavior of aerosols is difficult to estimate because of the dynamic nature of the atmosphere. Since the atmosphere is in continual motion one can guess but cannot determine where and how they affect the atmospheric processes.

The UV scattering albdo like ice and snow cover at a place also affects the amount of UV radiation at that location. Where there are snow or ice cover, it is obvious that the UV irradiance to some meters from the area increases. This is important in mountainous and polar areas.

The UV radiation underwater also decreases down depth. The deeper one goes the lesser erythemal UV he/she experiences. This is due to the scattering and absorption nature of the water solutes and solvents.

On remarkable point is, when the characteristics of all the determining factors are studies it is better also to know the atmospheric circulation, the lifetime of the particles in the air parcel, the formation and sink of the aerosols, and the influencing natural or anthropogenic factors.

Chapter Four

Data Types and Methods of Data Processing

In this section, data and methods used to attain the objectives laid down are discussed. In the first part, the data employed are explained and then the methods used are documented.

4.1 Datasets

Various data of satellite derived are used in this project; Total Ozone Mapping Spectrometer (TOMS) Nimbus 7, NOAA - 11, and NOAA - 16, among them. These are polar- orbiting Satellites launched by National Aeronautics and Space Administration (NASA) and National Oceanic and Atmospheric Administration (NOAA) in North America. Details of these sensors will be discussed in the sections ahead.

4.1.1 UV, Ozone and Aerosol Index data

The data used in this thesis project for the analysis of UV, ozone and aerosol index is taken from the Total Ozone Mapping Spectrometer (TOMS) on board Nimbus 7 spectrometer from NASA Goddard Space Flight Center and Earth Probe TOMS (EEPTOMS). These data are incorporated in to the International Research Institute (IRI) dataset. The Solar Backscattered Ultraviolet (SBUV) / TOMS vertical ozone profile aboard the Nimbus7, and NOAA - 11 and NOAA - 16 satellites is obtained from National Oceanic and Atmospheric Administration (NOAA). The data TOMS/Nimbus 7 and TOMS/ EPTOMS (Earth Probe Total Ozone Mapping Spectrometer) are available in both latitude and longitude in spatial and temporal values in the year from Jan 1979 to Dec 2003 on monthly and daily basis for the analyses of total column ozone, UV index, and aerosol index.

The vertical distribution of ozone is analyzed for ten years, the first five years from 1981 to 1985 and the second five years for the period 1999 to 2003. The former is

obtained from Nimbus 7 SBUV; the others are derived from NOAA - 11(1999 to 2000) and NOAA - 16 (2001 to 2003) satellites. The five years period are chosen deliberately based on trend analyses. This is to see the vertical ozone distribution in this range, increasing or decreasing.

4.1.1.2 TOMS Algorithm and Theoretical Background

TOMS measures total integrated ozone globally on a daily basis as well as monitoring smoke from biomass burning, desert dust and other aerosols, and sulfur dioxide and ash from volcanic eruptions. The first TOMS instrument was placed in orbit in 1978 aboard Nimbus 7, and TOMS continued to make measurements aboard Earth Probe since its successful launch in 1996. The measurements taken are processed by the National Aeronautics and Space Administration (NASA), and archived at the Goddard Space Flight Center (GSFC).

The satellite was orbiting at an altitude of 740 km, has an inclination of 98.385 degrees, a period of 99.675 minutes, and a field of view (FOV) at nadir of 39 km latitude x 39 km longitude. Its orbit allows for 90% daily global coverage. TOMS measures total column ozone on the principle of backscattered ultraviolet solar radiation. The satellite uses a single mono-chromator, with six exit slits at wavelengths of 308.60 nm, 313.50 nm, 317.50 nm, 322.30 nm, 331.20 nm, 360.440 nm, and scanning mirror to measure the radiance along a 35 point path at 3 degree intervals along a line perpendicular to the orbital plane, taking no measurements on the retrace and pausing for 8 seconds before starting another scan. Total ozone is derived from a normalized radiance, which is the ratio between backscattered Earth radiance and the incident solar irradiance.

4.1.1.3 Theoretical Basis of TOMS Data

To interpret the radiance measurements made by TOMS instrument requires an understanding of how the Earth’s atmosphere scatters ultraviolet radiation as a function of solar zenith angle. Incoming solar radiation undergoes absorption and scattering in the

atmosphere by atmospheric constituents such as ozone and aerosols and by Raylegh scattering. Radiation that penetrates to the troposphere is scattered by clouds and aerosols, and radiation that reaches the ground is scattered by surfaces of widely varying reflectivity. The basis for this discussion is section 2.3 where the radiative transfer theory was presented. Here a modification for the TOMS instrument is exposed.

The backscattered radiance at a given wavelength depends, in principle, upon the entire ozone profile from the top of the atmosphere to the surface. The three shortest wavelengths used in the TOMS ozone measurements were selected because they are strongly absorbed by ozone.

At all of the TOMS wavelengths, the backscattered radiance consists primarily of solar radiation that penetrates the stratosphere and is reflected back by the dense tropospheric air, clouds, and the Earth's surface. Primarily the total optical depth above the scattering layer in the troposphere determines the intensity. The amount of ozone below the scattering layer is small and can be estimated with sufficient accuracy to permit derivation of total column ozone. Because most of the ozone is in the stratosphere, the principal effect of atmospheric ozone at these wavelengths is to attenuate both the solar flux going to the troposphere and the component reflected back to the satellite.

The backscattered radiance emerging from the top of the atmosphere as seen by TOMS instrument, I_{m} is the sum of purely atmospheric backscatter I_{a}, and reflection of the incident radiation from the reflecting surface $\mathrm{I_s}$,

$$I_m(\lambda,\theta,\theta_o,\Omega,\mathrm{P}_0,R) = I_a(\lambda,\theta,\theta_0\phi,\Omega,\mathrm{P}_0) + I_s(\lambda,\theta,\theta_0,\phi,\Omega,\mathrm{P}_0,R) \tag{4.1}$$

Where λ = wavelength,

θ = Satellite zenith angle, as seen from the ground,

θ_0 = Solar zenith angle,

ϕ = azimuth angle,

Ω = Column ozone amount (DU),

P_0= Pressure at the reflecting surface, and

R = effective reflectivity at the reflecting surface.

The surface reflection term can be expressed as follows,

$$I_s(\lambda,\theta,\theta_0,\Omega,P_0,R)=\frac{RT(\lambda,\theta,\theta_0,\Omega,P_0)}{1-R_{sb}(\lambda,\Omega,P_0)} \quad \text{and} \quad (4.2)$$

$$T(\lambda,\theta,\theta_0,\Omega,P_0)=I_d(\lambda,\theta,\theta_0,\Omega,P_0)f(\lambda,\theta,\Omega,P_0)$$

Where S_b = fraction of radiance reflected from the surface that atmosphere reflects back to surface,

I_d = total amount of direct and diffuse radiation reaching surface at P_0,

F= fraction of radiation reflected toward satellite in direction θ that reaches satellite. The denominator of equation 4.2 accounts for multiple reflections between the ground and the atmosphere.

4.1.1.4 Data for the Vertical Distribution of ozone

The vertical ozone-mixing ratio used in this thesis is obtained from National Oceanic and Atmospheric Administration (NOAA). National Aeronautics and Space Administration (NASA) and NOAA prepare the data jointly. FORTRAN code is used to read the data for the respective latitude and longitude in Africa.

4.1.1.4.1 Backscatter Ultraviolet/ Total Ozone Mapping Spectrometer

Initial space borne ozone (O_3) observations started with the BUV (Backscatter Ultraviolet) sensor, a demonstration instrument flown on Nimbus 4 of NASA (launched April 8, 1970; sun synchronous near circular polar orbit, perigee = 1092 km, apogee = 1108, inclination = 80.1^0, period = 107.2 minutes). The sensor mass was 14.5 kg, and the

power was 7W.

The instrument consisted of a double mono-chromator containing all reflective optics and a photomultiplier detector. The double mono-chromator was composed of two Ebert-Fastie type mono-chromators in tandem. Each mono-chromator has a 52 mm x 52 mm grating with 2400 lines per mm. Light from a 0.05 sr. solid angle (subtending approximately a 222 km^2 area on the ground) entered the nadir pointing instrument through a depolarizing filter. A motor driven cam step rotated the gratings to monitor the intensity of 12 ozone absorption wavelengths. The detector was a photo multiplier tube.

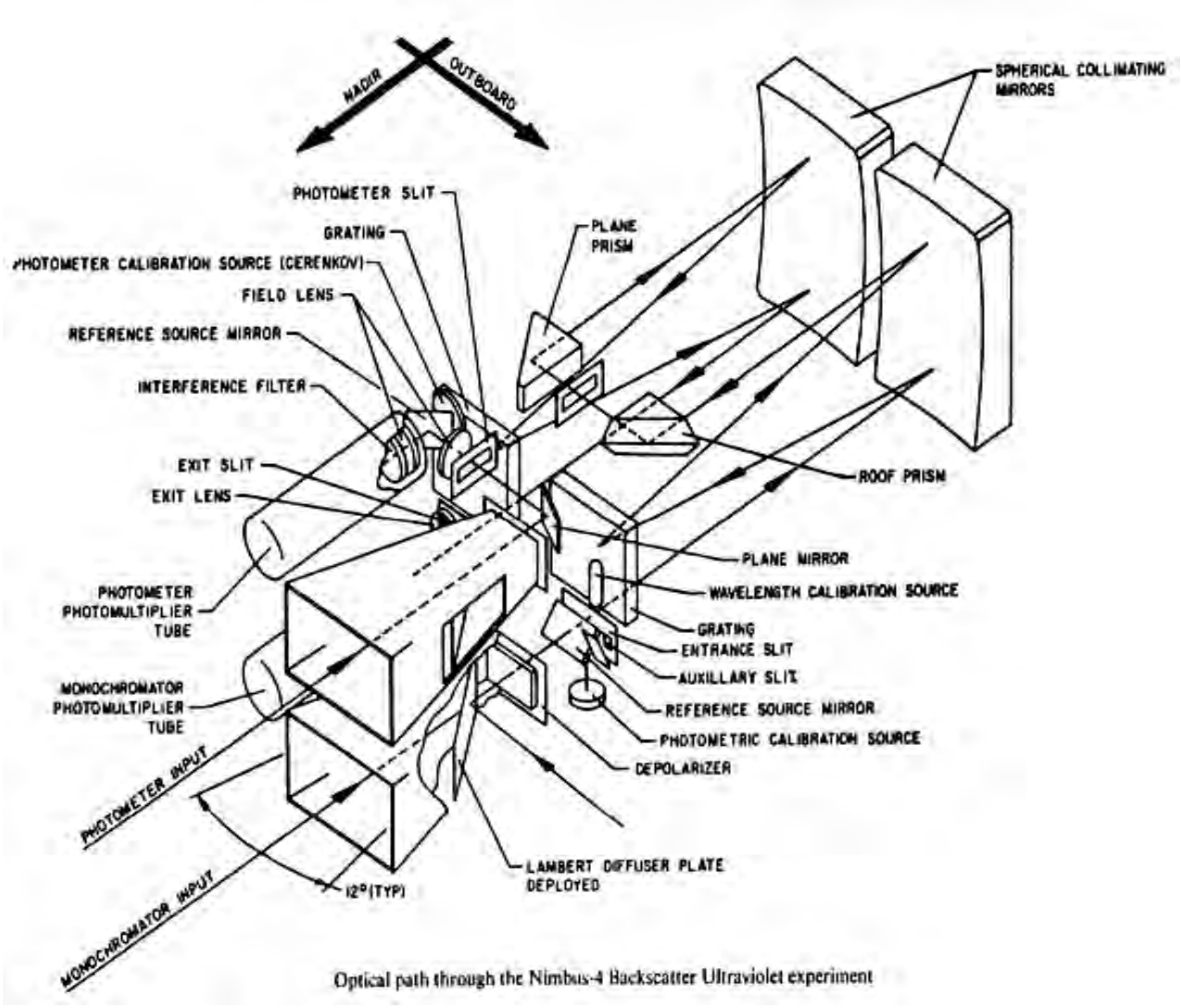

Figure 4.1: The BUV (Backscatter Ultraviolet) optics layout (Heath D.F. et al).

4.1.1.4.2 Solar Backscatter Ultraviolet/ Total Ozone Mapping Spectrometer

The mass of the instrument was 20 kg; power of the instrument was 20W. The data bit rate was 4 Kbit/sec. The main objectives of the instrument were to measure the vertical ozone profile, total column ozone amounts of atmospheric ozone, solar irradiance, and terrestrial radiances.

SBUV was a double Ebert-Fastie spectrometer and filter photometer, similar to the BUV used three detectors: a photomultiplier tube (PMT) and a photodiode for the monochromator; and one photometer for the photometer. Both the monochromator and the photometer have chopper wheels operating at 25 Hz. The SBUV used a depolarizer to eliminate the sensitivity of the grating monochromator to polarization of the backscattered radiation. The instrument's field of view (FOV) at nadir was 0.20 rad. A roughened aluminum diffuser plate viewed the sun for solar spectral irradiance by viewing a mercury-argon lamp. In one mode, SBUV serially monitored 12 selected narrow wavelength bands in the spectral region from 0.250, 0.340 μm.

The remarkable point here is SBUV instrument differs from the TOMS instrument in that the TOMS is a scanning radiometer which measure UV radiation at 6 distinct wavelengths. The TOMS can provide global coverage of the sunlight portion of the earth. The SBUV does not scan. Instead, it only looks down in the nadir direction. However, it measures UV radiation at twelve (12) variable wavelengths (See Figure 4.2). This allows for not only the determination of total ozone concentrations at various altitudes throughout the stratosphere.

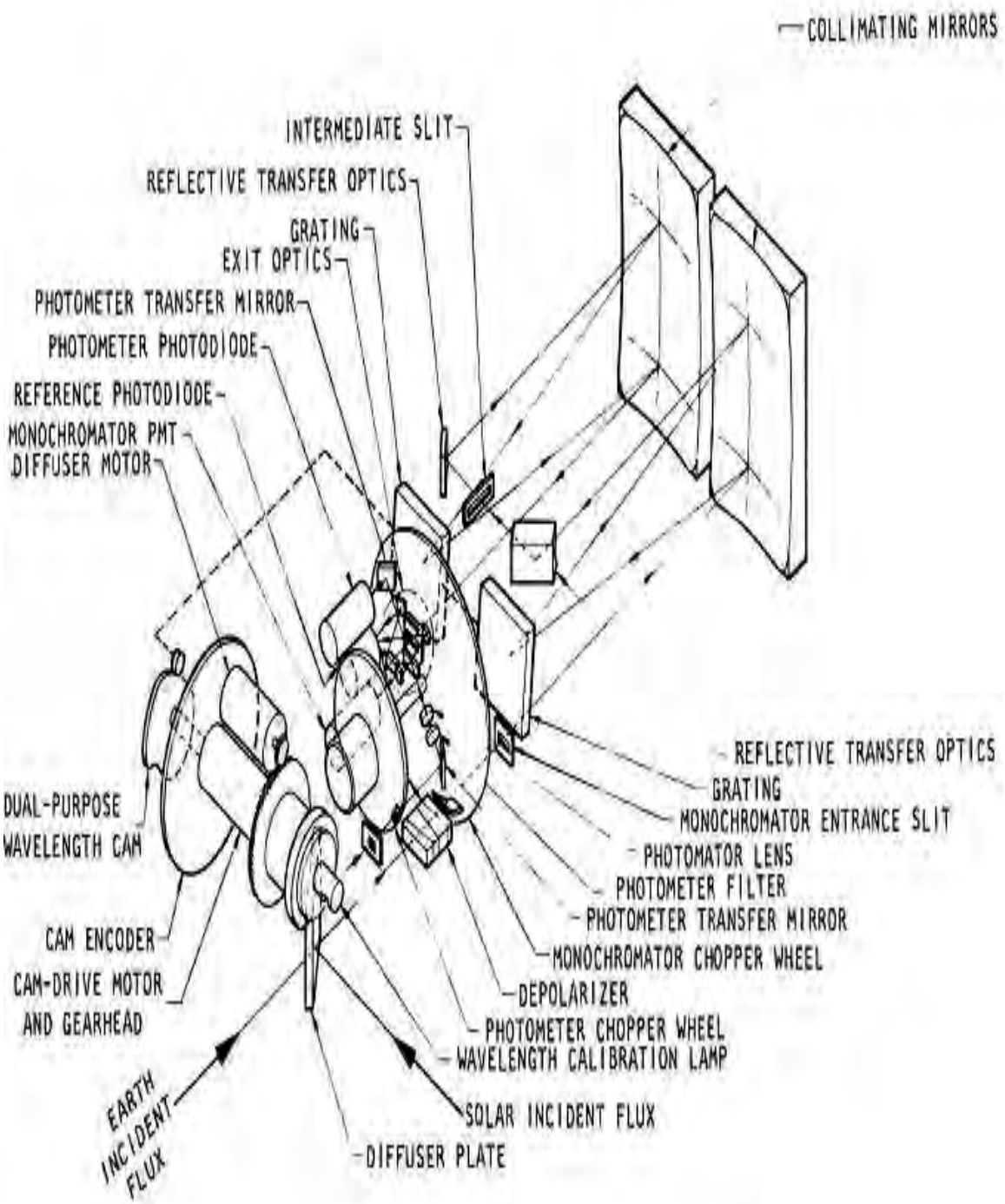

Figure 4.2 Optics of the TOMS instrument on board the Nimbus 7 (Heath D.F. et al.).

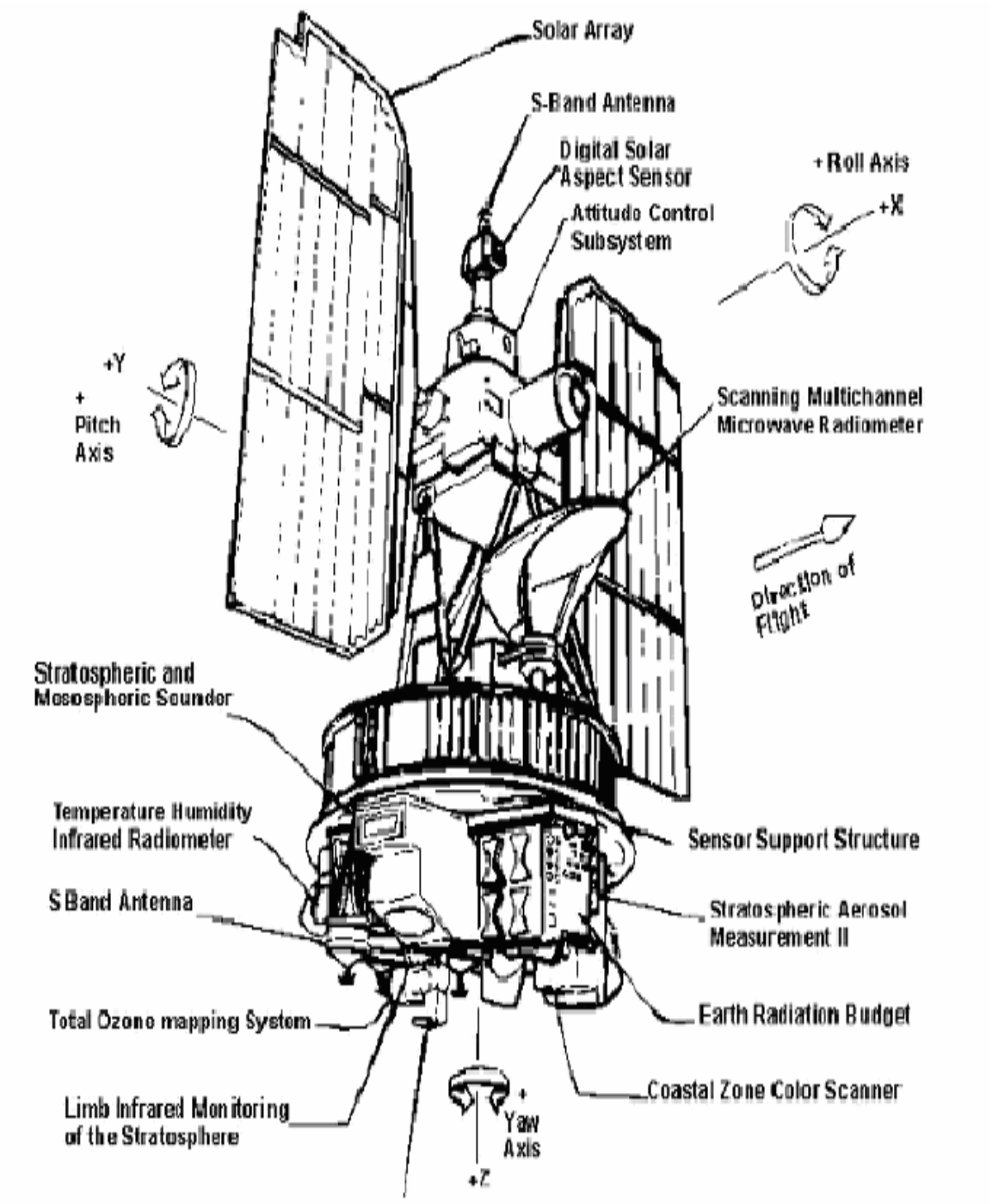

Figure 4.3 The Nimbus 7 Observatory.

(http://www.TOMS_sensors\Nimbus-7 Observatory.html.)

4.1.2 Cloud data

Cloud data is available from the International Satellite Cloud Climatology Project (ISCCP) from 1984 to 2001. This data is extracted and the singular value decomposition is applied. The interpolation of this data with the UV irradiance data is investigated.

4.2 Methods

The data analysis consists of Singular Value Decomposition (SVD), Regression and correlation analyses and variance analysis.

Since we have long-term data as is mentioned in the data part above, it is important to apply the SVD analyses. Singular value decomposition (SVD) is quite possibly the most widely used multivariate statistical technique used in the atmospheric sciences. The technique was first introduced to meteorology in a 1956 paper by Edward Lorenz, in which he referred to the process as empirical orthogonal function (EOF) analysis. Today, it is also commonly known as principal-component analysis (PCA).

Before going to details of the use of the SVD, it is better to present the techniques and theorem of SVD. Let A be an m x n data matrix, where m>n. Then A can be decomposed as follows:

$$A=UWV^T \qquad (4.3)$$

where U is an m x n orthonormal matrix: $UU^T = I_m$, W is an n x n diagonal matrix.

$$W = \begin{bmatrix} w_1 & 0 & \dots & 0 \\ 0 & w_2 & \dots & 0 \\ \dots & \dots & \dots & \dots \\ 0 & 0 & 0 & w_n \end{bmatrix} \qquad (4.4)$$

and V is an n x n orthonormal matrix: $UU^T = I_n$. The diagonal elements of W are called the singular values. I will refer to the singular value decomposition exists always and is unique up to 1) Same permutations in columns of U, W and V. 2) Linear combinations of columns of U and V with equal singular values.

If X is a matrix X_{ij} will represent the elements in the I^{th} row, J^{th} column, and X_j will represent the J^{th} column vector. Note $A_{ij} = \sum_{k=1}^{n} w_{kk} U_{i,k} V_{i,k}$. Thus, we can approximate A well by deleting columns of U and V with small singular values.

The variance matrix is

$$C_x = AA^1 \qquad (4.5)$$

We can then rewrite the variance matrix as C_x as $Cov = AA^1 = UWV^TVWU^T = UW^2U^T$. Thus U columns of U are the eigenvectors and hence the temporal values of Cx and the squared singular values are the eigenvalues of C_x. The spatial variability over a space is computed using the function

$$X = R \cos d \qquad (4.6)$$

Where $R = \sqrt{(x^2 + y^2)}$, here Y represents the longitude and X represents the latitude, d is the angle the line from the origin to the point forms with the latitude. This function is used to get the spatial modes of the variabilities of UV, aerosols, ozone and clouds. This method is applied on the data matrix stated as in the following.

The UV, aerosol index (AI), and total column ozone data are placed in such away as the first column is the time in months since 1979 to 1992 (Nimbus 7 data) and from 1997 to 2003 (EPTOMS data), the second column is latitude, the third longitude, the fourth column consists of column ozone, then erythermal UV (UVery), and aerosol index in each of the last columns. We filtered out only the latitudes and longitudes that incorporate Africa and its coastal regions (20W to 90E latitudes and 40S to 40N longitudes).

The purpose of singular value decomposition is to reduce a dataset containing a large number of values to a dataset containing significantly fewer values, but which still contains a large fraction of the variability present in the original data. The dependence of UV radiation with the other parameters often exhibit large spatial correlations. SVD analysis results in a more compact representation of these correlations, especially with

multivariate datasets and can provide insight into spatial and temporal variations exhibited in the fields of data being analyzed.

The first structure is the single pattern that represents the most variance in the data. The structures are the elements of the eigenvectors of the variance-covariance matrix of the data. The first eigenvector (EOF) points to the direction in which the data vectors jointly exhibit the most variability. Essentially, a new coordinate system is created, with each axis aligned along the direction of maximum joint variability.

The second structure is the pattern that describes the second largest amount of variance, calculated the same way as the first structure. A very important property of the second structure is that it is completely uncorrelated with the first structure, as well as all other following structures. The second eigenvector is perpendicular to the first eigenvector, which is perpendicular to the third eigenvector and so on. This property is what led Lorenz to call the technique empirical orthogonal function analysis. All structures are mutually uncorrelated.

The variance of the nth principal component is the nth eigenvalue. Therefore, the total variation exhibited by the data is equal to the sum of all eigenvalues. Eigenvalues are normalized such that the sum of all eigenvalues equals 1. A normalized eigenvalue will indicate the percentage of total variance explained by its corresponding structure. Structures have also been normalized so that the root mean square equals 1. This way, the structures can be expressed in terms of standard deviation. Singular values are equal to the square root of the eigenvalues. Since eigenvalues are automatically normalized in the Data Library, they do not easily provide information into the total amount of variance they explain. However, you may calculate the total variance explained by each EOF by squaring the singular values.

There is a time series associated with each structure. These time series are also known as principal components. The first time series is calculated by projecting the data matrix onto the first eigenvector of the variance-covariance matrix of the data, the second time series by projecting onto the second eigenvector, and so on. The time series values indicate the amount of the given structure needed to complete the data field. It follows that the structure (dimensionless) multiplied by the time series value at a single point in

time (units of the data), summed over all structures, and yields the original data at that point in time.

Mathematically, there are as many eigenvectors as there are elements in the vector data set. The first few eigenvectors will point in directions where the data jointly exhibits large variation. The remaining eigenvectors will point to directions where the data jointly exhibits less variation. For this reason, it is often possible to capture most of the variation by considering only the first few eigenvectors. The remaining eigenvectors, along with their corresponding principal components, are truncated. The ability of SVD to eliminate a large proportion of the data is a primary reason for its use.

The regression analysis is employed to incorporate the dependence of UV radiation on aerosol, cloud cover, altitude, ozone, and other trace gases. It will be used to get the relation (correlation) amid the UV as a medium and the other dependencies.

The interpretation of the analyzed data will be followed. Comparisons are also made with the work of other countries based on the available literature review. The results of the above methodologies are retrieved both in spatial and temporal values in time and space.

4.3 Chapter Summary

Various data of polar orbiting satellites are used. The TOMS/ Nimbus 7, TOMS/ EPTOM, NOAA-11 and NOAA-16 satellites data are used to achieve the result in this thesis.

Data analyses methods of different kind have also been used. The Empirical- Orthogonal-Function (EOF), which points to the data with the highest variance, contained in the total long-term data. The first few spatial structures only are enough to show the total variability of the data.

Chapter Five

Results and Discussion

In this section, the dose of the erythemal UV (UVery) in UV index (UVI) values will be calculated and the latitudinal dose comparison will also be made. Then the spatial and temporal characteristics of UV and independent variables that determine the surface UV will be presented. The seasonal variability of UVery, Ozone, and aerosols will be highlighted and physical association will be made. Finally, those clouds which have sufficient relationship will be sorted out of the 20 cloud types and 5 parameters (cloud amount, cloud optical thickness, cloud top temperature, cloud top pressure and cloud waterpath) each based on correlation and regression analysis. Then the contribution of all of the variables in this UVery on the surface of the earth will be documented. The overall work plan in this section is as shown in the diagram below (Figure 5.1).

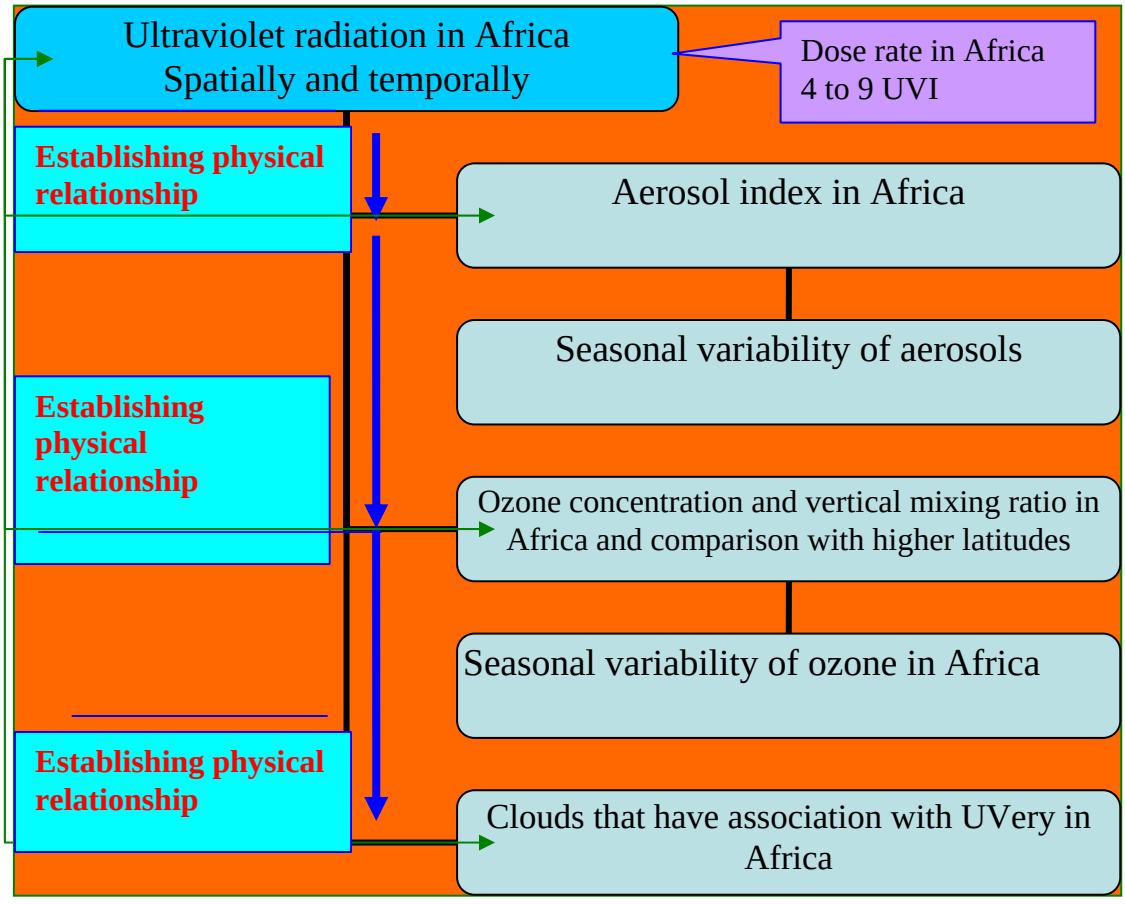

Figure 5.1: The overall outline of work plan of the results obtained and discussed.

5.1 Ultraviolet Radiation in Africa

As most parts of Africa are situated in tropical latitudes and deserts, it could be possible that the amount of UVI (skin burning) radiation could be greatest. Pertaining to the altitudinal dependence of UV radiation, those regions with high altitude within the continent receive higher amount of UV radiation during clear sky times. Around 18N latitude the maximum value of UV irradiance could be depicted (5500 J/m^2). Figure 5.2 shows the latitudinal variation of average UV irradiance in Africa for all of the months in a year at sea level. Here we can see that this integrated ultraviolet radiation over the biological action spectrum at the tropics is much greater than that of the high latitudes.

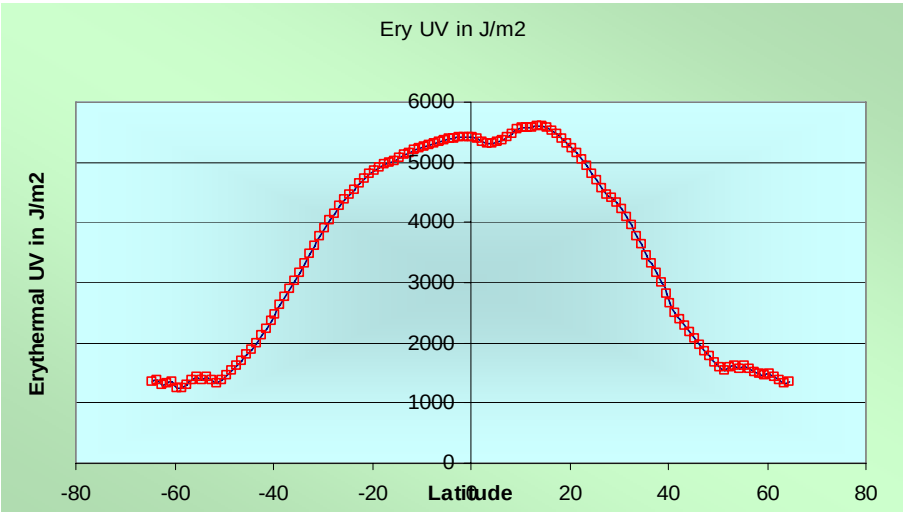

Figure 5.2 Latitudinal variability of average UV (J/m^2) TOMS/ Nimbus 7 (1979 – 1992).

This value of skin burning radiation can be changed in to the UV index (UVI). This is made changing the number to power per unit area which is called dose rate. Then multiplying the value obtained to 20 m^2/mW. Mind here that the value obtained is on average. But it varies from latitude to latitude. The dependence on altitude can be viewed in such away that those altitudinal countries get more UVI values than the lowland areas. To get exact values for a given location one could use this value and could do adjustment

to sea level. The possible range of values of UVI in Africa is between 4 and 9. This index number is rated according to its action on plants and animals called action spectra.

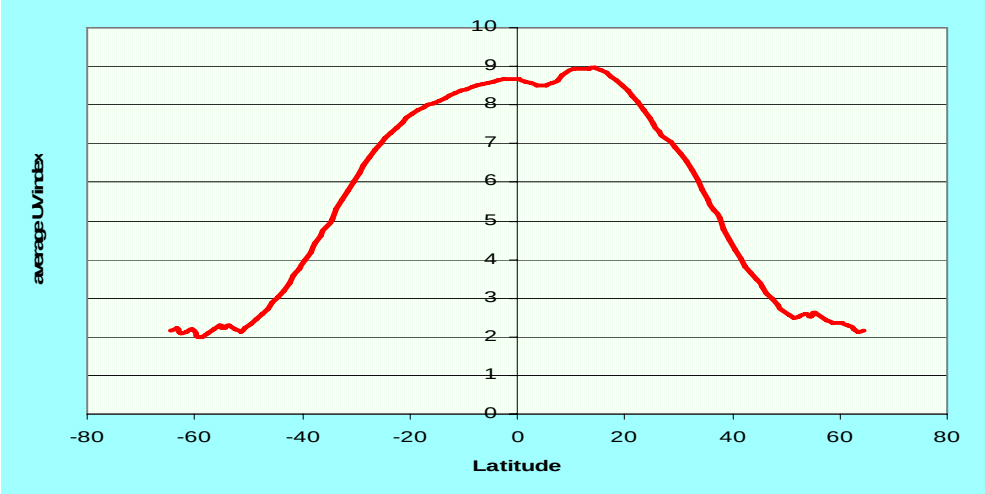

Figure 5.3 Latitudinal variation of UV index (UVI) from TOMS/Nimbus 7 data (1979 – 1992).

The UV index over different countries varies. For example, the UV exposure categories over America, Canada and WHO is compared as shown in Figure 5.4. Based on this Figure the value of UVI in Africa is moderate to very high according to the WHO standard.

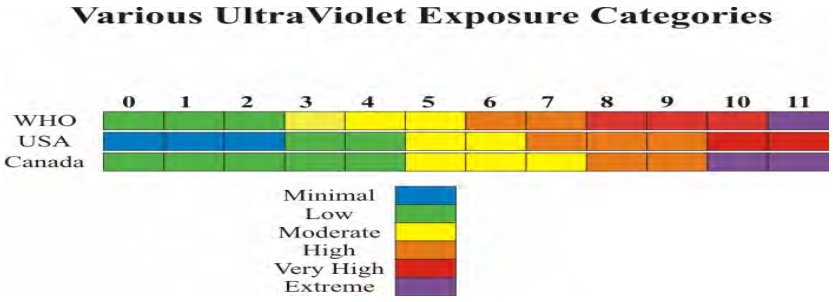

Figure 5.4 Différent ultraviolet exposure categories. The values are different in different countries as compared to the WHO category[1].

[1]Taken from National Oceanic and Atmospheric Administration (NOAA), National Weather Service, and National Center for Environmental Prediction, Climate Prediction Center. Craig S.Long, National Oceanic and Atmospheric Administration(NOAA).

5.2 Temporal and Spatial Results

The SVD function computes the singular value decomposition of the datasets weighted over the cosine of the latitude. Often, spatial data will be weighted over the cosine of the latitude to account for area changes between meridians at varying latitudes. A weight term, however, is not necessary to complete the SVD analysis. Other variables also exist in conjunction with the weight function. Some of which are structures, eigenvalues, and time series. All of which give useful information about the data.

The eigenvalues associated with the first few eigenvectors are much larger than the eigenvalues associated with subsequent eigenvectors. The first few eigenvalues account for most of the variation present in the original data.

5.2 The Spatial and Temporal Results of UV, AI and Ozone over Africa

In this section, the spatial and temporal values of UV, aerosols and ozone will be investigated. The seasonal variability also is shown.

5.2.1 TOMS/ Nimbus 7 and EPTOMS UV analysis

From the principal component analysis (PCA), the first normalized eigenvalue represents 0.193, the second eigenvalue is 0.091, the third 0.061, and the fourth normalized eigenvalue represents 0.049. Recall that normalized eigenvalues represent the fraction of variance explained by the structure associated with that eigenvalue. Therefore, the first structure explains 19% of the variance, the second structure 9%, and so on. Looking at the eigenvalue table, there are 84 structures. Yet, the first four structures alone account for over 39% of the variance.

The first structure that explains 15% of the total variance can be seen divided in to two oppositely varied parts (see Figure 5.5: a), structure 1). The region around the equator (10N to 10S, Figure 5.5: a), structure 1; marked region 2) is the most energetic part (positive). This indicates that the maximum amount of UV irradiance is concentrated around the equatorial region. In contrast, the first region (the region around 20N to 35N,

Figure 5.5: a), region marked as 1) is in the negative spatial region. This implies that the region gets the minimum amount of energy of ultraviolet compared to the equator.

In addition, the central and southern parts experience more amount of erythemal ultraviolet radiation than the Northern part of Africa. The cause of the variation is due partly to the all year round overhead ultraviolet rays coming from the sun and the northern hemisphere is more prone to absorbing aerosols due to the Sahel dust, sand and salt aerosols.

The second structure, which explains about 7% of the total variation, also shows more or less the same pattern as the first structure; but a certain drift to the west of the second region around the equator. The reason for UV radiation being highest at the equator is the overhead sun rays cover small spatial area and go very small distance through the atmosphere. The third and the fourth structures are different from the first two structures. This is attributable to the positive values around the southwestern and southern tips and the negative values around east coast, especially the negative region of the Indian Ocean (see Figure 5.5: a), structures 3 and 4).

The reason for this is the clouds of the Indian Ocean carried by the westerly winds and its influence in the east coast of Africa. This could be shown in the cloud part where much of clouds coming from the Indian Ocean carried by winds can easily be understood from the spatial distribution of the clouds. See Figures of the clouds in section 5.3.

The temporal characteristics of UV show two distinct characteristics. As can be seen from the respective spatial modes, the UV has shown a slight trend decline from the years 1979 to 1992 (see Figures 5.5, b). The years from 1997 to 2003, on contrary, are the periods in which the erythemal UV is increasing slightly (see Figure 5.5: c).

The reason why UV irradiance has shown a decrease in the period from 1979 to 1992 is ozone has shown an increase in this same period (see Figures 5.8 b, and 5.9: a). In the second period, (1997 to 2003) UV has shown an increase due to the slightly normal nature of ozone trend in the period given (see Figure 5.8: c and 5.10: b). Ozone on the

one hand is produced from the ultraviolet radiation (the cause here is UV and the effect is ozone production as stated in section 3.4.1.1), on the other hand ozone absorbs the UV radiation and is wavelength dependent as explained in section 2.2. This absorption of UV by ozone results in the decrease in the surface UV irradiance. Ozone reemits the absorbed UV as thermal long wave radiation, much the same as the surface of the earth does to the visible light. This is the main temperature source which heats the stratosphere. It is due to the existence of ozone in the stratosphere that the temperature of the stratosphere is varied from the troposphere and hence the name stratosphere. The high correlations between the altitudes at which the ozone increases and the altitude at which temperature increases in the stratosphere is due to that behavior of ozone in which it changes the UV light spectrum to thermal long wave radiation.

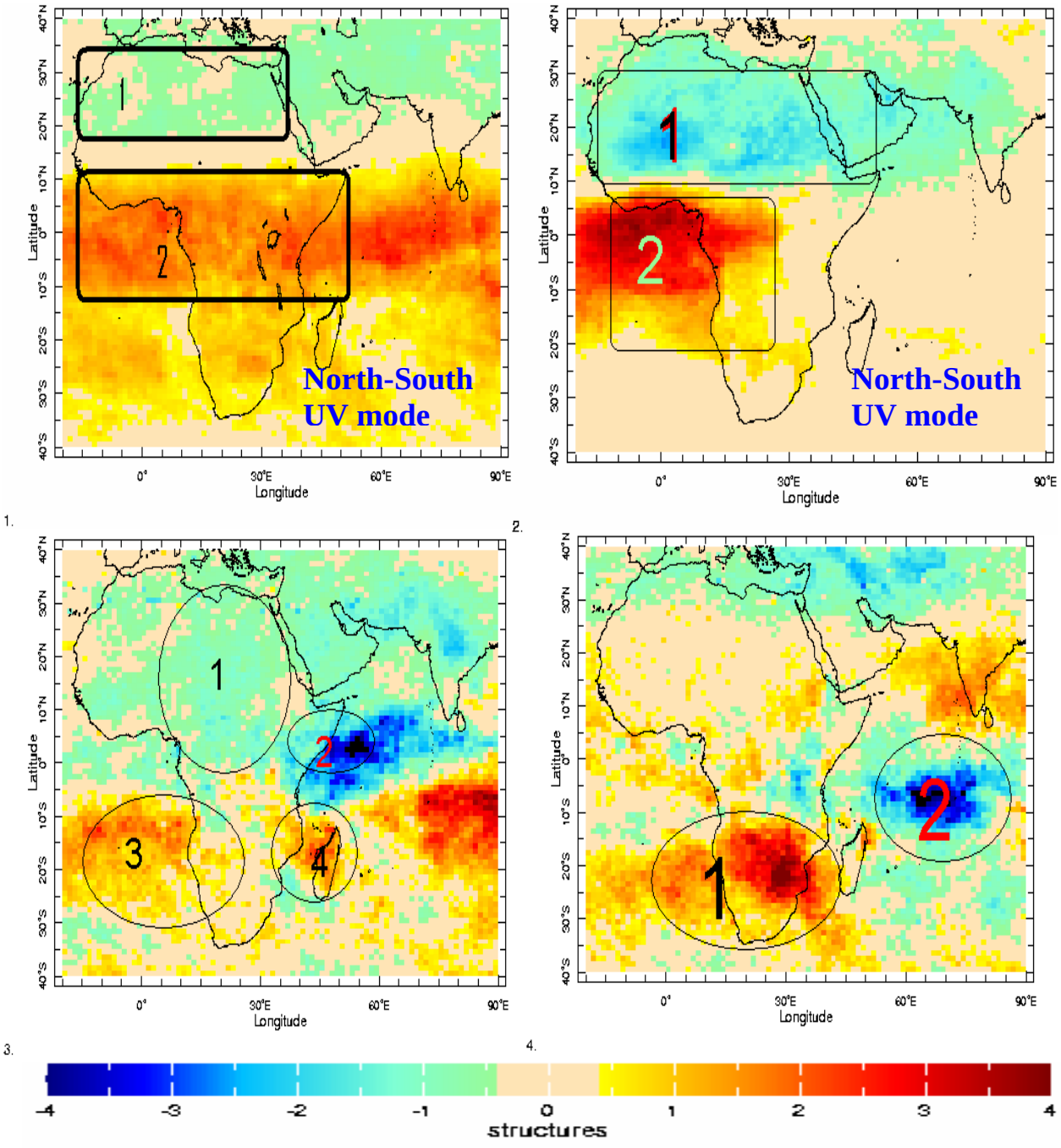

Figure 5.5: a) The spatial results of UV ery over Africa Continent. Some regions are marked for explanation. The four maps show the four structures in their respective order.

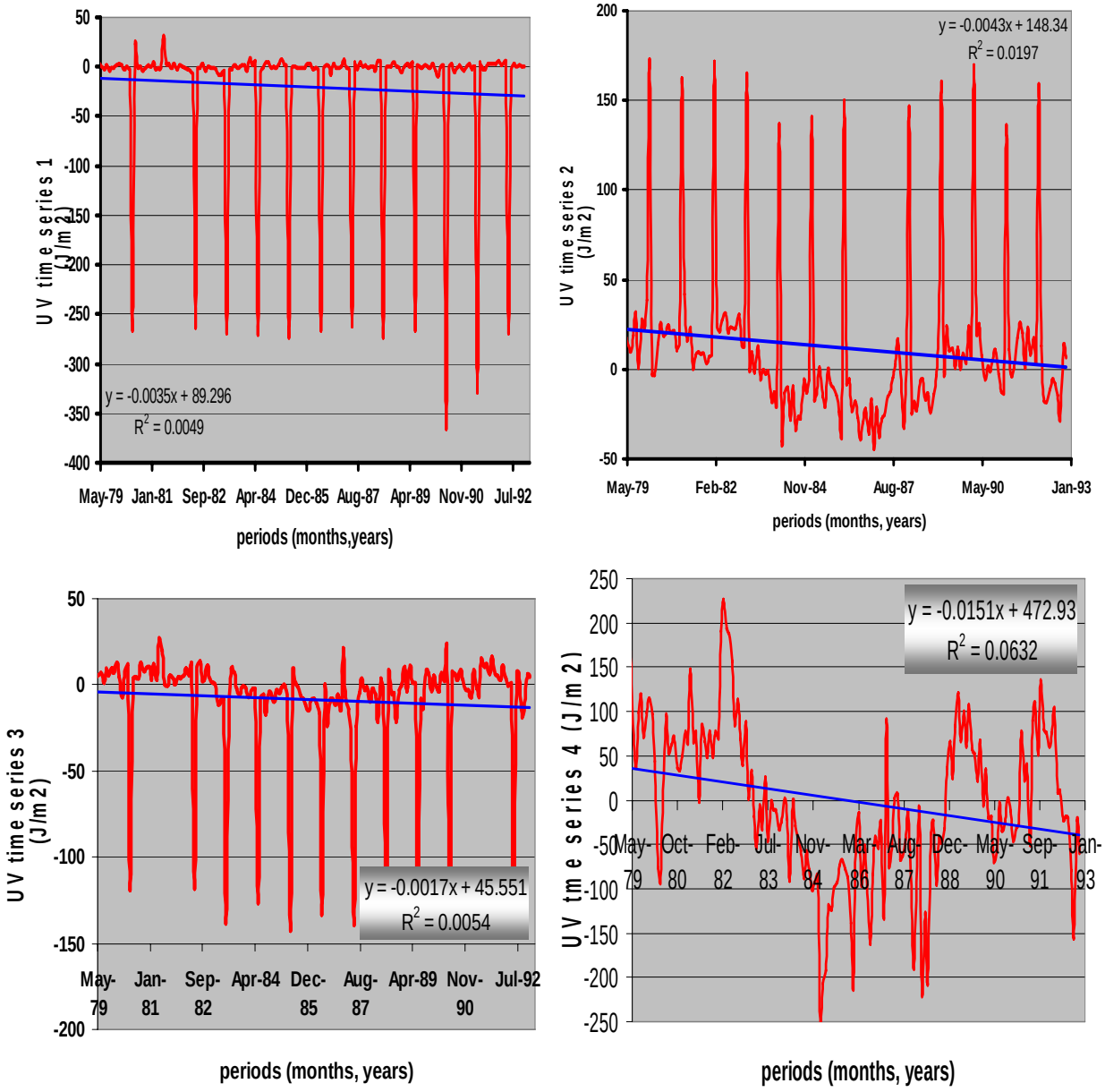

Figure 5.5: b) The corresponding time series of UVery irradiance for spatial structure 1 (Nimbus 7, 1979 to 1992).

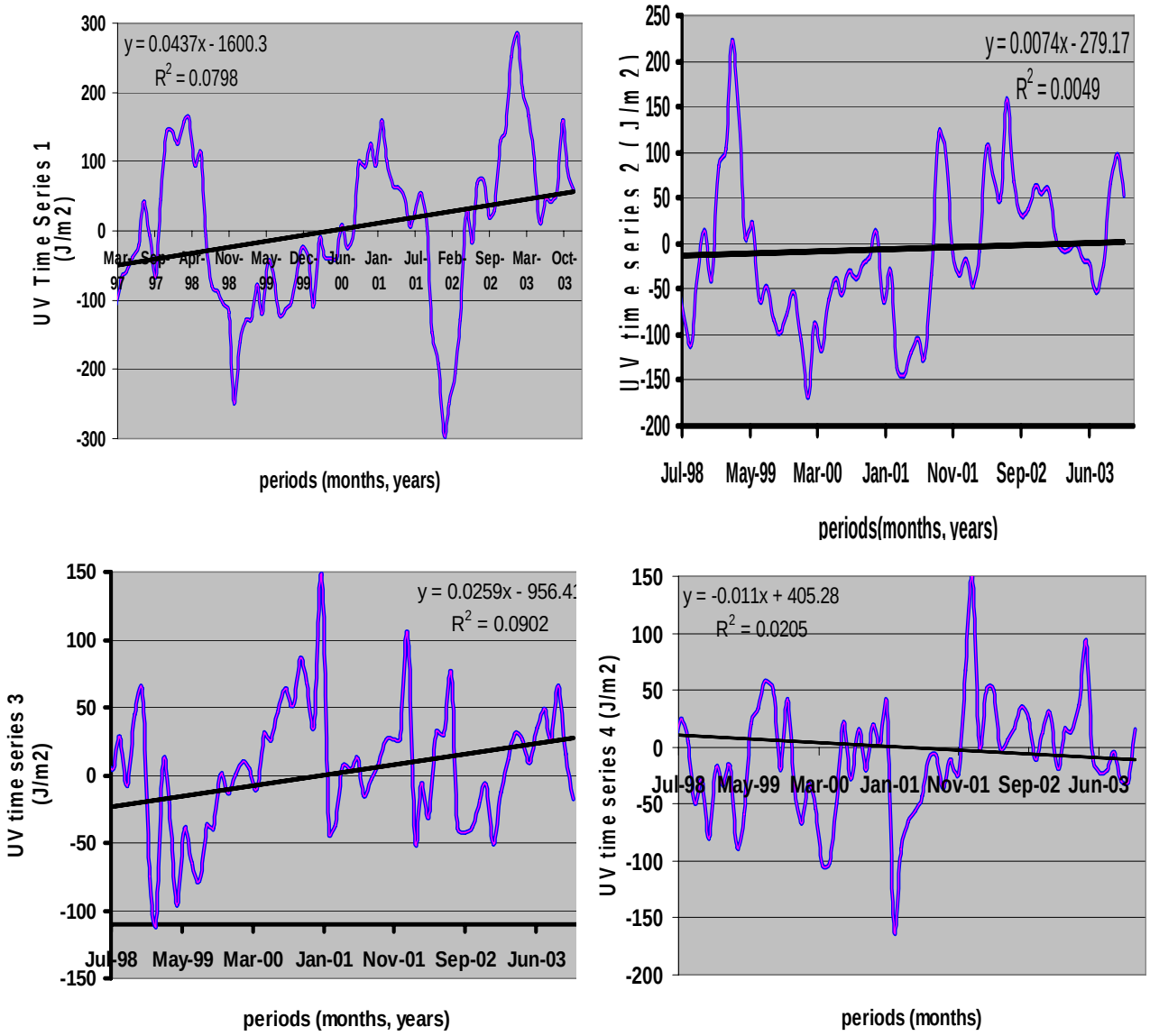

Figure 5.5: c) The temporal mode of the first structure of UVery from 1997 to 2003 using TOMS/ EPTOMS.

5.2.1 Seasonal Distinction of UV in Africa

The sun burning UV in Africa is relatively decreasing significantly during the JJAS (June, July, August, and September) (see Figure 5.6: a). The linear line fit for this season explains 66%. In all of the seasons from 1980 to 1992 based on TOMS/Nimbus7 data, the

UVery shows decreasing. The Earth Probe Total Ozone Mapping Spectrometer (EPTOMS) data, on the other hand, shows an increase of UVery in the same season. For an illustration look at the Figure 5.6: b.

The result of the decrease in UV radiation in the period shown is due to the increase in ozone (see Figure 5.10, a). Remember that ozone absorbs UV radiation and decreases the surface irradiance. The ozone variability in season shows highest in boreal winter season ONDJ (October, November, December, and January) and lowest in boreal summer season JJAS but in all of the seasons it is increasing.

However, the increasing of UV radiation in the year 1997 to 2002 can be explained as ozone in the same period has shown a slight drop though in increasing order (Figure 5.10, b). The other phenomena associated to an increase in surface UV is the abrupt drop in the amount of aerosol index in Africa (see Figure 5.8 b). UV-absorbing aerosols contribute to the surface UV radiation decrease on the surface of the earth as they absorb and scatter the incident light.

The other variable responsible for the increase in recent UV radiation is the decrease in the cloud (altocumulus cloud top temperature) (see Figure 5.26). The line fit for the trend of this cloud has shown 47% percent decreasing.

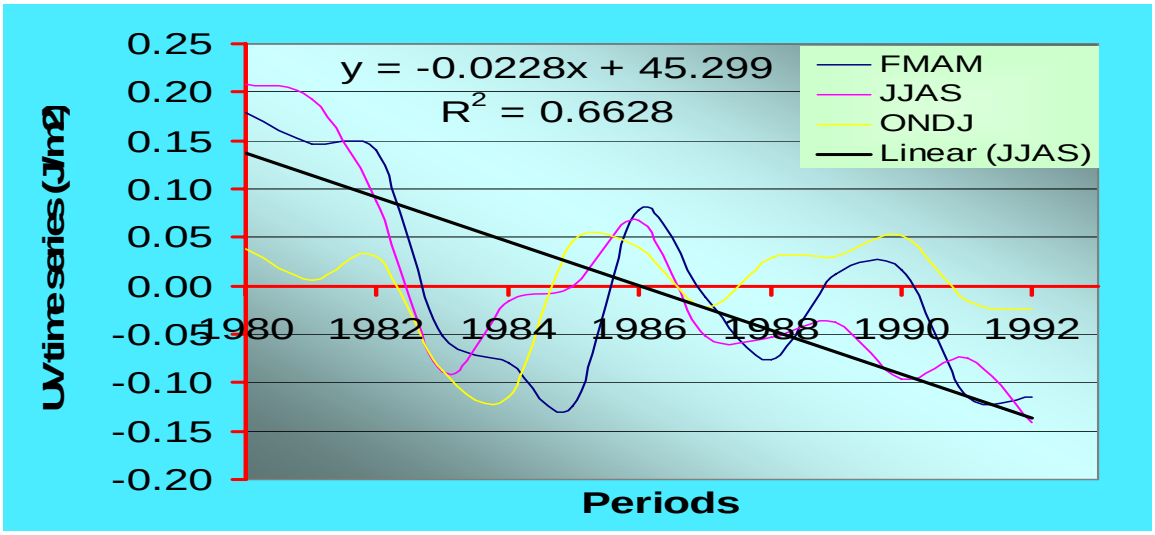

Figure 5.6: a) Seasonal variability of erythemal UV values in Africa. The trend shows 66% decrease during JJAS (boreal summer season). This is based on TOMS/Nimbus7 data (1980-1992).

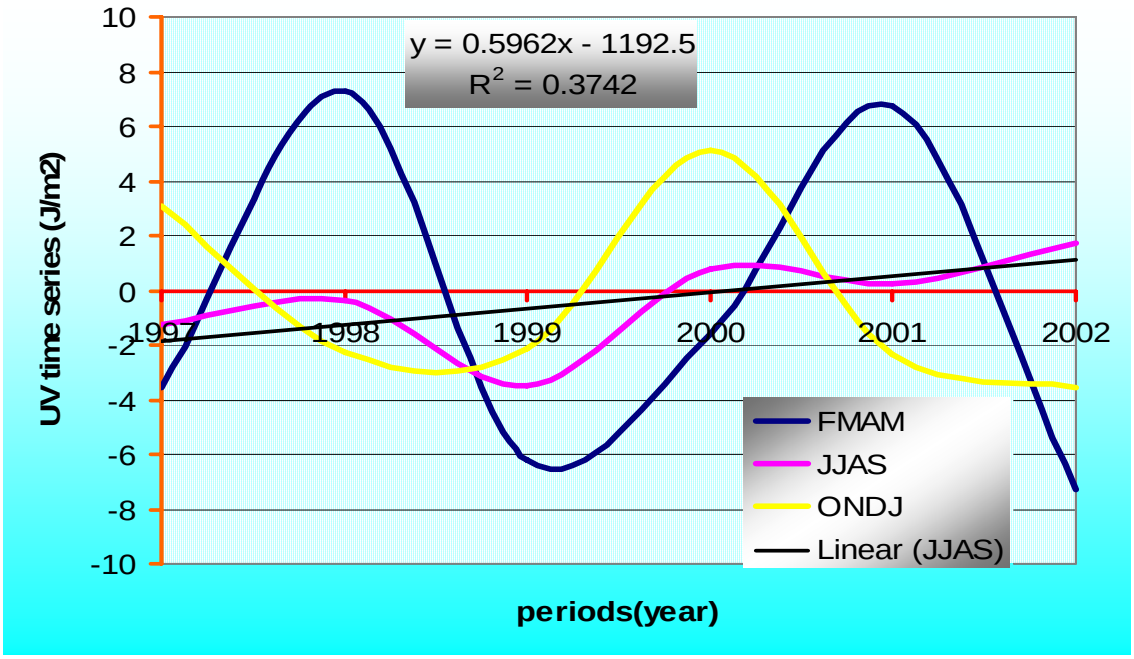

Figure 5.6: b) Seasonal distinction of erythemal UV values in Africa. The trend shows 37% increase during JJAS (boreal summer season). This is based on TOMS/EPTOMS data (1997-2002).

5.2.2 TOMS/Nimbus 7 and EPTOMS Aerosol Index analysis

Here the first normalized eigenvalue represents 28% of the total variance, the second represents 10%, the third 7% and the fourth eigenvalue represents 5%. In general, the first four represent a little over 50%. Hence, the first four normalized eigenvalues alone are enough to explain the total variability of the whole data.

The first structure which accounts for the 28% of the variance shows the highly negative value in the Northern part of Africa. The negative spatial value is due to the non-absorbing aerosols or hardly any aerosols in that particular region. As discussed in section 3.2.4 the non-absorbing aerosols are sea salt aerosols and sulfate particles. This aerosol seams to cover Tunisia, North-east Algeria, and eastern Libyan Desert. According to M. Prospero Joseph et al., the greatest dust activity takes place near an extensive system of salt lakes and dry lakes found in the lowlands south of the Tell Atlas. The most intense and persistent activity occurs in the region immediately to the south of the salt lakes (called “chotts” here). The dusty region extends to the south and southeast, down to

~30N, abutting the Atlas Mountains to the West, Maps show many ephemeral drainage channels from the Atlas to the lowlands to the east.

The second structure can be seen divided in to two regions, the central west coast which is highly positive region (10S to 10N, Figure 5.7: a), marked region 2) and the Northern negative region (10N to 35N, Figure 5.7: a), marked region 1).

The negative region (10N to 35N, Figure 5.7: a), marked region 1) has the same reason as for the structure 1. As explained above, Tunisia and Northeastern parts of Algeria are the sources of salt aerosols.

The positive AI values are due to the absorbing aerosols. These are the aerosols which absorb UV radiation. The positive spatial variation region (10S to 10N, Figure 5.7: a), marked region 2) shows absorbing aerosols. These aerosols are the aerosols from the lowest part of the Kalahari Desert. Dust activity is centered over the western end of the Makgadikgadi (foremerly Makarikari) Depression, a region of sandy alkaline clay pans located southwest of the Okavango Delta, in the lowest part of the Kalahari desert, where a variety of lacustrine, fluvial, and Aeolian land forms are in close juxtaposition (Cooke and Verstappen, 1984), as referenced by M. Prospero Joseph et al.

The third structure, which explains 7% of the variance, can also be seen divided in to two regions. The negative region at the North Western part of Africa (Figure 5.7: a), structure 3, marked 1) and the South Western (Figure 5.7: a), structure 3, marked 4) and the Eastern parts of Africa (Figure 5.7: a), structure 3, marked 2, and 3), which shows a positive pattern.

The marked regions 1 and 4 are similar to the regions as explained in structures 1 and 2 above. However, the Easter parts (Figure 5.7: a), structure 3, marked regions 2 and 3) are aerosols from Egypt, eastern Libyan Desert, the Ethiopian Riftvally, and Djibouti. As discussed by M. Prospero Joseph et al. the eastern extreme of the dust source is located over the southwestern end of the Qattara Depression. The active region extends in a relatively narrow corridor to the southeast to 22 -23 N, 15 E, bounded on the west by the Al Haruj al-Aswad hill range (maximum altitude 1200 m) and the Jabal Bin Ghunaymah mountains and the Sarir Tibasti (Tibasti) highlands on the border with Chad.

The fourth structure has two distinct regions the North western (15N to 35N, structure 4, marked 1) and the South Western (3S to 15S, structure four, marked 3),

positive, and the Middle Western, negative, (0 to 15N, structure 4, marked 2) parts of Africa. (See figure 5.2. b). This structure is quite different from the other structures in that the other structures 1, 2, and 3 shows the opposite of the structure 4. Here the northern and southern tips show positive while the middle of Africa in the tropics is negative spatial aerosol distribution. Mind that this structure expresses only 5% of the total variability. This shows in most parts of Africa where there are non-absorbing aerosols there are also absorbing aerosols.

The first temporal structure (Figure 5.7: b), which accounts for 28 % of the total variability, shows a trend decline. The line fit for the same graph represents 22% trend decline. The second and the fourth temporal modes show no trend increase or decrease. While the third (Figure 5.7: b) shows 14% and 0.7% trend increase but this mode only accounts for 7% of the total modal variability. Hence, in general, due to the maximum variability expression of the first mode, the overall trend of aerosols in the year from 1979 to 1992 was decreasing and slightly decreasing from 1997 to 2003.

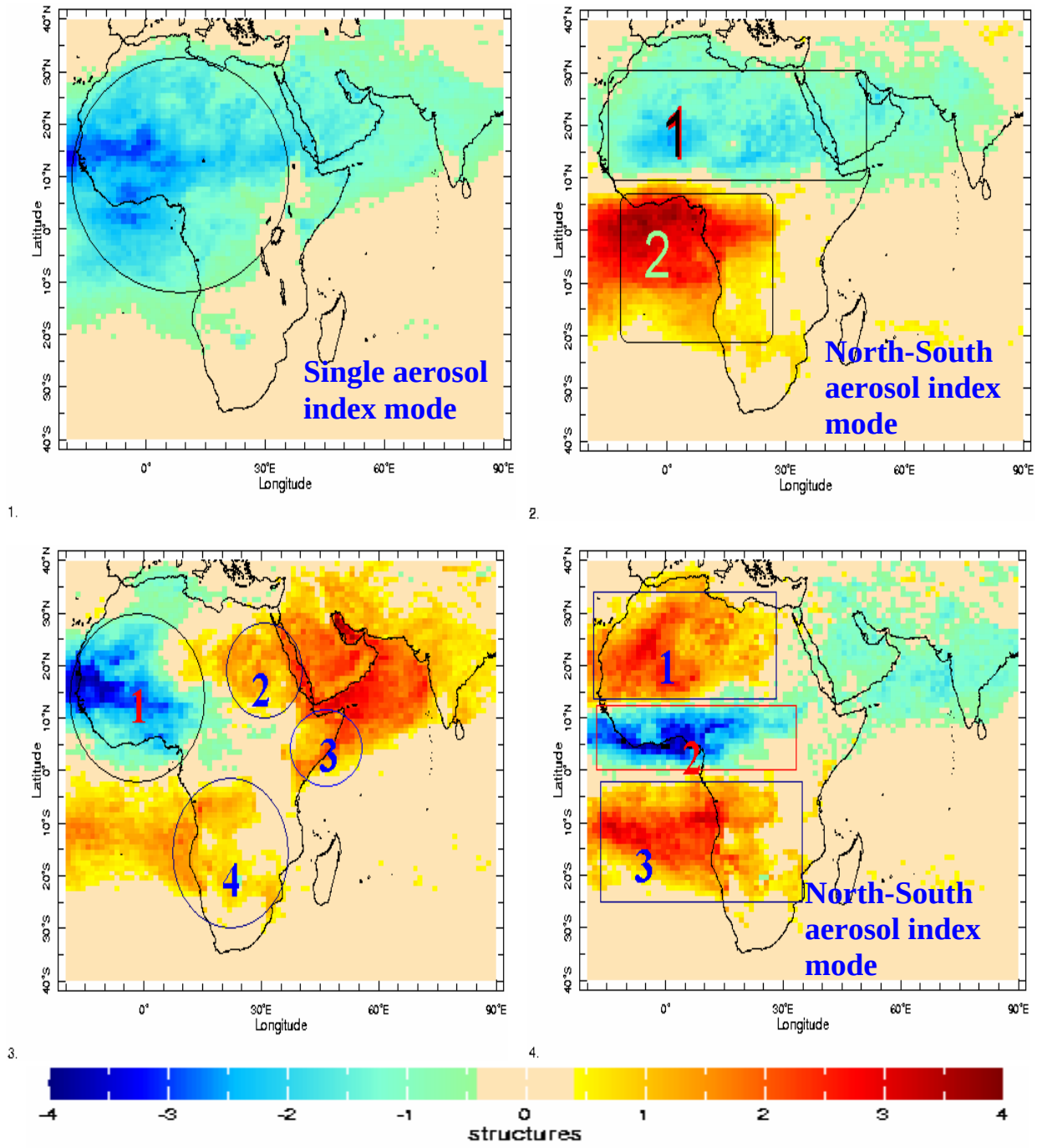

Figure 5.7: a): The spatial results of aerosol index over Africa. The marked regions are for explanation and show the negative and the positive variability of the data.

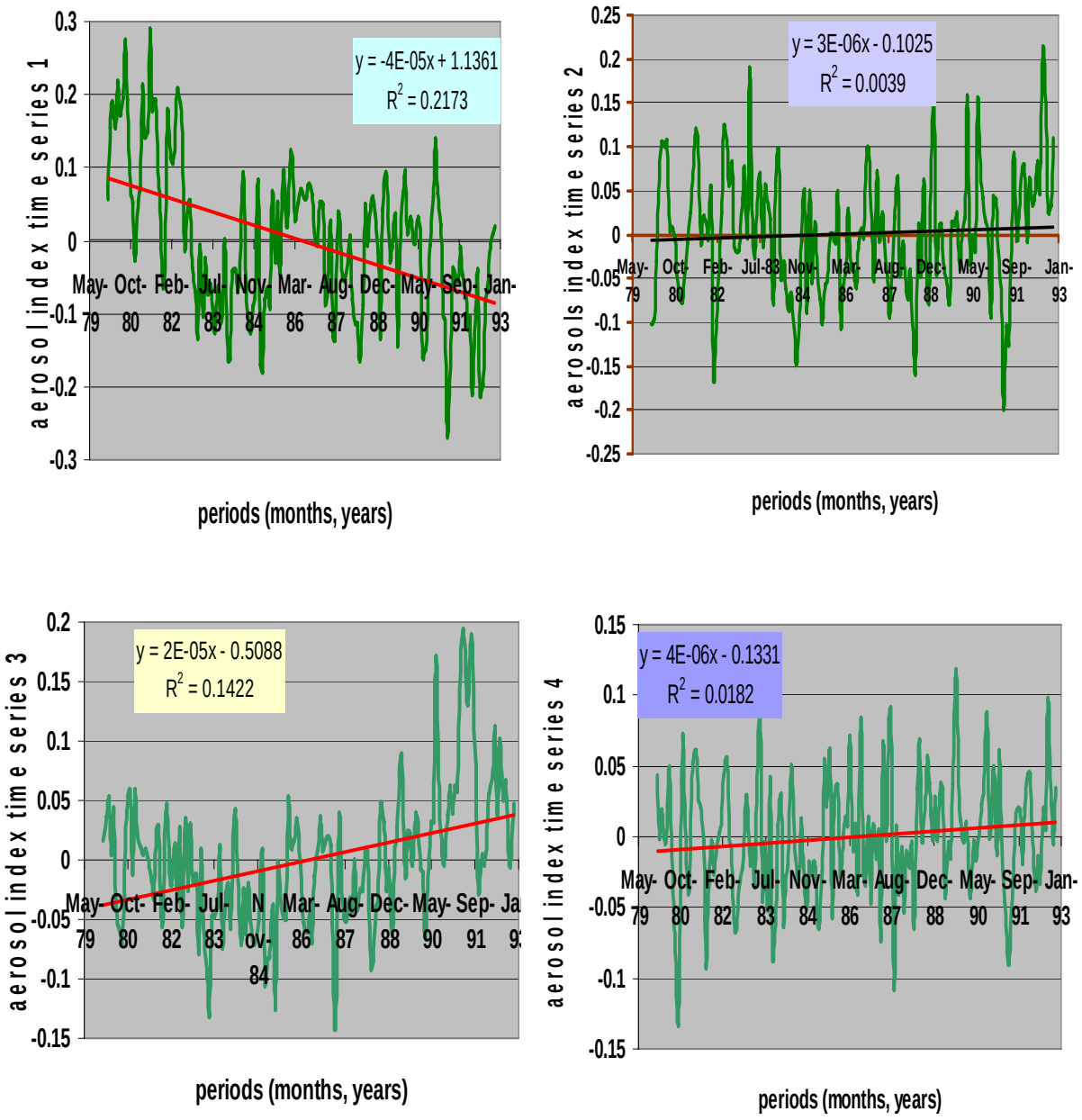

Figure 5.7: b) The temporal mode of the second eigenvalue of aerosol index based on TOMS/Nimbus 7 (1979 to 1992) data.

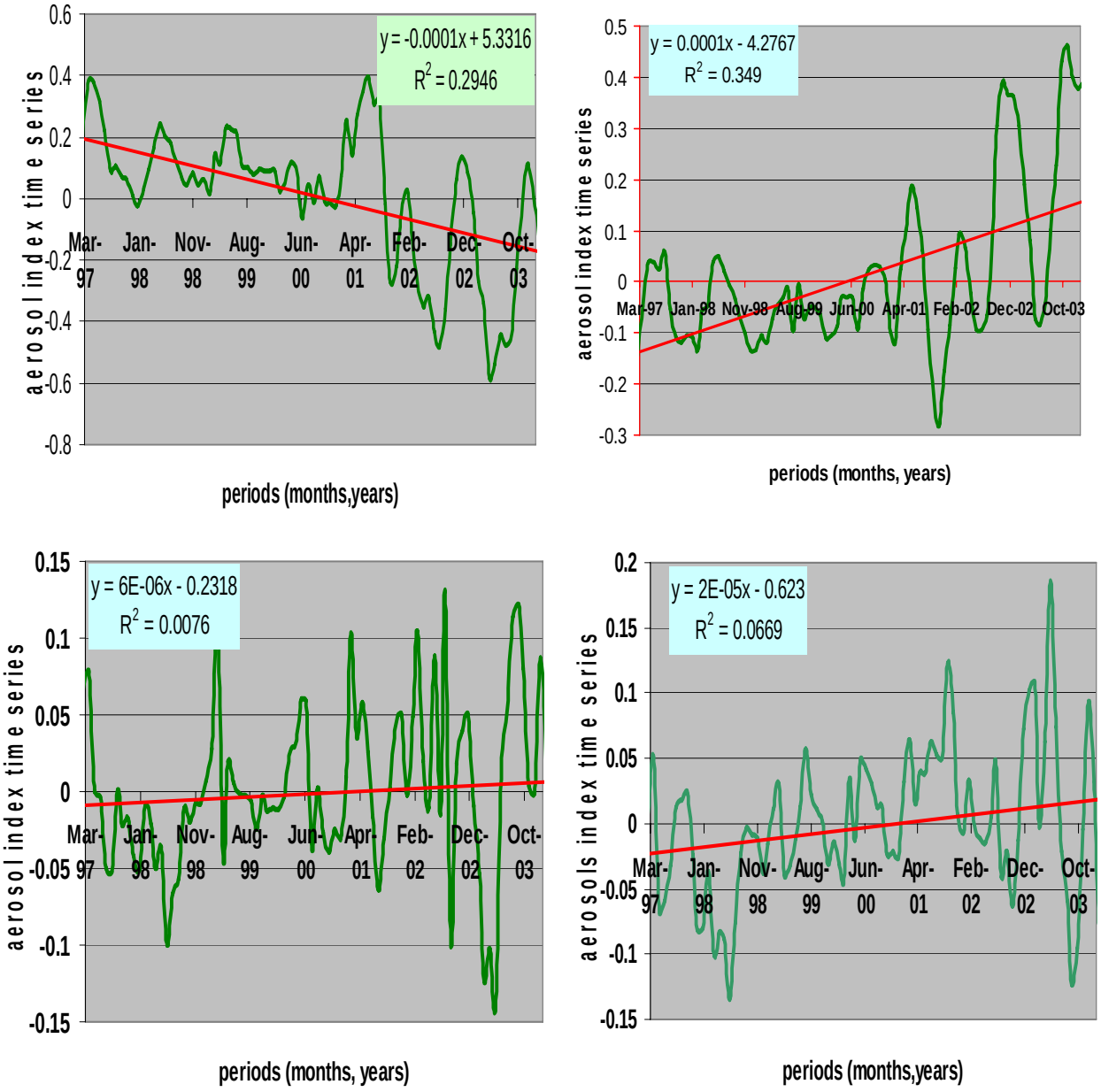

Figure 5.7: c) The temporal mode of the first eigenvalue of aerosol index based on TOMS/EPTOMS (1997 to 2003) data.

In summary, the aerosols from northern part and eastern parts of Africa are those aerosols which are UV-absorbing aerosols (e.g. dust and smoke) and non-absorbing like sulfate aerosols, salts, sands etc. On the other hand, the UV-absorbing aerosols (e.g. dust

and smoke) exist in greater strength in Middle Western parts of Africa. In southern Africa hardly the absorbing aerosols can be found.
In general, the northern hemisphere aerosol is greater than the southern hemisphere aerosols. The trend analyses shows aerosols in Africa are decreasing.

5.2.2.1 Seasonal variation of Aerosol Index over Africa

The TOMS aerosol index values declines in all of the seasons. The line fit shows 0.6628, which explains 66% of the data in the JJAS (boreal winter) using TOMS/Nimbus 7 (see Figure 5.8: a). The TOMS/EPTOMS data also shows a turn down of aerosol index in Africa from 1997 to 2004(see Figure 5.8: b). The line fit for the winter-Africa explains 47% of the aerosols declining. Here both polar orbiting satellites show a decline in aerosol index over Africa. This same value suggests there is certain features of the aerosol have changed.

Pertaining to the decline of the aerosols, the erythemal UV could also changes. This is discussed in section 3.4.4. Aerosols affect the amount of erythemal UV at ground in such away that they attenuate the incident radiation. This does imply simply as aerosols over a space declines the UV over that space increases and vise versa. From 1979 to 1992 the amount of UV over Africa does not show and icrease, it rather shows a decrease and a line fit to the down welling of the erythemal UV explains 66% of the winter season. The periods from 1997 to 2002, on the other hand shows an increase of the UVery in the same season. The line fit explains 37% of the total increasing pitch.

In general, aerosol index shows a decline trend, while UVery indicates a trend down for the first 14 years, while in slow increasing trend from 1997 to 2002. This shows the trend of aerosols is increasing in the future and hence decreases the amount of surface ultraviolet radiation in the Northern, western and eastern parts of Africa.

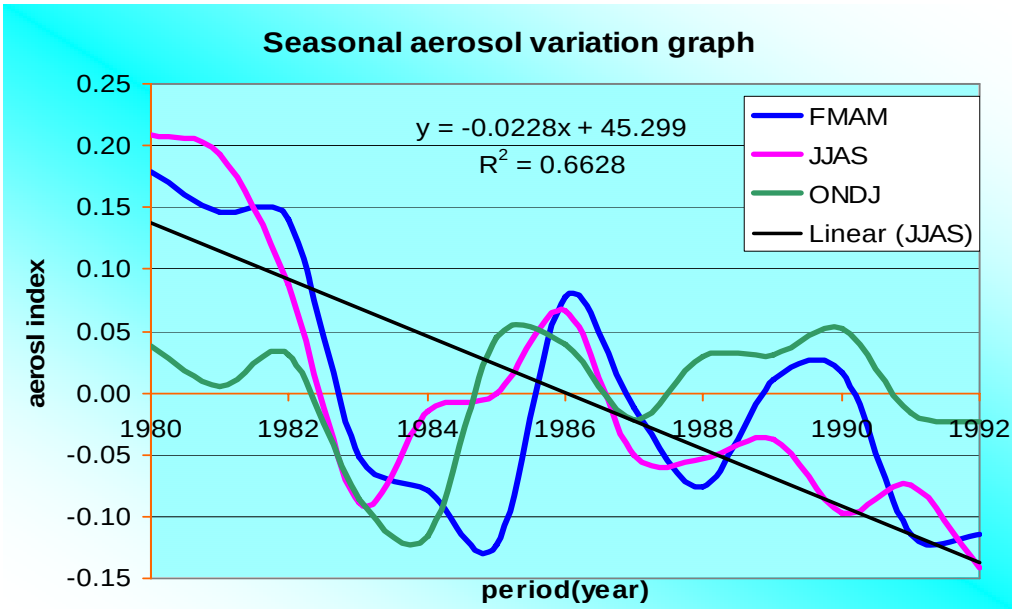

Figure 5.8: a) The seasonal variability of TOMS/ Nimbus 7 aerosol index in Africa (1980-1992).

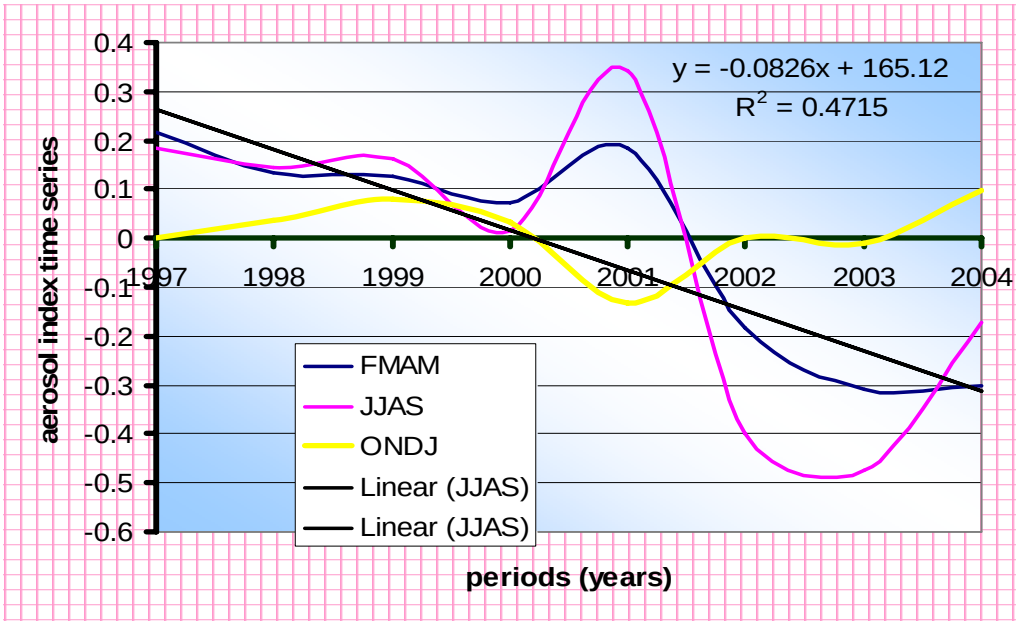

Figure 5.8: b) The seasonal variability of TOMS/EPTOMS aerosol index in Africa (1997-2004).

5.2.3 TOMS/NIMBUS 7 and EPTOMS Ozone Amount (DU) analysis

Structures pertaining to the ozone amount (DU) can be explained 30% by the first normalized eigenvalue, hence the first structure, 17% by the second eigenvalue (the second structure), 11% by the third normalized eigenvalue (the third structure) and 5% by the fourth normalized eigenvalue (the fourth structure). In general, the first four normalized eigenvalues represent 50% of the total variance in the total ozone amount (DU).

The first structure (Figure 5.9: a), structure 1) can be explained through three regions. The region showing positive variance (10S to 10N, Figure 5.9: a), structure 1, marked region 3) and the two negative regions (15N to 35N, Figure 5.9: a), structure 1, marked region1) and (15S to 40S, Figure 5.9: a), structure 1, marked region 5) show a marked difference.

The positive value in the equatorial region (10S to 10N) is due to the high production of ozone in the Equatorial region as a result of the high energetic value of ultraviolet radiation explained in section 5.4. From section 3.4.1.1, ozone production is based on the high energetic part of the electromagnetic radiation from the sun. In all the year round the Equatorial region gets overhead sunrays. This helps the production of ozone in the equator. The one unique feature of the equator is it is the region with high value of UV and ozone, both at same time. The notion, ozone is produced in the Equatorial region and transported to the mid and high latitudes is in this regard acceptable. We can also see the vertical distribution of ozone in this region for further explanation.

The second structure, which explains 17% of the variance, is divided in to two regions (Figure 5.9: a), structure 2). The first part is 7S to 35N latitude and shows negative variance, the second part 15S to 35S shows the positive variance (Figure 5.9:a), structure 2, marked as 1 and 3). This drift of ozone south of Africa is as a result of transport of ozone more due South than North. This may result because of the high aerosol concentration in the north than south as explained in section 5.2.2.

The third structure explains 11% of the total variability. One could see the positive region (Figure 5.9: a), 0S to 35S, structure 3, and marked region 2). This is a region, which has the highest ozone amount in cross section. The reason behind this is partly the Brewer-Dobson Circulation discussed in section 3.4.1.3.

The fourth structure, which explains 5% of the variability, shows a little concentrated ozone amount in the North West and northeast tips of Africa. The region marked 3, is the negative ozone region for this particular structure. This means the ozone production is irregular in amount. This is to mean that, at some unique spots the ozone amount is greater than at other spots. This is the reason why ground based observations are necessary to compare with the satellite observations.

Considering the temporal modes of ozone from 1979 to 1992, the first temporal mode (Figure 5.9: b) shows an increasing trend; while the other modes (Figure 5.9: c to e) show neither an increase nor a decrease. The temporal modes for the periods from 1997 to 2003 show two different trends. The first and third temporal modes (Figure 5.9: f and h) are an increasing mode while the second and fourth (Figure (5.9: g and i) slightly decreases. When we see the overall seasonal trend in section 5.2.3.1, ozone is increasing in Africa (see Figures 5.9: a) and b)).

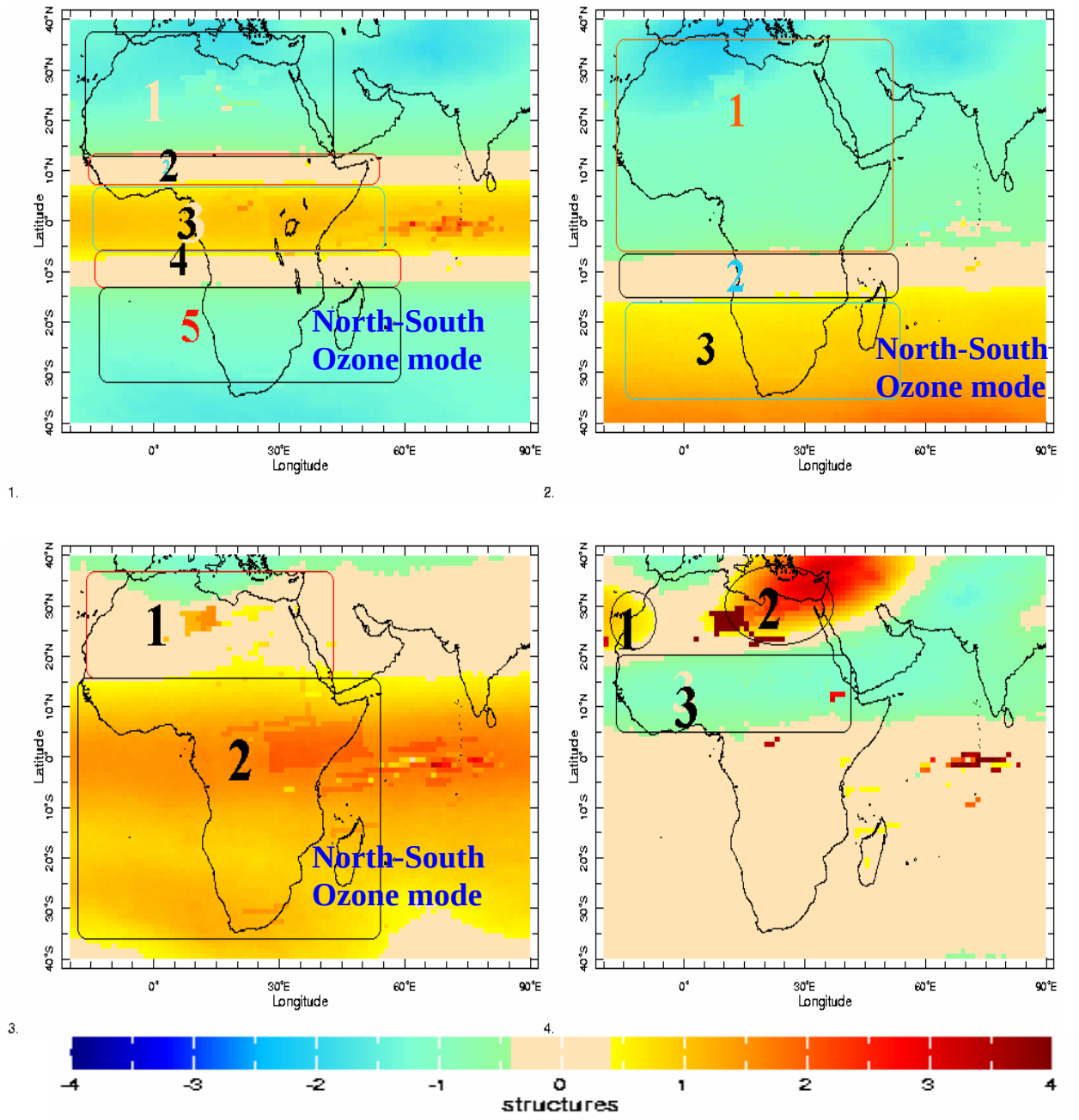

Figure 5.9: a): The spatial distribution of ozone amount (DU). The marked regions are for explanation. These are the first four structures, which show 60 % of the total variability of the data.

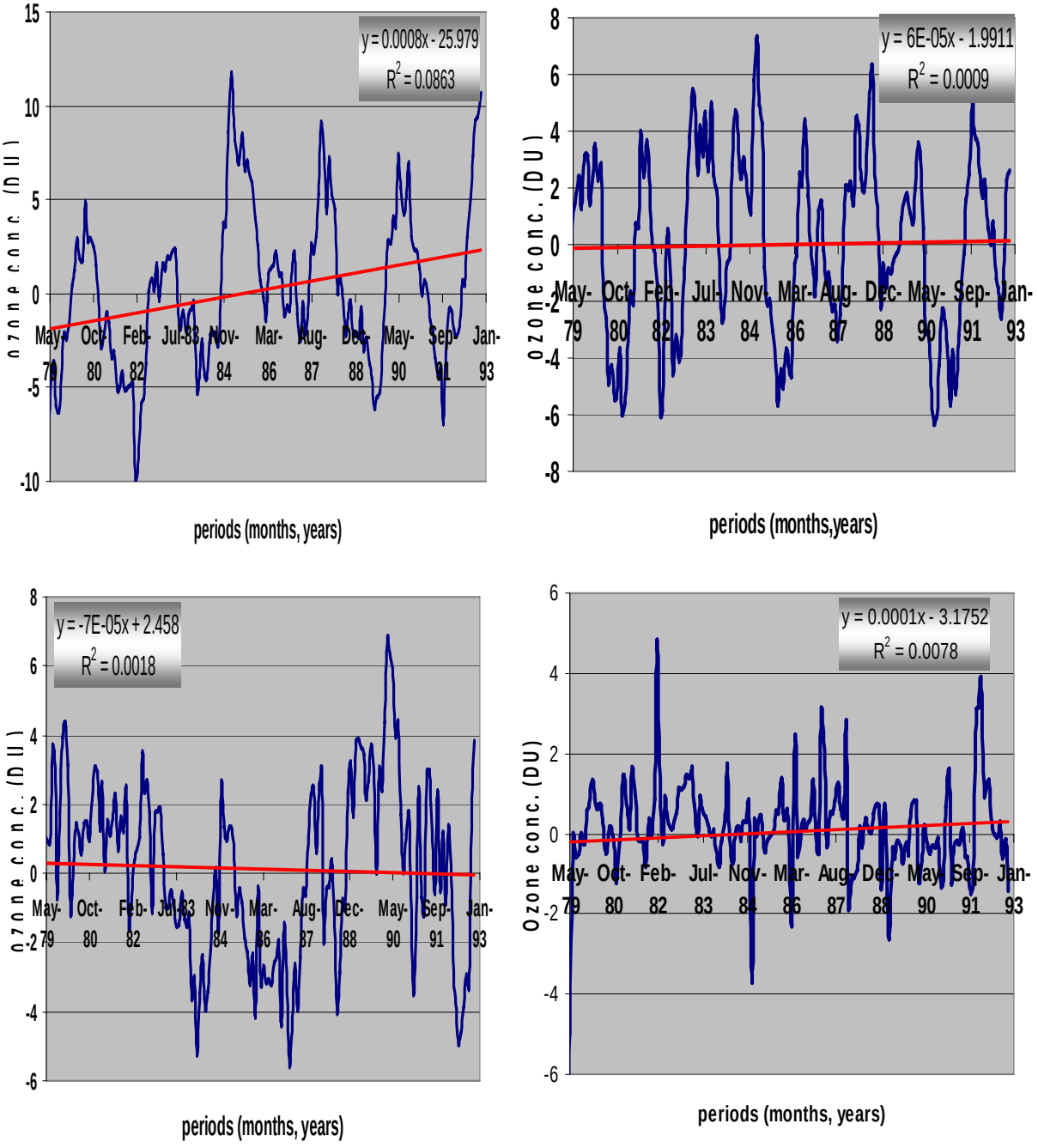

Figure 5.9: b) The temporal modes corresponding to the ozone structures using TOMS/ Nimbus 7 data (1979 to 1992).

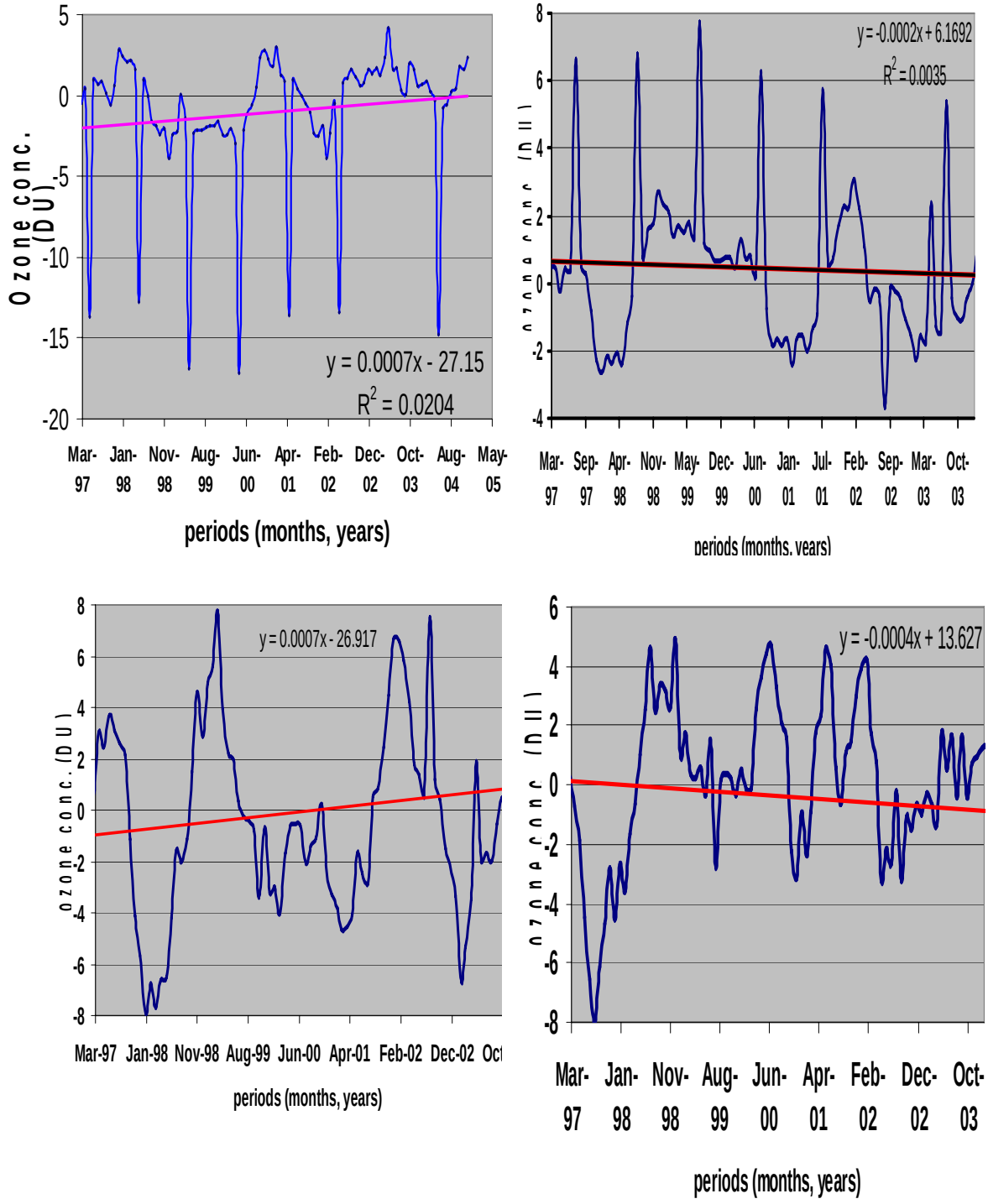

Figure 5.9: c) The temporal modes corresponding to ozone structures using TOMS/ EPTOMS data (1997 to 2003).

5.2.3.1 Seasonal variation of ozone over Africa

The ozone amount is relatively highest in the ONDJ season. Here the possible fit (54%) explains an increase of ozone amount from year to year in this season. The ozone trend in Africa is generally increasing in the period from 1979 to 1992. This is shown in figure 5.10: a). The ozone amount in the pre 1982 was very low.

The cause is many amendments (Montreal Protocol 1987, and others) were made since the discovery of the ozone hole. These amendments could trigger a decrease in the amount of ozone depleting chemicals produced from industries, and hence a little relieve in the higher latitudes ozone means, slower transport of ozone from tropical regions. The Ozone dynamics is too slow for the ozone to be transported to the high latitudes. Hence an increase in the ozone amount in the tropical Africa. The other thing worth considered here is the amount of terrestrial ultraviolet radiation arriving the Earth's atmosphere. This possibly affects the amount of ultraviolet radiation in the surface. As extraterrestrial UV radiation increases, the amount of ozone produced in the tropics also increases, and vise versa.

There is unusually maximum ozone in 2003 (see Figure 5.10, b)). Here the possible reason could be the amount of solar energy increasing in this year. As the amount of solar UV radiation increases in the stratosphere, then there will be a broke down of O_2 molecule to produce each of the individual oxygen atoms which further combines with O_2 molecule to produce ozone hence, an increase in ozone in the stratosphere.

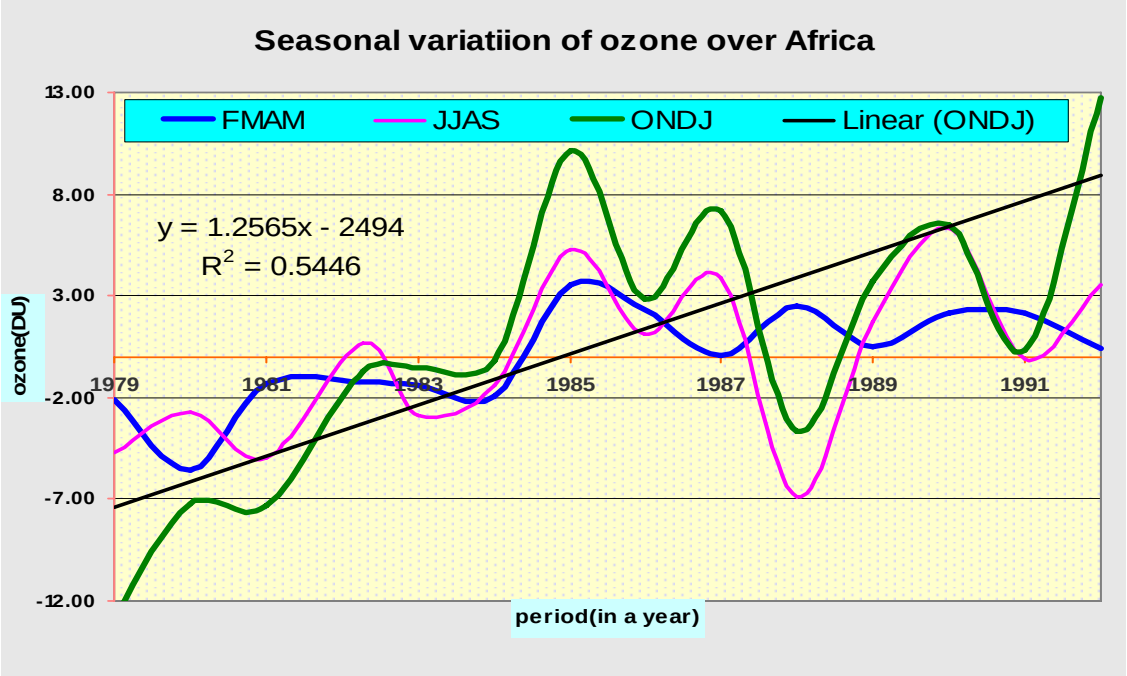

Figure 5.10: a) The seasonal changeability of ozone concentration (DU) in Africa from the TOMS/Nimbus 7 data (1979-1992).

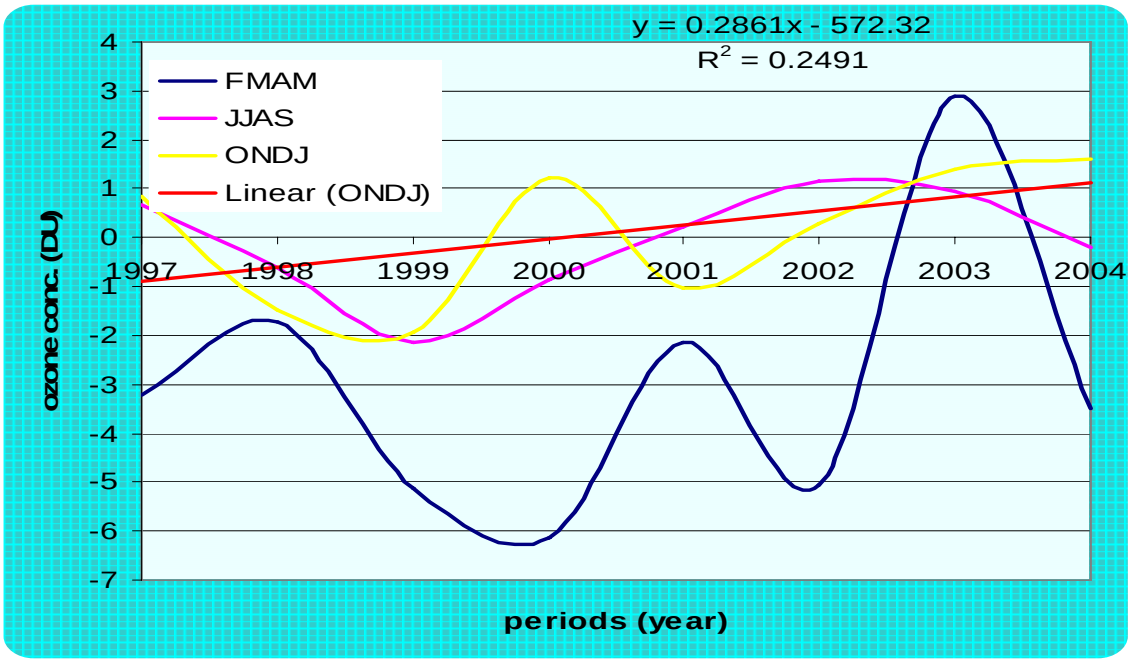

Figure 5.10: b) The seasonal irregularity of ozone concentration (DU) in Africa from the TOMS/Nimbus 7 data (1997-2004).

5.2.3.2 Vertical Distribution of Ozone in Africa

The vertical ozone distribution in Africa was computed from SBUV/TOMS/Nimbus 7, SBUV/NOAA-11 and SBUV/NOAA-16 polar orbiting satellites data for 10 years in the period in which ozone amount (DU) is highest in Africa. This period as shown in section 5.2.3.1 above is October, November, December and January. The vertical ozone distribution varies latitudinally and solar zenith angles (SZA).

The latitudinal cross section is obtained for structure 1, which explained 11% of the total variability. See Figure 5.2.3.1 structure 1. The SZA taken roughly for all the 10 years of data is 70^0. For the positive spatial variability of ozone (10S to 10N), October shows the highest vertical ozone amount parts per million volume (ppmv), 8.761 ppmv, in the period of 10 years while December shows the least vertical ozone (ppmv), 8.225 ppmv in the stratosphere. This has a difference of 0.536 ppmv, 6% lower than the larger value. See Figure 5.11.

On the other hand, in the troposphere, November outweighs (2.255 ppmv). There is 13% decrement in general. January shows the least value (1.968 ppmv).

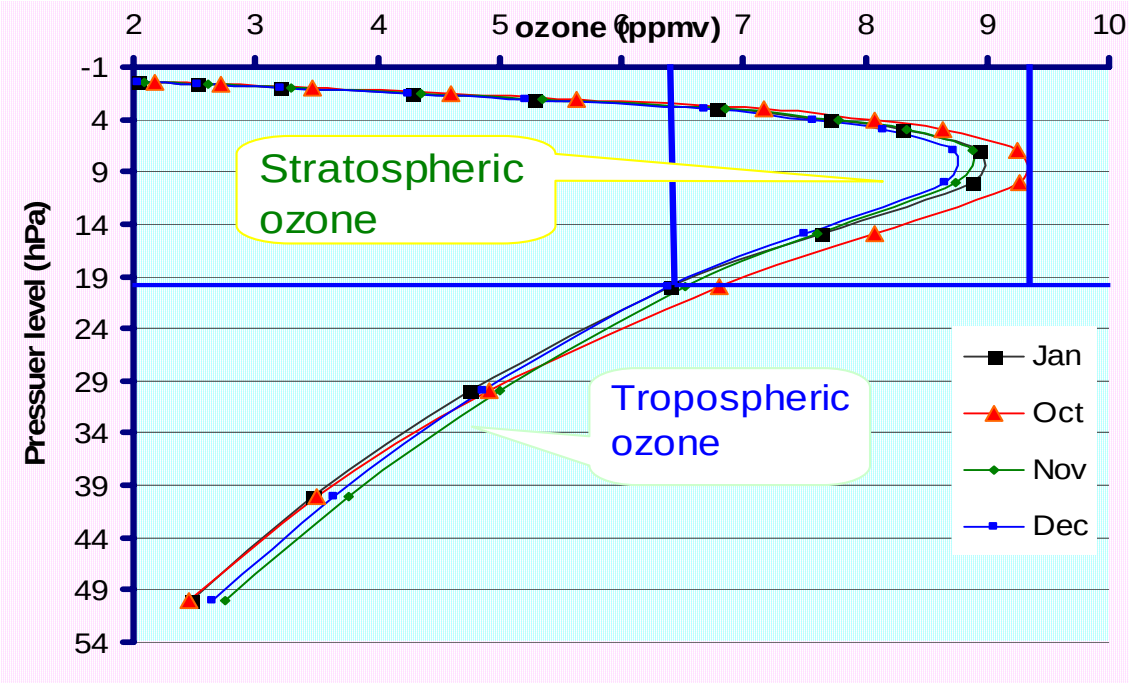

Figure 5.11: The monthly variability of ozone vertical distribution for the 10 years average (10S to 10N).

Figure 5.12 shows the yearly variability of ozone vertical distribution in parts per million volume (ppmv). In the stratosphere, here we took the maximum points (the turning points), the periods 1999 and 2000 shows the least and the next least ozone vertical distribution respectively.

The 2002 and 2003 period shows the highest ozone value in vertical ozone distribution in the stratosphere. The difference between the highest (2002) and the least ozone vertical concentration is 0.2599 ppmv, which is 26% less than the highest vertical column ozone (see Figure 5.12). In the troposphere, the vertical column ozone decreases from 1999 to 2002 by 25%. This is more or less the same difference observed in the stratosphere, but opposite concentration of ozone is observed (see Figure 5.12).

If ozone concentration is highest in the stratosphere in the period, it is also the least in the troposphere in the same period. In general, the vertical ozone concentration shows opposite quantitative variability in the two spheres of the atmosphere.

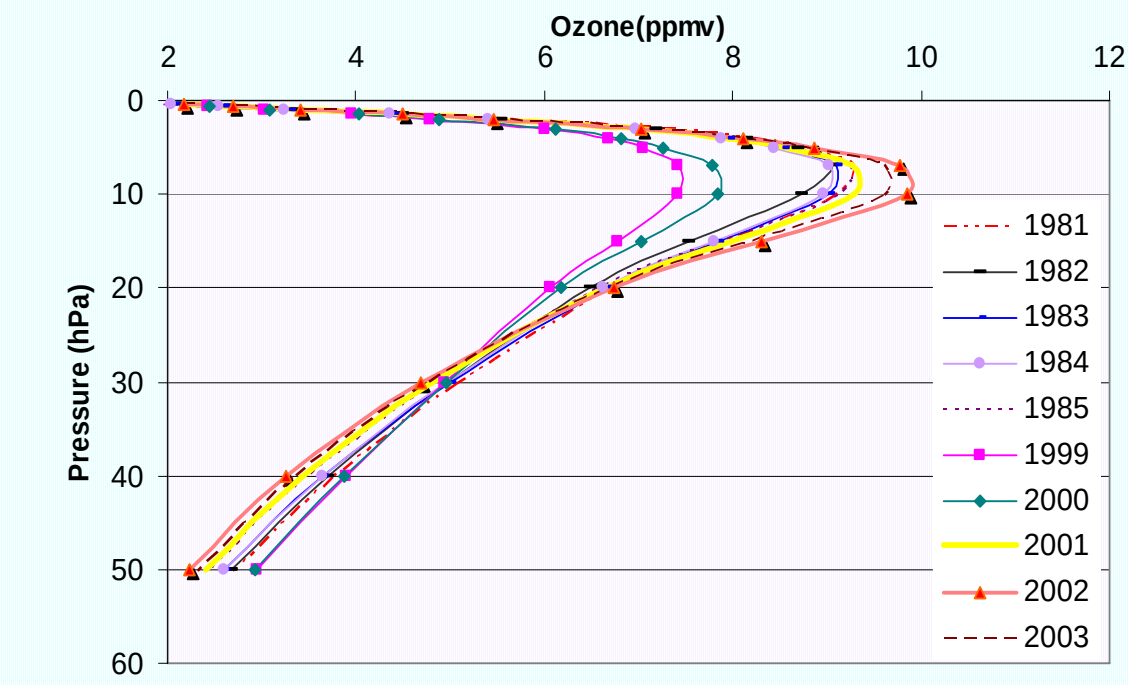

Figure 5.12 Yearly average of vertical ozone distribution (SBUV/Nimbus 7 (1981-1985), SBUV/ NOAA - 11 (1999-2000), and SBUV/NOAA - 16 (2001-2003)).

For the other cross sections ~30S and ~30N is taken and compared with the other latitudes, ~0, ~60S, ~60N, ~90S and ~90N. Here we took the above 10S to 10N as ~0 for simplicity. The vertical ozone concentration is relatively highest in October for 60N (9.544 ppmv), and least for 60S (8.48 ppmv). The difference is 11% lower than the peak. This is in the stratosphere. In the troposphere, the opposite, i.e. the ozone vertical concentration is upper limit at 60S and minimum at 60N, it overturns that of the stratosphere (see Figure 5.13).

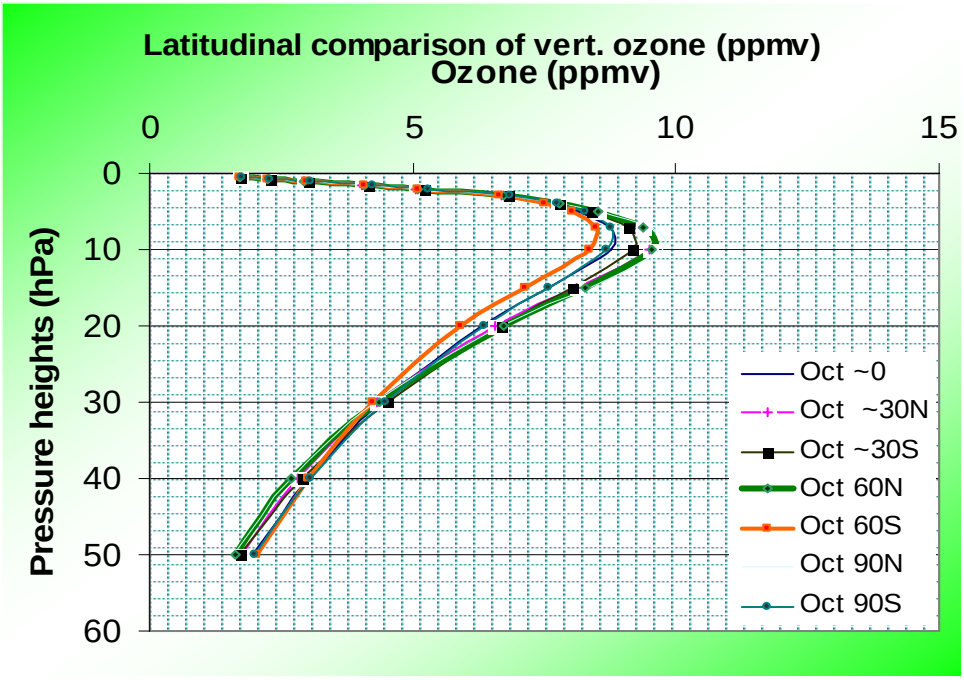

Figure 5.13 Latitudinal comparison of vertical ozone distribution for the month October (SBUV/Nimbus 7 (1981-1985), SBUV/ NOAA - 11 (1999-2000), and SBUV/NOAA - 16 (2001-2003)).

In November, the ozone-mixing ratio is least in values at and around 90N and 90S in the stratosphere. These are in compromise with great ozone depletion observed in the Arctic and Antarctic regions. There is a little difference at 10-hPa pressure level, at which the 90S value is a little greater than the 90N value. In the same month, the greatest ozone-mixing ration is observed for 30S and its nearest locations. This is because of the ozone transport from the equator to higher latitudes through Brewer-Dobson Circulation.

Ozone is produced in the stratosphere of the equatorial latitude due to the overhead sun there. This high amount of solar energy breaks down the oxygen molecule and combines it with another oxygen molecule in the stratosphere, and form ozone – a three atom of oxygen combined. Though ozone is produced in the tropics, it is transported to the higher latitudes though Brewer-Dobson circulation. This is transportation through zonally averaged sense that is averaged around a latitude circle. The Brewer-Dobson circulation additionally explains the observed latitudinal (i.e. north south) distributions of long-lived constituents like nitrous oxide and methane. For more discussion, see section 3.4.1.3.

The values obtained are more or less in conformity with the previous studies. For more Clarity look at the Figure 5.14. The other months also show more or less similar ozone mixing ratio to Figure 5.14.

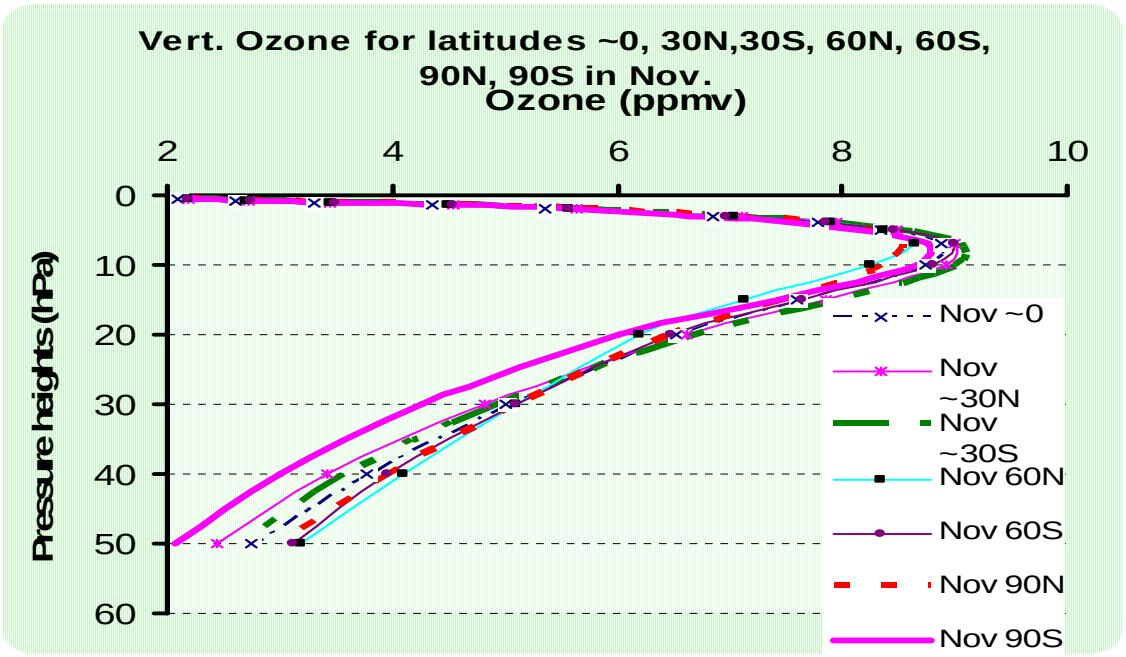

Figure 5.14: Latitudinal comparison of ozone mixing ratio (ppmv) for the month November (SBUV/Nimbus 7 (1981-1985), SBUV/ NOAA - 11 (1999-2000), and SBUV/NOAA - 16 (2001-2003)).

The poles ozone-mixing ratio is in between two extremes, maximum and least in different years. January 1999 and 2000, October 1981 and 1985, November 1999, and December 1999 is the periods in which the least ozone-mixing ratio at the Antarctic is

observed. This is in good agreement with the Ozone hole years and seasons. For more illustration, see Figures 5.15.

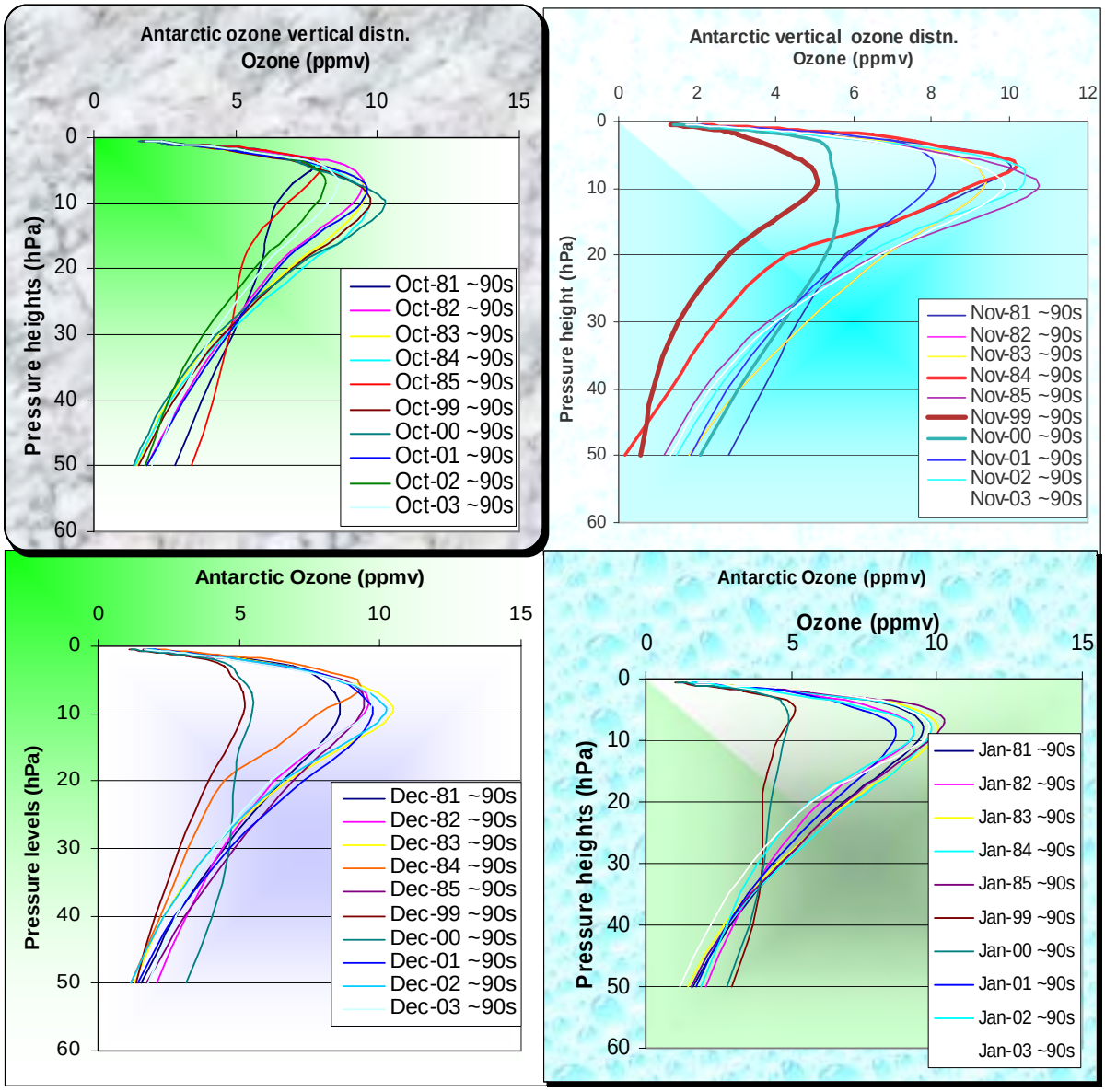

Figure 5.15: Ozone mixing ratio in the Antarctic region (SBUV/Nimbus 7 (1981-1985), SBUV/ NOAA - 11 (1999-2000), and SBUV/NOAA - 16 (2001-2003)).

On the other hand, in the Northern Pole there are periods in which maximum ozone-mixing ratio can be observed and a period in which a depletion of ozone was seen.

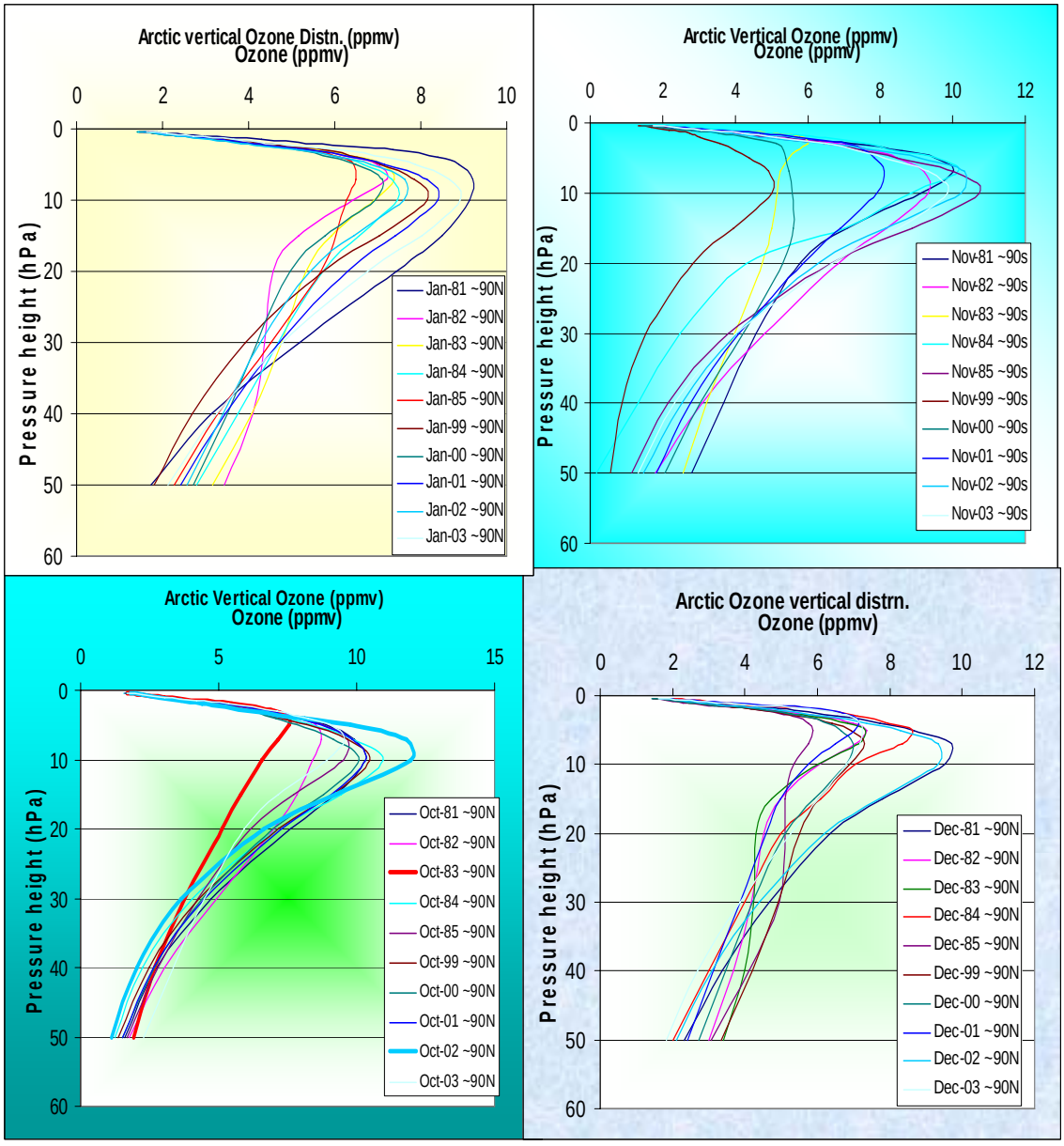

Figure 5.16: Ozone Mixing-ratio in the Arctic region (SBUV/Nimbus 7 (1981-1985), SBUV/ NOAA - 11 (1999-2000), and SBUV/NOAA - 16 (2001-2003)).

January 1982 and 1985, October 1983, November 1989 (the least value) and December 1985 are the periods in which the vertical ozone-mixing ratio has shown an unusual depletion based on this data. For more illustration, see Figure 5.16.

In summary, the variability in ozone vertical distribution or mixing ratio is greatest in the high latitudinal regions. Therefore, the UV irradiance level rises during the drop in ozone amount in the atmosphere. The gap in the highest ozone-mixing ratio in one year and a drop in the other in the winter season is the main problem in higher latitudes. This is because of the high variability of UV irradiance due to low and high ozone amount in the atmosphere respectively.

In contrast to the higher latitudinal zones, the ozone-mixing ratio has shown relatively stable. This shows that, no matter how high the amount of UV irradiance reaching the surface of the tropical region, there is calm variability of UV irradiance. This slow variability of UV irradiance is important for adaptation purposes. This is the reason why tropical dwelling people, animals, and plants are relatively resistant to the high sun burning UV developing adaptive pigments like melanin to people and animals as enzymes to plants.

5.3 Latitudinal Comparison of Average UV irradiance, Column Ozone (DU) and Aerosol Index

a) Latitudinal Comparison of UV and ozone

The ozone column amount is highest in the mid-latitudes (30N/S to 60N/S), lowest in the Polar Regions (60N/S to 90N/S). At the Equator (~30S to 30N), the value of ozone amount is in the range between the mid-latitude ozone amount and that of the polar ozone amount. Look Figure 5.17 a) and b) for an illustration.

This difference could be because of the zonally averaged circulation in the meridional-height plane, i.e., a circulation of rising and pole ward motion accompanied by sinking and equator ward flow. Note that, the velocities involved are much smaller than the zonal wind, but still important for transport on long time scales (see Figure 5.18). But the UV index amount on the other hand is relatively greater than that of other parts of the world. This is attributable to the overhead sunrays in the equator the whole year and p

possibly due to the relatively lesser ozone amount which does absorb the UV radiation than the mid-latitudinal regions.

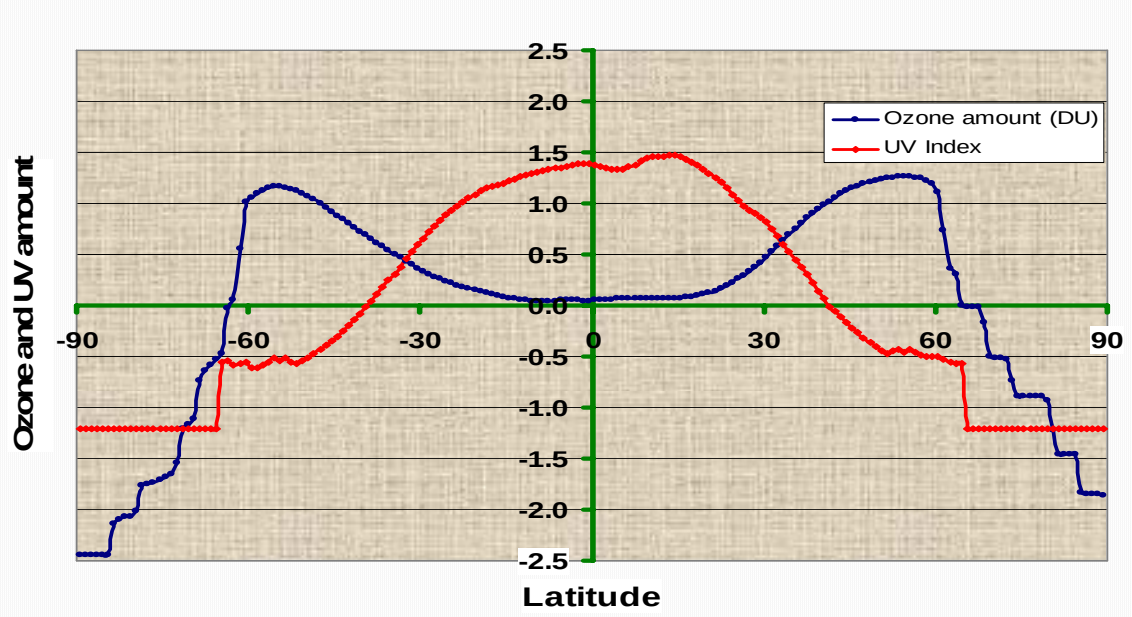

Figure 5.17: a) The latitudinal comparison of Ozone and UV distribution using the TOMS/Nimbus 7 data.

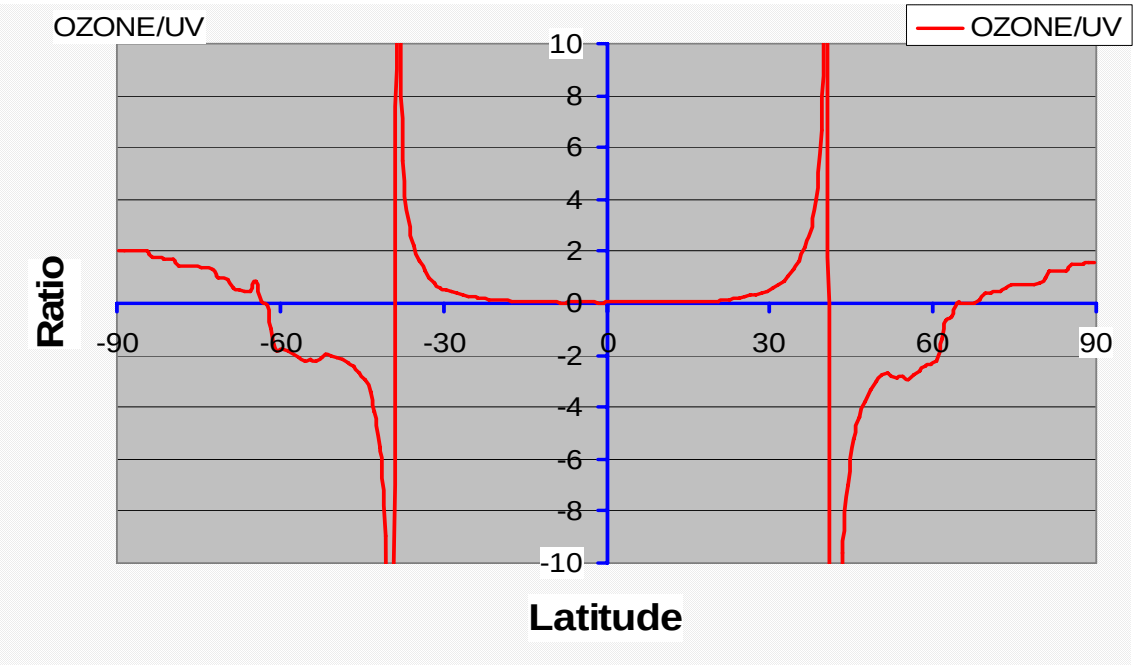

Figure 5.17: b) The ratio of Ozone to UV.

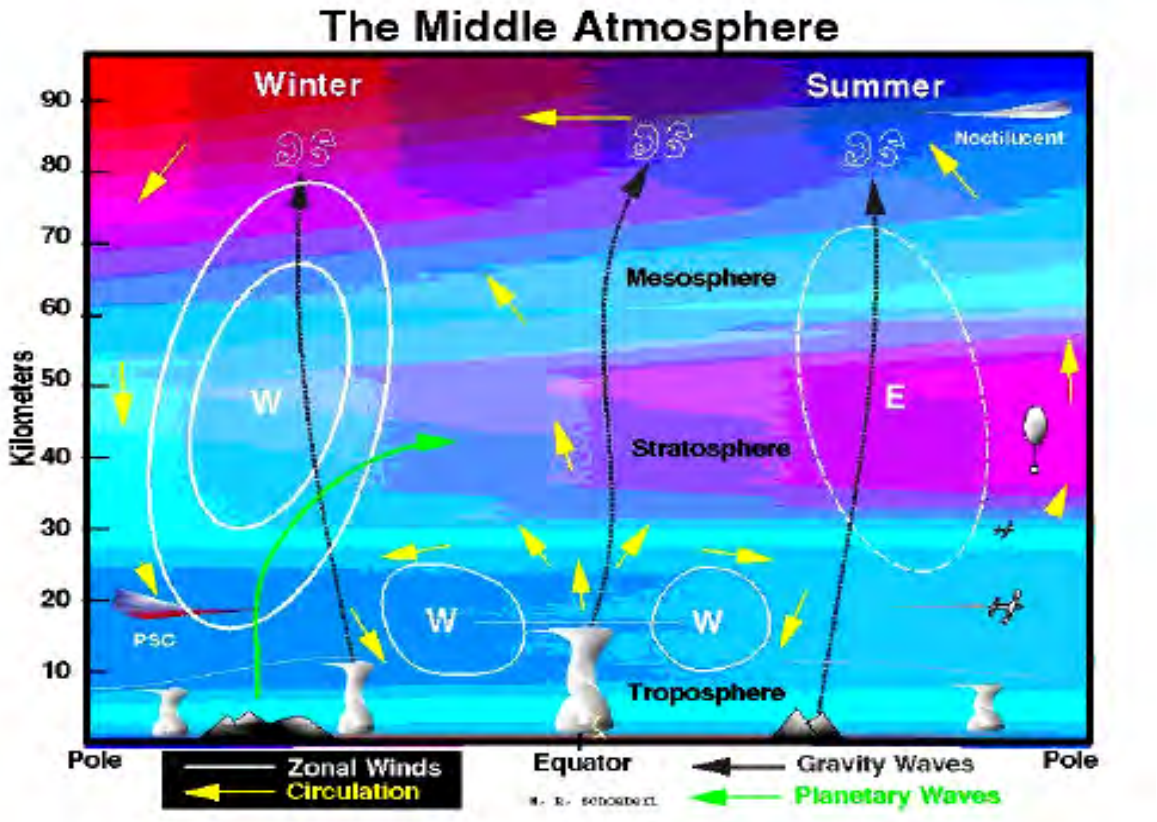

Figure 5.18 Circulation in the middle atmosphere.
(http:// see.gsfc.nasa.gov/edu/SEES/strat/class/S_class.html).

b) Latitudinal Comparison of UV, ozone and Aerosol Index

The aerosol index value is highest in the latitude range from 5N to 30N (Figure 5.19). The non-symmetricity of the aerosol profile against the equator is due to the ample source of dust in the Sahara desert and Arabian Desert. This is discussed briefly in section 5.2.2. Aerosol index amount is most in the Northern hemisphere than the Southern hemisphere. This is due to the Saharan and Arabian Desert dust aerosols, sand aerosols, and playas in the northern hemisphere. Human factors could also be at stake, since industrialized regions lay in the Northern geographical zone than the south.

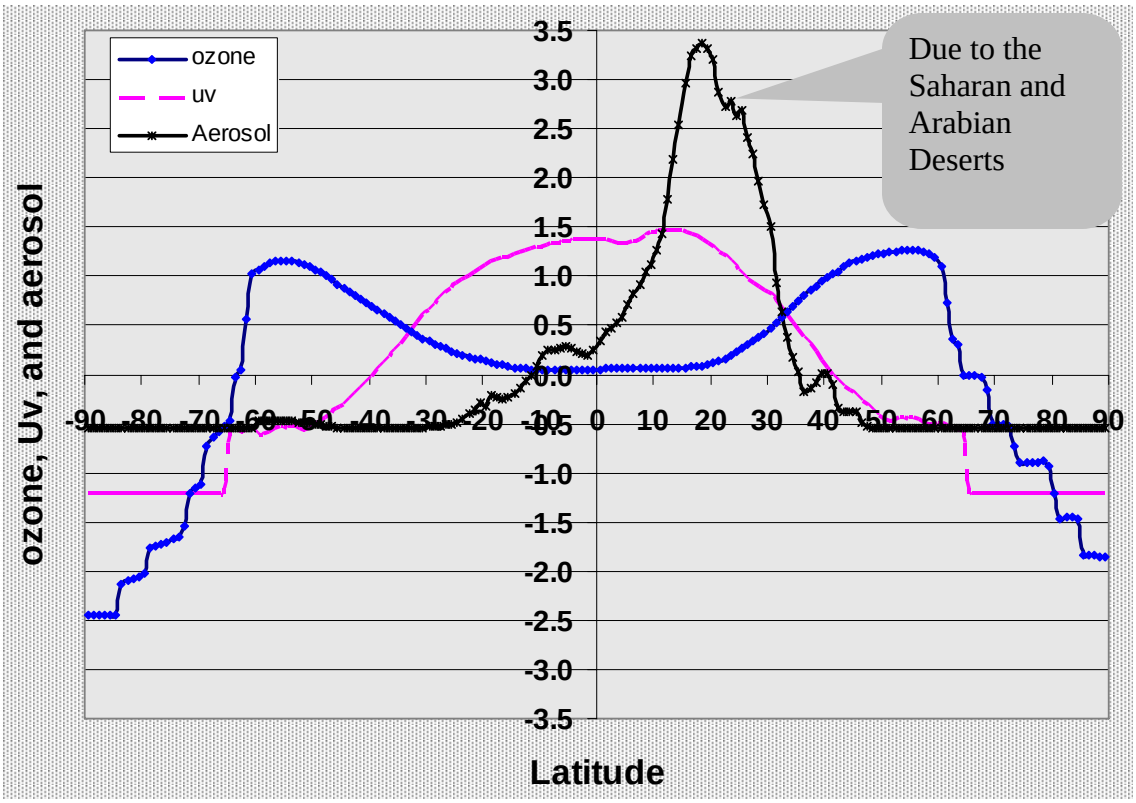

Figure 5.19: The latitudinal comparison of Ozone, UV and aerosol index.

5.4 The Relation of ozone, and aerosols with UV

a) Ozone and UV Association

As discussed in section 3.4.1, less stratospheric ozone results in an increase in the ultraviolet radiation reaching the surface of the Earth. This peculiar characteristic can be explained using the ozone and UV relationship established in Figure 5.20. Here we can see that UV radiation at the surface is inversely proportional to the ozone amount in the stratosphere. The line fit for the regression and the model summary explains 41% of inverse proportionality between ozone and UV. The governing equation for this relationship is

$$UV\ (O_3) = -18.595 - 12.233x\ O_3 \qquad (5.1)$$

Model	R	R Square	Adjusted R Square
1	.636	.405	.399

Model		Unstandardized Coefficients		Standardized Coefficients	
		B	Std. Error	Beta	t
1	(Constant)	-18.595	6.304		-2.950
	Oz_NMBS_1	-12.233	1.441	-.636	-8.488

Table 5.1: Model summary of the regression between ozone concentration and UV.

From this formula, we can calculate that 1% decrease in ozone results in about 30% increase for UV irradiance on the surface of the Earth. This shows the ozone depletion is disastrous for living things dwelling in that area as it increases harmful UV radiation on the surface of the Earth.

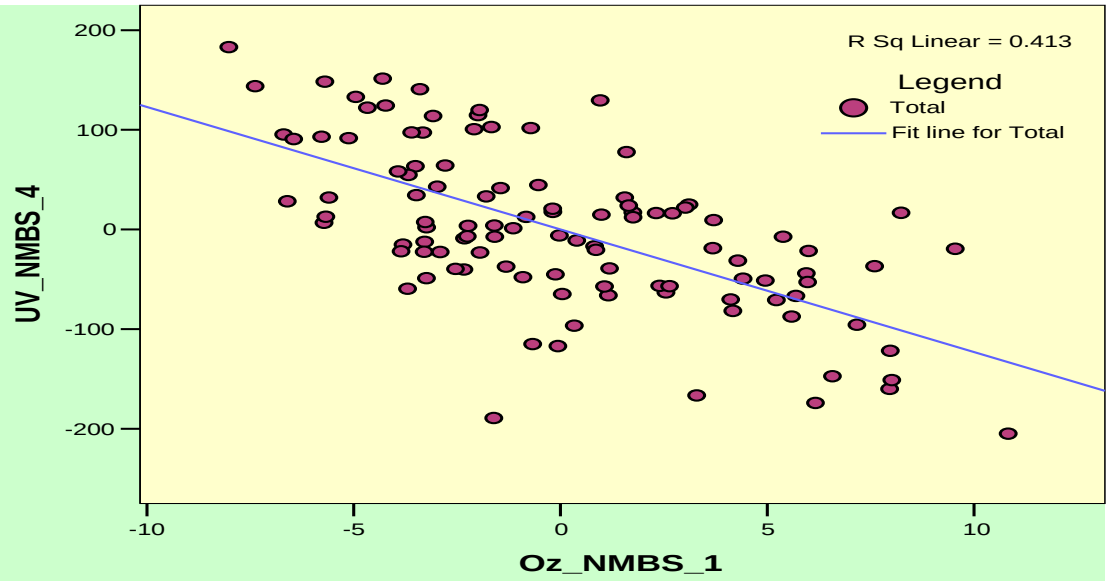

Figure 5.20: The ozone and UV association. The increase in ozone results in the decrease in UV.

b) Aerosols and UV Association

Varieties and spectral optical depths are essential inputs to regional and global aerosol impacts to the spectral UV irradiance. Here we can see that UV and aerosols have shown little relationship. This is to mean, only 7% of the total variability of UV over the African continent can be expressed by aerosols. Aerosol should contribute to UV irradiance at surface in such a way as to absorb and decrease its amount.

$$UV = -4.085 - 210.140 \times AI\ (Ts\_1) - 187.982 \times AI\ (Ts\_2) - 717.297 \times AI\ (Ts\_4) \quad \ldots\ldots (5.2)$$

where Ts-n means respective time series of the eigenvalue n.

Model	R	R Square	Adjusted R Square	Std. Error of the Estimate
1	.267	.071	.044	140.071486

Model		Unstandardized Coefficients		Standardized Coefficients	t
		B	Std. Error	Beta	
1	(Constant)	-4.085	14.421		-.283
	ARSL_NMBS_1	-210.140	159.531	-.126	-1.317
	ARSL_NMBS_2	-187.982	192.118	-.094	-.978
	ARSL_NMBS_4	-717.297	326.648	-.209	-2.196

Figure 5.2: The aerosol and ozone relationship model summary.

5.5 The Spatial and Temporal Results of Clouds Having Association with UV over Africa

Propagation of radiation through the atmosphere is affected by absorption and scattering by particulates (e.g. haze, dust, fog and clouds) suspended in the air. The effect of dust aerosols and other types of aerosols is discussed in the aerosols section above. Here what is going to be dealt with is the effect of clouds on the UV irradiance level reaching the earth's surface.

There are 20 cloud types considered along with UV radiation. Though it is difficult to parameterize and consider the effects of all of the 20 cloud types in previous works, it is attempted here to include the cloud effect on UV irradiance. To remind you here with previous discussion on chapter three, as radiation enters to the atmosphere, it is subjected to absorption and scattering. The same thing applies when radiation confronts clouds in its way. If the cloud is in overcast condition, it absorbs and reflects almost all transmitting little. However, during broken cloud circumstances it is almost unpredictable whether it increases or decreases the amount at surface. Nevertheless, it is studied that UV irradiance at surface is greater during broken cloud time than overcast cloud condition.

The influence of clouds on erythemal UV irradiance shows a large diversity. The equivalent cloud optical depth (homogeneous plane-parallel cloud layer between 3000-4000 m a.s.l.) ranges between 8 and 120. The increase of UV radiation due to multiple reflections between a snow covered ground and an overcast cloud cover ranges between 40% and 80%. Erythemal irradiance varies strongly on days with a broken as well as an overcast cloud cover.

The all cloud cover in Africa is snow free. The clouds with ice Altostratus ice-amount, Cumulus ice all the variables (i.e. Cloud amount, cloud optical thickness, cloud top pressure, cloud top temperature, and cloud water path), Nimbostratus ice-cloud amount, Stratocumulus ice-all of the other variables, Stratus ice-all of the variables and Surface ice are negligible and found at margins of the African continent. This surface ice

value implies that, the African continent is ice free -except those areas of the mountains peaks like Mount Kilimanjaro in Tanzania.

The clouds, which have shown significant correlations with UV irradiance, are to be investigated. The tables show only those of the clouds, which predicted the relationship significantly. The most known cloud type in the tropics is convective type of clouds. But, the convective type of clouds does not show significant relationship with UV irradiance in Africa. This deserves further study.

The associations presented here are in such a way that those cloud types, which have shown relationship with ozone, should also be taken in to account in the UV study.
Note that, the significant relationship of clouds with UV is only depicted for the UV time series 4, which shows only 5% of the total UV variability.

The clouds, which have shown significant relationship, are as follows:

a) All clouds- Top Temperature
b) Altocumulus Liquid clouds – Optical Thickness and top temperature
c) Cirrostratus cloud – Top Pressure
d) Cirrus cloud – Water Path

The other cloud types show very little relationship and hence are neglected.

a) All Clouds – Top Temperature

This cloud parameter shows 13% of the 204 total eigenvalues. As can be seen from Figure 5.21, only single mode (positive spatial variability) with much of the values of the structure are concentrated in the southern Africa mode, Congo mode and Sahel mode. These mean that, these regions clouds have high top temperature, which affects the surface ultraviolet radiation negatively. The temporal value of the same mode shows a decrease from the years 1984 to 1992 and an abrupt increase from 1992 to 1999. The perfect significant fit explains 42% of the total variability in the top temperature of the all clouds in the respective regions. For more illustration, the trend is given in Figure 5.22.

When we see its association with UV ery, we used regression and the R-square is 0.316. This implies that the relationship is significant as 32% of the UV can be explained by this cloud top temperature in Africa.

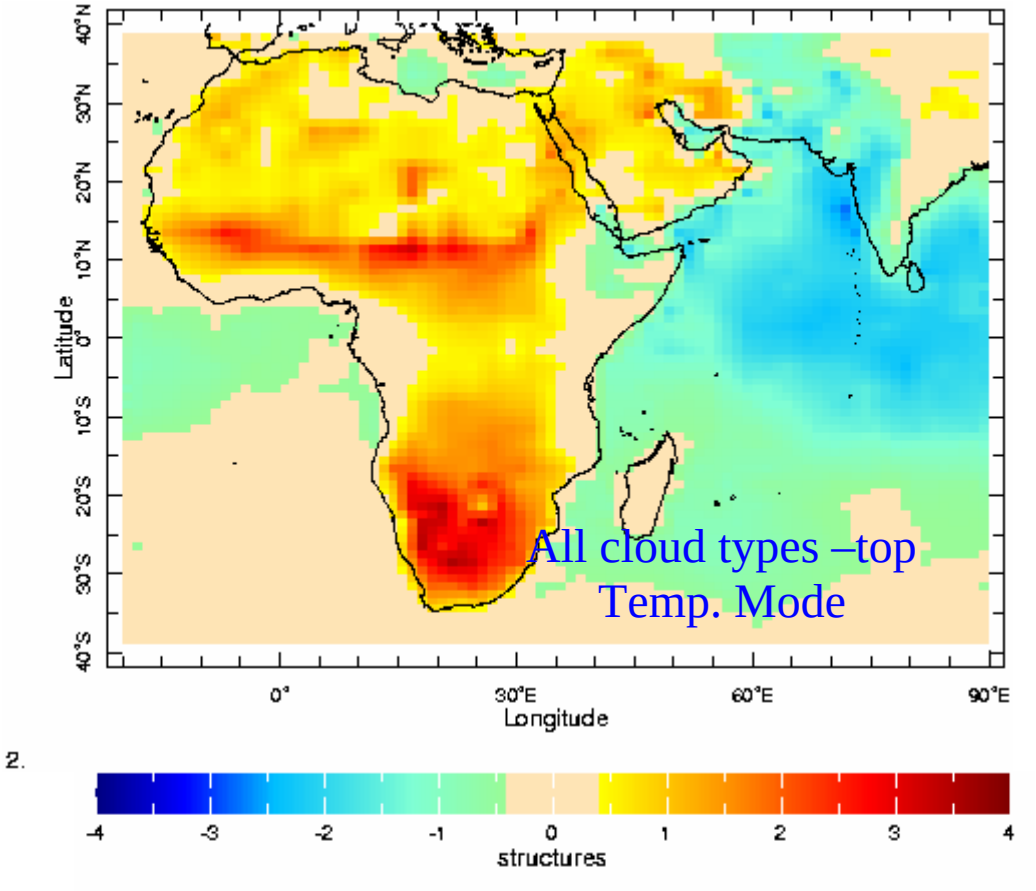

Figure 5.21: All cloud types – Top Temperature. Here we can see only a single mode within Africa.

From the model we get,

$$UV = -34.996 - 19.578 \times \text{all-cloud-top-temp.} \quad (5.3)$$

Model	R	R Square	Adjusted R Square	Std. Error of the Estimate
1	0.568(a)	0.323	0.316	66.986791273

Model		Unstandardized Coefficients		Standardized Coefficients	t	Sig.
		B	Std. Error	Beta		
1	(Constant)	-34.996	6.448		-5.428	.000
	All,cld_tem_2	-19.578	2.756	-.568	-7.105	.000

Table 5.3: The model summary of the all cloud top temperature and ultraviolet radiation.

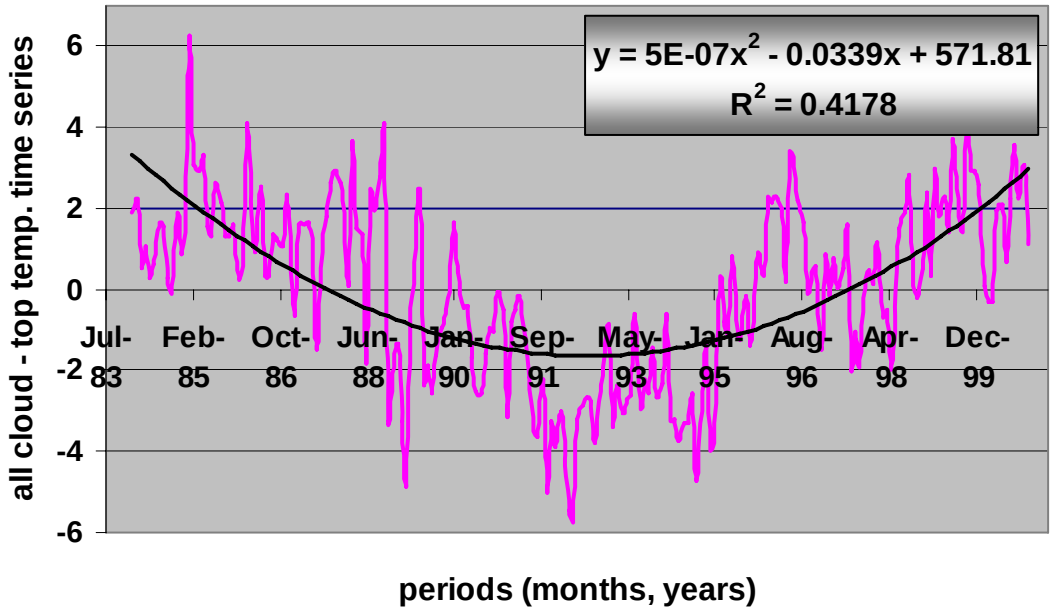

Figure 5.22: The temporal characteristics of the All Clouds types – Top Temperature. The trend shows abrupt increasing order of the top temperature of the clouds in Africa.

b) Altocumulus Liquid Cloud – Optical Thickness and Top Temperature

Altocumulus liquid cloud optical Thickness is the only optical thickness of the all clouds, which has shown significant association with UV. This cloud parameter represents 15% of the total variability existed in the 204 eigenvalues. This cloud type shows negative spatial region in the tropical Congo, the west cost of Africa and the Indian Ocean region (see Figure 5.23). It indicates that, there is little difference in the amount of optical thickness of the cloud altocumulus liquid cloud. The temporal value also shows little trend decrease (Figure 5.24). This indicates that the clouds, which are found in the African continent, have little optical thickness so that it attenuates the solar radiation to the minimum.

The relationship between altocumulus liquid and the ultraviolet radiation is depicted as

$$UV = -33.127 - 362.739 \times \text{altocumulus-liquid-optthick} \quad (5.4)$$

Model	R	R Square	Adjusted R Square	Std. Error of the Estimate
1	.371	.138	.130	75.5736996

Model		Unstandardized Coefficients		Standardized Coefficients	t	Sig.
		B	Std. Error	Beta		
1	(Constant)	-33.127	7.274		-4.554	.000
	Altcmls,lqd_opt_1	-362.739	88.137	-.371	-4.116	.000

Table 5.4: Model summary of the regression between altocumulus liquid optical thickness and ultraviolet radiation.

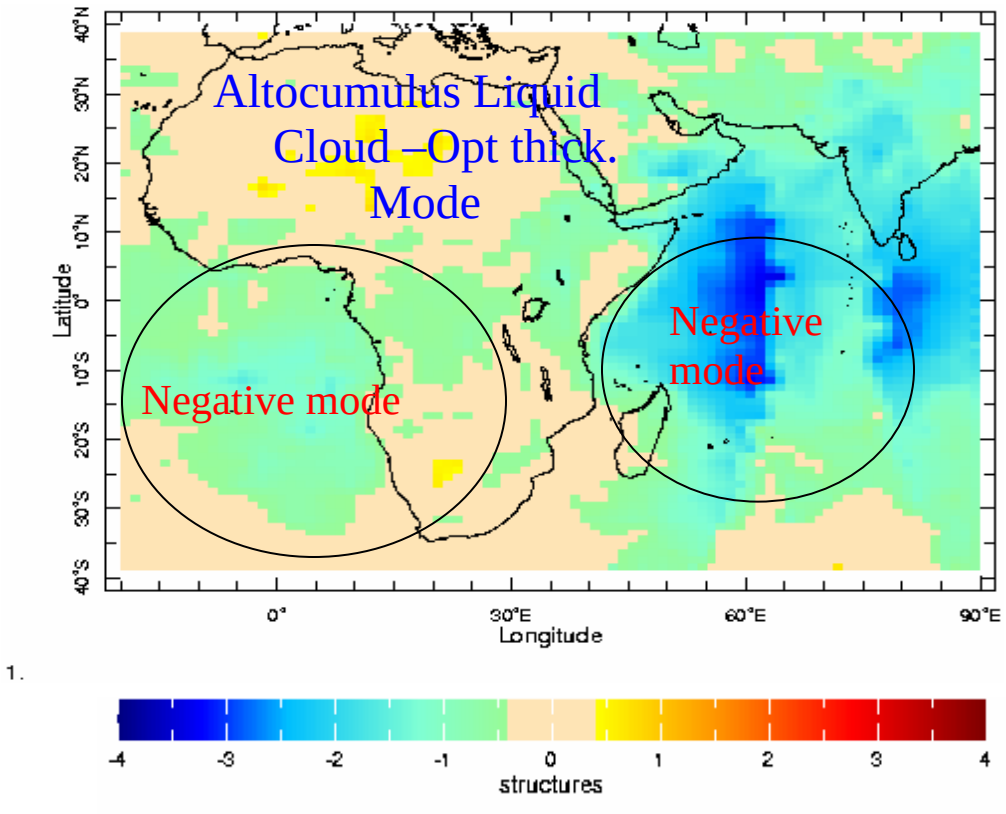

Figure 5.23: The spatial characteristics of the Altocumulus liquid cloud optical thickness. Here one can see the negative spatial region in central Africa, South Atlantic Ocean and Indian Ocean. The other regions of Africa are neutral.

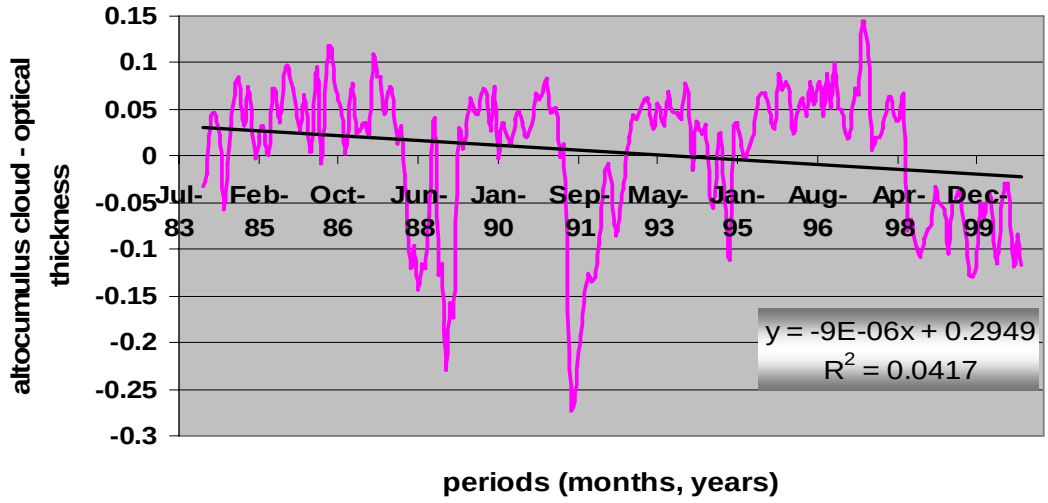

Figure 5.24: The temporal trend of altocumulus cloud – optical thickness in Africa. The possible fit explains a trend down of 4%.

The other altocumulus liquid cloud parameter, which has shown significant correlation with ultraviolet radiation, is its top temperature. Temperature affects UV radiation by increasing the catalytic breakdown of ozone. That is temperature affects ozone transport and catalysts dynamics in the atmosphere. The positive mode in the whole of Africa except the southeastern part is the high amount of temperature. The negative mode is the southwestern cost of Africa. Here this negative temperature is due to the South Atlantic Ocean, which radiates cool air to the west cost of Africa. For more clarification, see Figure 5.25.

The corresponding time series is slopping down, i.e. showing 47% significant trend fit decline in the temperature of the altocumulus cloud (Figure 5.26).

In most of the cases, oceans show negative spatial top temperature of clouds. This is due to the specific heat of water in ocean, which is lower than the clouds temperature, and this ocean absorbs the temperature of the clouds. On the other hand, the specific heat of the land is greater than that of the ocean and takes less heat from the atmosphere and hence the temperature of the clouds on a land surfaces is greater than that of the same cloud on oceans.

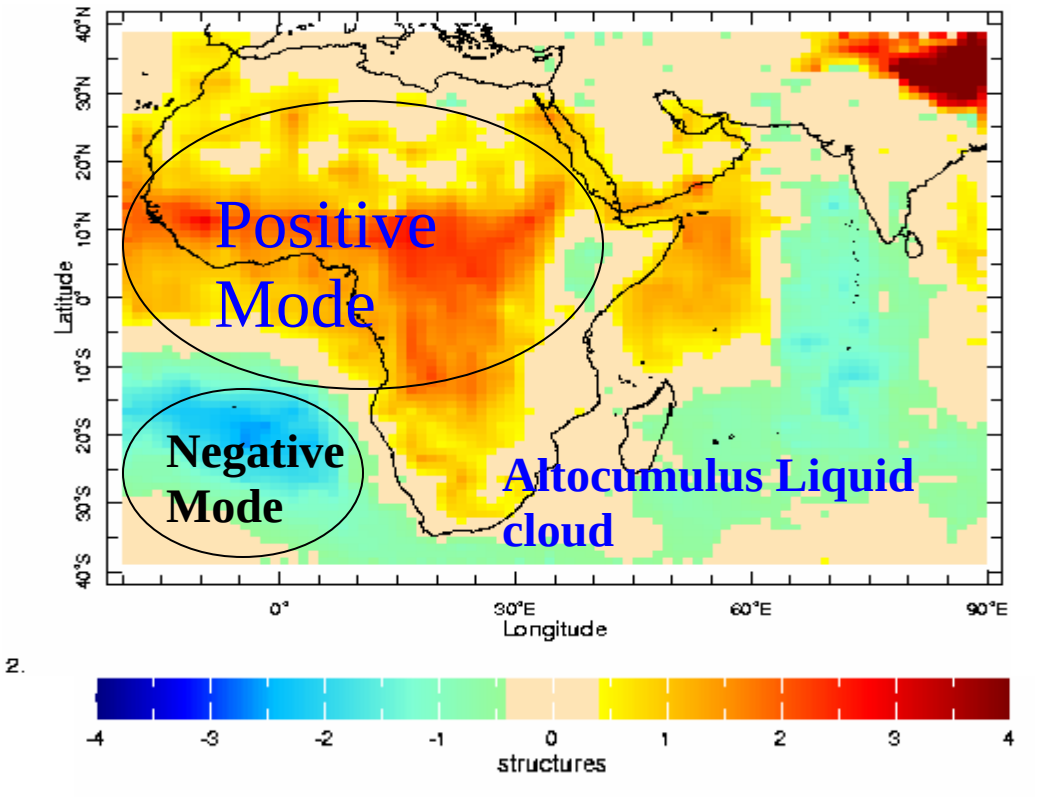

Figure 5.25: The spatial characteristics of altocumulus cloud top temperature having significant association with ultraviolet radiation.

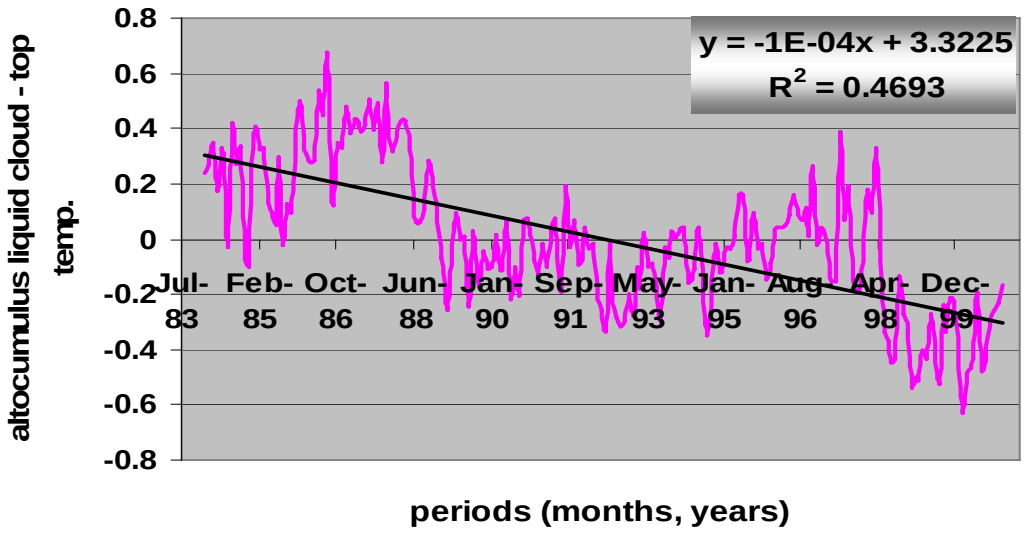

Figure 5.26: The temporal characteristics of Figure 5.25. The trend shows the declining of the top temperature of the altocumulus cloud top temperature.

Twenty-four percent of the UV radiation can be explained by altocumulus liquid cloud top temperature, keeping the other factors constant. The regression result and model equation for the association between altocumulus top temperature and ultraviolet radiation is

$$UV = -12{,}677 - 169.906 \times \text{altocumulus liquid-temp} \qquad (5.5)$$

Model	R	R Square	Adjusted R Square	Std. Error of the Estimate
1	.492	.242	.235	70.8547203

Model		Unstandardized Coefficients		Standardized Coefficients	t	Sig.
		B	Std. Error	Beta		
1	(Constant)	-12.677	7.727		-1.641	.104
	Altcmls,lqd_tem_2	-169.906	29.199	-.492	-5.819	.000

Table 5.5: Model summary of the relationship between UV and altocumulus liquid cloud top temperature.

c) Cirrostratus Cloud – Top Pressure

Based on the spatial variability of the Cirrostratus cloud- top pressure we can see it dividing in to four but two distinct regions. The northern, the south western, and the southeast positive regions and the northeastern and the Arabian negative regions. The southeastern part positive region shows high pressure due to the Indian Ocean influence and the southwestern region is due to the South Atlantic Ocean influence. As warm air rises from these oceans, it radiates to the cooler air and hence exerting pressure on the clouds in this respective regions. On the other hand, the northern hemisphere is prone to aerosols which rises from the Sahara desert in so doing they could possibly exert pressure on the top of the cirrostratus cloud.

The negative spatial region shown in Figure 5.27, the north eastern and Arabian region can possibly be due to the light air and the cloudless arid area of the Arabian Desert. The other parts of Africa shows nearly neutral spatial mode- in between the

positive and negative eastern Africa and Arabian modes. For more illustration and visual clarity, see Figure 5.27.

The important regression model shows this cloud type alone explains 11% of the UV variability over the surface of Africa. The equation which show relationship is

$$UV = -34.511 - 6{,}358 \times \text{cirrostratus cloud top-press} \qquad (5.6)$$

Model	R	R Square	Adjusted R Square	Std. Error of the Estimate
1	.343	.118	.109	76.4481418

Model		Unstandardized Coefficients		Standardized Coefficients	t	Sig.
		B	Std. Error	Beta		
1	(Constant)	-34.511	7.358		-4.690	.000
	Cirrstrts,cld_press_4	-6.358	1.691	-.343	-3.761	.000

Table 5.6: Model summary of the relationship between cirrostratus cloud pressure and UV.

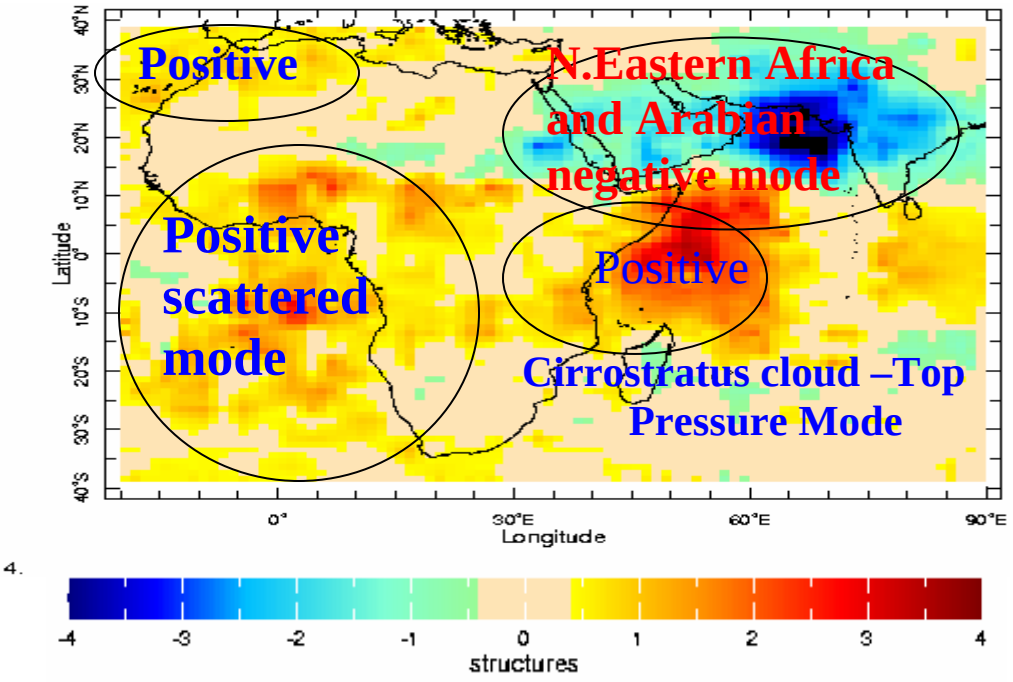

Figure 5.27: The spatial characteristic of the African Cirrostratus cloud top pressure.

A temporal characteristic of the same cloud shows a slight decrease from the year 1984 to 1992 and slight upheaval from 1993 to 2000. The quadratic fit explains 5% of the total variability of the trend (Figure 5.28).

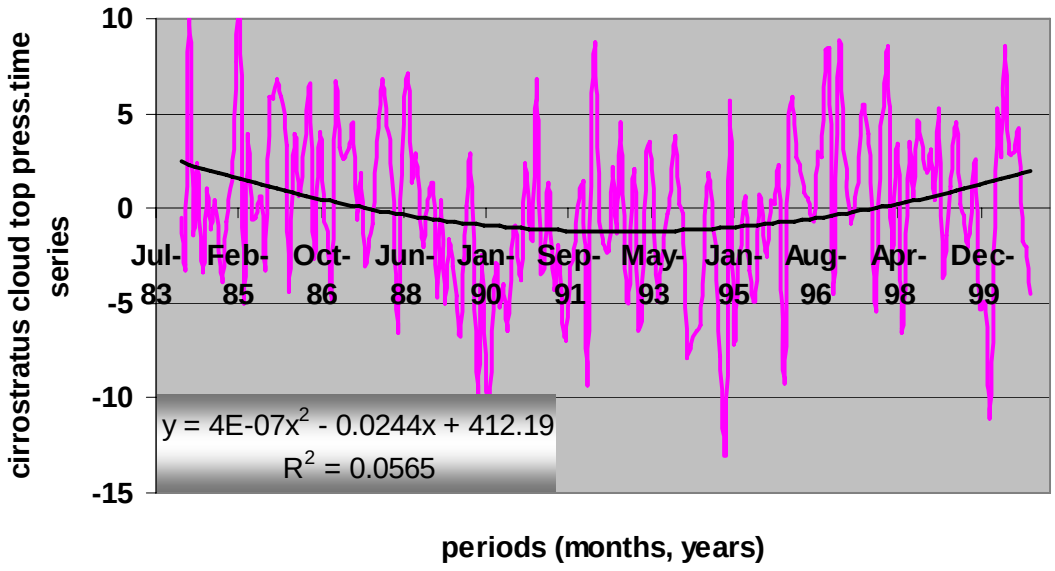

Figure 5.28: Temporal variability of cirrostratus cloud top pressure. The quadratic fit explains 6% of the total variability.

d) Cirrus Cloud Water path

This cloud type explains 26 % of the total variability of the 204 eigenvalues. The overall coverage in Africa of this cloud water path is neutral and negative spatial modes at the coastal regions (see Figure 5.29). The trend of the temporal variability shows a decrease in the period 1984 to 1992 and increasing from then (see Figure 5.30). This characteristic is the same in the entire cirrostratus top pressure mode (Figure 5.28) and all cloud type top temperature (Figure 5.23).

The regression model equation is

$$UV = -39.785 - 25.042 \times \text{cirrus cloud water path} \qquad (5.7)$$

Model	R	R Square	Adjusted R Square	Std. Error of the Estimate
1	.491	.241	.234	70.9189954

Model		Unstandardized Coefficients		Standardized Coefficients	
		B	Std. Error	Beta	t
1	(Constant)	-39.785	6.901		-5.765
	Cirrs,cld_wtr_path_1	-25.042	4.320	-.491	-5.797

Table 5.7: The regression model summary of cirrus cloud water path and UV.

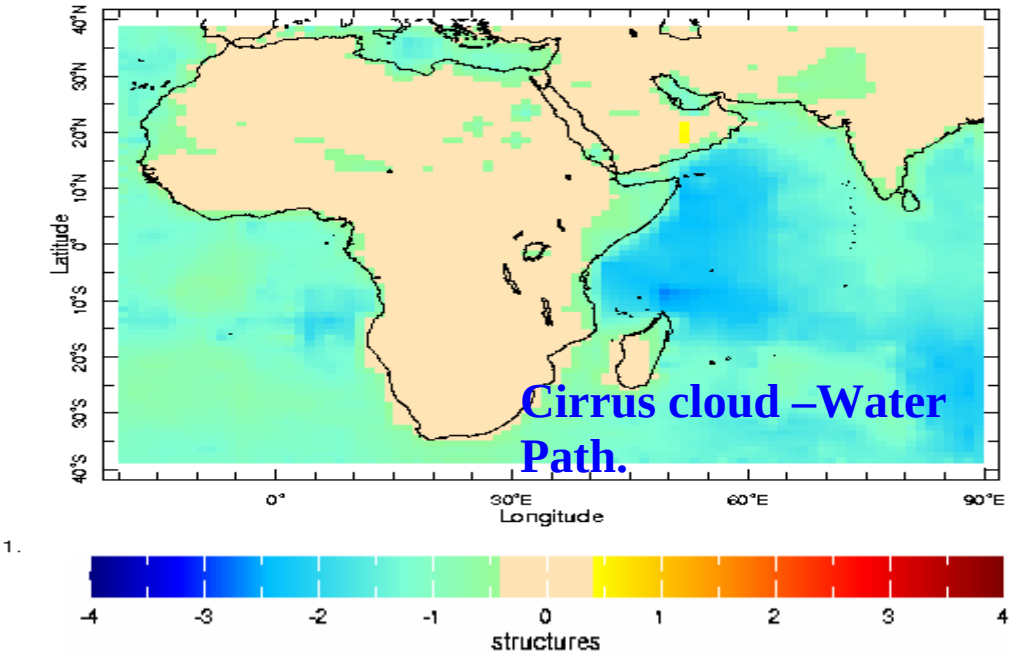

Figure 5.29: The spatial characteristics of cirrostratus cloud water path. Null value in the entire African continent except some spots in the Libyan and Egyptian countries.

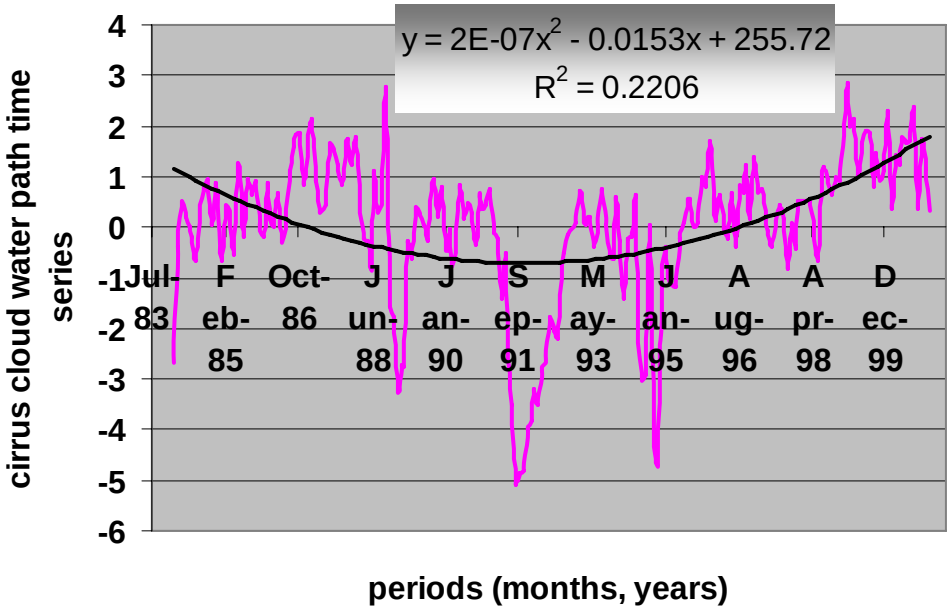

Figure 5.30: Temporal trend analysis of cirrus cloud water path. Abrupt decreasing for 1984 to 1992 and increasing trend after 1993.

The overall contribution of clouds to the UV analysis is around 39%, and hence during cloudy days of the types investigated the sea level UV calculation needs a decrease of 39%.

The general model which accounts for the clouds in this UV investigation is

UV = -30.293 – 11.492 x (all-cloud-temp.) – 56.791 x (altocumulus Liquid-top-opt.) – 49.453 x (altocumulus liquid – temp.) – 3.488 x (cirrostratus cloud – top - press) – 7.029 x (cirrus cloud water path) ……(5.8)

Model	R	R Square	Adjusted R Square	Std. Error of the Estimate
1	.643	.414	.385	63.5392386

Model		Unstandardized Coefficients		Standardized Coefficients	
		B	Std. Error	Beta	t
1	(Constant)	-30.293	7.972		-3.800
	All,cld_tem_2	-11.492	3.894	-.333	-2.951
	Altcmls,lqd_opt_1	-56.791	129.045	-.058	-.440
	Altcmls,lqd_tem_2	-49.453	35.206	-.143	-1.405
	Cirrstrts,cld_press_4	-3.488	1.520	-.188	-2.295
	Cirrs,cld_wtr_path_1	-7.029	7.887	-.138	-.891

Table 5.8: The total account of the clouds having significant relationship with UV.

5.6 Chapter Summary

As estimated, the amount of erythemal UV (UVery) in Africa is high. The possible range of values of UV index (UVI) obtained in Africa is between 4 and 9. This value is on average, but those areas within the equatorial region and mountainous areas get more than the above values as UV increases up an altitude and overhead sun around the equator. The value of UVI obtained is moderate to high according to the WHO standard.

According to this study, the central and southern parts of Africa experience more amount of erythemal UV radiation than the Northern part of Africa. The reason is the presence of UV absorbing aerosols in the Sahel (north), Kalahari (central western), the east Libyan deserts, the Ethiopian rift valley and Djibouti.

The erythrmal UV (UVery) in Africa has shown highest values during the JJAS (June, July, August, and September) season. The overall trend of the UVery is decreasing in all of the seasons. The period from 1980 onwards is the period in which the ozone amount was decreased significantly due to emission of CFCs from industries and refrigerators.

Ozone on the other hand, has shown highest value in the ONDJ (October, November, December, and January) season and minimum amount in the JJAS season. This indicates that the reason why erythemal UV increased in the JJAS season.

Aerosol has shown a highest in the JJAS season and declining trend. So the Northern and central parts of Africa where these aerosols dominate, the amount of UV radiation is low. The aerosols from the northern part and eastern parts of Africa are those aerosols which are UV-absorbing aerosol (e.g. dust and smoke) and non-absrobing aerosols like sulfate aerosols, salts, sands etc. The UV- absorbing aerosols (e.g. dust and smoke) exist in greater strength in Middle Western parts of Africa. In Southern Africa, hardly the absorbing aerosols could be found.

Here it is clear that, the Northern hemisphere is more prone to aerosols than the southern hemisphere. This implies the Southern hemisphere experiences highest value of erythemal UV than the north.

The positive spatial region around the Equator (10S to 10N) in the ozone total amount (DU) is due to the production of ozone around the equator. This is the region, which experiences relatively higher amount of ozone and UVery in Africa. The ozone trend in Africa in general shows an increase. The line fit to the ONDJ shows 0.5546. The reason could be the increase in 4.3% of the solar UV since 1700 which has results in increase in stratospheric ozone.

For the positive spatial variability of ozone (10S to 10N) and the boreal summer (ONDJ) October shows the highest vertical ozone amount parts per millionth of volume (ppmv), 8.761 ppmv, in the period of 10 years while December shows the least vertical ozone (ppmv), 8.225 ppmv in the stratosphere. This has a difference of 0.536 ppmv, 6% lower than the larger value. On the other hand, in the troposphere, November outweighs (2.255 ppmv). There is 13% decrement in general. January shows the least value (1.968 ppmv). Moreover, the 2002 and 2003 period the highest ozone value in vertical ozone distribution in the stratosphere is recorded.

Latitudinally, ozone has shown small stratospheric ozone in vertical mixing ratio (ppmv) for 90N and 90S. The 30N and 30S show relatively higher stratospheric ozone.

The correlation results of UV and clouds are also considered. One peculiar, result from the association is the convective type of cloud, which is supposed to have high

coverage in the tropics, has shown no relationship with UV. This needs further investigation.

Chapter Six

Summary, Conclusions, and Recommendations

6.1 Summary

Ultraviolet radiation is a little over 8% of the total black body radiation; but it is the most energetic and influencing part of the solar spectrum. The purpose of this thesis is hence to improve an understanding of UVery radiation over the African continent. In addition, the characterization of different determining factors of UV radiation has been made.

That part of UV called erythemal UV (UVery) or UV-B and UV-A in the wavelength range from 280 nm to 400 nm are tribulations at the surface. This is the bad part of the sunrays. The reason is, UVery is associated with skin cancer (melanoma), eye disease (cataract), suppressed immune system, and degradation of infrastructure to mention some of its effects.

Africa is a continent where the number of black skins dominates, with some albino, and fairy skins. Though these non-melanoma types are affected, there is also significant effect on the melanoma type skin. This is when we consider the skin cancer based on study in mixed race countries like USA and South Africa. The effect on eye (cataract) is believed to be the cause for significant number of people in blindness in Africa. The human immune system suppression is also one factor why we study UV radiation. This is particularly important for patients of viruses, which attack the immune system of animals, and the prevalence of infectious diseases in the weak immune system developed due to continual over dose of UVery. The effect on infrastructure also is worth considered here. The color of our cloths most vulnerable to UV radiation fades (loses color) easily; the lifetime of plastics in buildings reduced significantly if unprotected; the asphalt breaks easily and many more. These are due to the breakdown of polymers put in the UV radiation. The effect on ecosystem is large. Plants produce enzymes to protect their leaves from the UV radiation in a way to adapt to the UV over dose. This enzyme in plants body is poisonous for animals that dwell on these plants. There are also reports on the decrease in yield of plants during the increased UV radiation.

In general, the UV study is important to protect and know our environment from radiation hazard, and design protection schemes of our environment. These are made through dose-rate calculation, which helps one know the effect and strength of the UV radiation. The dose rate calculated is in mW/m^2, this value then is multiplied with 40 m^2/mW. The result obtained is a unitless UV index (UVI). UVI value is the number that should be announced if possible daily or monthly for the people, to make them aware the values.

The UVI values calculated here for Africa on average is 4 to 9 which is moderate to high. These are high values compared to other countries values in the higher latitudes and polar areas. Therefore, it is necessary to take some measures of protection for those people working outdoors. The measures could be to wear eyeglasses, hat, and full body cover clothes, to quote a few. The period at which the UVery is highest during the days is from 10 a.m to 4 p.m. In Africa, except a few of the cloudy days all of the days are worth taken care of. Especially, the equatorial region is highly vulnerable. The reason is the all year round overhead sun.

UV radiation which is produced by the sun and coming to the surface of the Earth interacts with many scattering and absorbing gases, aerosols, clouds, water droplets, and scattering albedo. The absorbing gases are ozone, nitrogen, SO_2 through Rayleigh scattering. The absorbing and scattering aerosols are salt, sand, smoke, and dust aerosols through Mie scattering. The sky looks blue due to gaseous scattering; but the clouds look white due to Mie scattering.

The stability of solar radiation should also be taken in to account. In general, the increase in UV radiation of 3% for wavelength less than 300 nm and 1.3% for the band from 300 nm to 400 nm was studied. This increasing trend of UV radiation from the surface is the most important part of increase in ozone and UV radiation on the equatorial region. Here further investigation is required.

Ozone affects UV radiation at surface by absorbing the whole of UV-C (280 nm to 100 nm), partially UV-B (280 nm to 315 nm), and none of UV-A (315 nm to 400 nm). At surface the amounts of UV – A is 94%, UV – B is 6% and UV – C is 0%. This is due to the absorption and scattering of gaseous species, aerosols, clouds and water droplets. In

Africa, the UVery does show significant decrease since from 1979 to 1992 and a slight increase from the period 1997 to 2003.

In addition, the central and southern parts experience more amount of erythemal ultraviolet radiation than the Northern part of Africa. The cause of the variation is the aerosol coverage in the Northern part of Africa is higher due to the Sahara desert and Libyan Desert dust aerosols. The northern, the western and eastern parts are more prone to absorbing aerosols due to the Sahel, Kalahari, and the great rift valley dust, sand and salt aerosols.

When we compare the latitudinal difference of ozone within Africa, the equatorial region (10S to 10N) has shown maximum ozone amount. This is due to the production of ozone in the equatorial region and slow transport of ozone to the higher latitudes within Africa. In this study, the equatorial region has shown highest UVery and ozone amount (DU). This is different in that, previously it is known that the ozone is relatively less around the equator. When we consider the globe as a whole, well it is the mid latitude with high value of ozone amount (DU). But, when we consider Africa (40S to 40N, and 3E to 50W) equatorial region has shown remarkable difference in that both UV and ozone are highest than the other latitudes. The reason for the difference may be the production of ozone and its transport is not regular; maximum on one spot and minimum or none in another spot. This non-regularity in concentration of ozone is the as a result of aerosols effects and ozone dynamics.

Unlike the UVery, the ozone trend in Africa has shown an increase. Especially for the ONDJ season, a 0.5546 line fit, trend jump a ladder is recorded. The reason behind is, the increase in UVery of the extraterrestrial radiation, which needs further investigation.

Ozone can be measured either in total column amount (DU) or vertical ozone mixing-ratio in parts of per million of volume (ppmv). The vertical ozone distribution, here shows where, and when it is maximum in the stratosphere, it shows minimum in troposphere. The reason could be explained by the photolysis reaction and full absorption in the stratosphere, which leads to decrease in the amount of UVery to penetrate to the troposphere. The years 2002 and 2003 have shown the highest stratospheric ozone

(ozone mixing ratio) of the 10 years studied (10S to 10N). Of the seasons, as explained above, ONDJ (boreal winter) has shown relatively the maximum ozone amount in the atmosphere. Of these four months, October is the month in which the maximum ozone is recorded. This month is considered, in most part of Africa, hottest. The year 1999 in contrary has shown the least amount of stratospheric ozone. This is 26% less than the highest value in 2002. The opposite happened, as explained above, in the troposphere.

From the latitudinal comparisons, the stratospheric ozone is highest in October around 60N latitude and least around 60S. The difference is 11% lower than the peak value. In November, the ozone-mixing ratio is least in values at/ around 90N and 90S in the stratosphere. In the same month, the greatest ozone-mixing ration is observed for 30S and its nearest locations. This is because of the ozone transport from the equator to higher latitudes through Brewer-Dobson Circulation.

In summary, the variability in ozone vertical distribution or mixing ratio is greatest in the high latitudinal regions. Therefore, the UV irradiance level rises during the drop in ozone amount in the atmosphere. The gap in the highest ozone-mixing ratio in one year and a drop in the other in the winter season is the main problem in higher latitudes. This is because of the high variability ozone amount in the atmosphere of higher latitudes.

In contrast to the higher latitudinal zones, the ozone-mixing ration has shown relatively stable. This shows that, no matter how high the amount of UV irradiance reaching the surface of the tropical region, there is calm variability of UV irradiance. This slow variability of UV irradiance is important for adaptation purposes. This is the reason why tropical dwelling people, animals, and plants are relatively resistant to the high sun burning UV developing adaptive pigments like melanin to people and animals as enzymes to plants.

The effect of aerosols on UV is in such a way that they attenuate UV radiation. The strength of aerosols in Africa varies from hemisphere to hemisphere and region to region. The UV-absorbing and the non- absorbing factors are also one peculiar characteristics of aerosols effect on surface irradiance.

The aerosols from northern western, and eastern parts of Africa are those aerosols which are UV-absorbing aerosols (e.g. dust and smoke) and non-absorbing like sulfate aerosols, salts, sands etc. On the other hand, the UV-absorbing aerosols (e.g. dust and

smoke) exist in greater strength in Middle Western parts of Africa. In southern Africa, hardly the absorbing aerosols can be found.

In general, the northern hemisphere aerosol is greater than the southern hemisphere aerosols. The amount of UVery that arrives at the surface, then is, relatively heavy in the southern African regions. Unlike the UV and ozone, aerosol in Africa has shown a trend slow down, -0.6628 line-fit in the JJAS season according to TOMS/Nimbus 7 data.

Lastly but not least, the effects of clouds on UVery is studied. There are some clouds which have shown association with UV through interplay analyses. Interesting results come out from the UV and cloud relationships:

a) UV interplayed with all cloud type and properties except cloud amount (top pressure, top temperature, water path, and optical thickness)
b) All clouds account for 39 % of the total variability of UV irradiance.
c) Deep convective clouds does not show significant relationship with UV but are the main cloud types in tropical Africa

This is an attempt to consider the cloud effects, but needs further investigation as to the clouds strictures are complex and fragmented over a space.

This is part of an effort to adjust the cloud free, ozone free, and aerosols free UVery radiation measurement. Ozone established, according to this study, 41% relationship with UV, aerosols 7% and clouds 39%. This indicates that the most determining factor for UVery at the surface is ozone, then clouds and least aerosols. Conceptually, this is shown as in Figure 6.1.

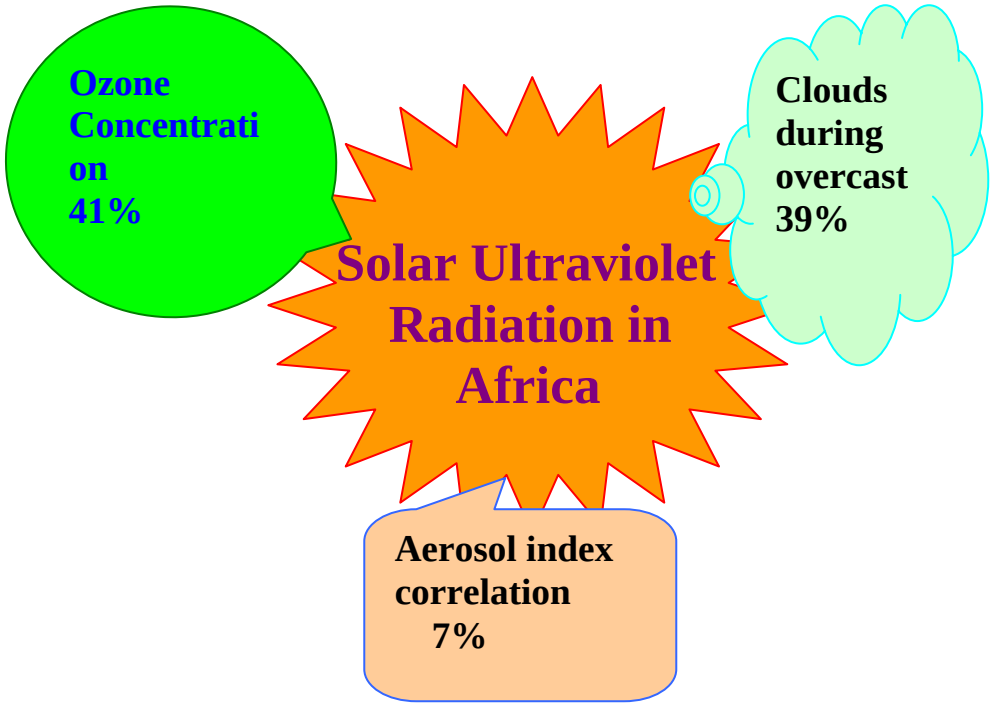

Figure 6.1: The generally established conceptual UV- ozone, UV-aerosol, and UV-ozone relationship.

6.2 Conclusions

The UVery amount in Africa is moderate (4) to high (9) in Africa according to the WHO standard. This amount of UVery is common in all of the years and hence should be taken care of during sunny days. UVery is decreasing for 1979 to 1992 and is slightly increasing for 1997 to 2003. This is due to increasing ozone in the period 1979 to 1992 while still a slight increase, though not as in previous, from 1997 to 2003.

The northern, western and eastern parts of Africa experience less UVery than the central and southern parts of Africa. The reason is aerosols are concentrated in these respective African regions. On the other hand, aerosols have shown a trend decline in all of the years studied. This trend decline is expected to increase the UVery in Africa.

Clouds have shown more association with UVery than aerosols. It has 39% established relationship in Africa with UVery.

UVery is in decline from 1979 to 1992, and is increasing since 1997 while ozone is increasing (55% line fit) from 1979 to 1992 and slightly increasing (25% line fit).

Latitudinally, UVery and ozone are highest around 10S to 10N within Africa. Globally, mid- latitudes (around 30S and 30N) have greater amount of ozone than the other latitudes. UVery does not vary, both in Africa and in world as a whole shows greatest dose in the tropical latitudes.

Of the seasons, ONDJ (boreal winter) has shown the highest amount of ozone recorded in the given period from 1979 to 1992 and from 1997 to 2003. 2002 and 2003 are the periods in which highest amount of ozone in the stratosphere in tropical Africa is recorded. Aerosols are declining in Africa. In general, Ozone trend increase results in UVery decrease, and decrease in aerosols increase the UVery irradiance. Since ozone accounts for 41% dependence on UV, then the UVery is expected to be decreasing in Africa.

Clouds, which have shown significant relationship with UVery in Africa, were decreasing from 1984 to 1992 and increasing since 1993. The increasing trends in recent years of clouds in Africa also have a shielding effect and contribute 39% decrease in UVery during cloudy days.

6.3 Recommendations

In this work, the amount of UVery (dose rate) and the association of UVery with aerosols, ozone and clouds have been investigated. The contribution of altitude and albedo needs further work. This needs the altitude data and respective topographies of the points to be studied. The amount of ozone increase in Africa should also be investigated. One possible explanation here is the amount of solar radiation increasing in solar cycle (every 11 year), which could produce high amount of ozone and hence UV is decreasing and ozone is increasing in Africa.

References

Aoki, T., T. Aoki, M. Fukabori, and T. Takao, Comparison in ultraviolet Irradiance at Syowa Station, Antarctica, between the observation and the Simulation with a Radiation Transfer Model, in Atmospheric Ozone, Proc.Quadrennial Ozone Symp., Sapporo, Japan, 3-8 July 2000, edited by R.D. Bojkov and K. Shibasaki, 91-292, NASDA/EORC, Tokyo, 2000.

Athas, W.F., W.C. Hunt, and C.R. Key**,** Changes in non-melanoma skin cancer Incidence between 1977-1978 and 1998-1999 in north central New Mexico Cancer Epidemiology Biomarkers Prev, 2003. **12**(10): p. 1105-8.

Bais A. F. and D. Lubin: Surface Ultraviolet Radiation: Past Present and Future, Scientific Assessment of Ozone Depletion, ch. 7, 2006

Bais, A. Kazantzidis, K. Tourpali (2003), Climatological UV maps over Europe from Ground based and Satellite Measurements, EDUCE project: WP 1, Laboratory of Atmospheric physics, Aristotle University of Thessalonki.

Blinskii, V.A., Garadzha, M.P., Mezhannaya, L.M., Nezbal, E.I. (1968). Ultraviolet Radiation of the Sun and Sky. Moscow University Press, Moscow.

Craig S. Long and Alvin J. Miller, UV Index, Climate Prediction Center, NOAA, USA, 1998.

Dahlback A. and Stamnes K., A new spherical model for computing the radiation field Available for photolysis and heating at twilight, Planet. Space Sci. Volume 39, pp 671-683, 1991.

Detwiler, C.R. Garret, D.L., Purcell, J.D. and Tousey, R. (1961). The intensity Distribution in the Ultraviolet Solar Spectrum. Ann. Geophys. 17, 263-272.

Fioletov, V.E., L.J.B. McArthur, J.B. Kerr, and D.I.Wardle, Long-term Variations of UV-B irradiance over Canada estimated from Brewer observations and derived from ozone and pyranometer Measurements. Geophys. *Res.*, *106*, 23009-23027, 2001.Fioletov, V.E., J.B. Kerr, D.I. Wardle, N. Krotkov, and J.R.

Flaggie M., and S.K. Solanki, The Solar Spectral Irradiance since 1700, Geophys. Res. Lett., 27, 2157-2160, 2000.

Heath D.F., L.M., Carlton, A.J. Krueger, The Nimbus4 Backscatter Ultraviolet

(BUV) Atmospheric Ozone Experiment Two Years' Operation, Pure and Applied Geophysics, Vol. 106108, pp.1242.

Heath D.F., A.J. Krueger, H.A. Roeder, B.D. Henderson, The Solar Backscatter Ultraviolet and Total Ozone Mapping Spectrometer (SBUV/TOMS) for Nimbus, Optical Engineering 14, 323332 (1975).

Human S. and V.Bajic, Modeling Ultraviolet Irradiance in South Africa, Radiation Protection Dosimetry, Vol. 91, Nos 1-3, pp. 181-183(2000), Nuclear Technology Publishing.

Human S. and V.B. Bajic. Estimation of UV index by neural networks. Development and Practice of Artificial Intelligence Techniques, pages 75-77. IAAMSAD, South Africa, 1999.

Ilyas, M., A. Pandy, and S.I.S. Hassan, UV-B radiation at Penang, Atmos. Res., *51*,141-152, 1999.

Iqbal M., An Introduction to Solar Radiation, Academic Press, Toronto, Canada.

Jacobson, M.Z., Global direct radiative forcing due to multicomponent Anthropogenic and natural aerosols, *J.* Geophys. *Res.*, *106*, 1551-1568, 2001.

Joseph M. Prospero, G.Paul, T. Omar, E. Nicholson Sharon, and E. Gill Thimas, Environmental Characterization of Global Sources of Atmospheric Soil Dust Identified with the Nimbus 7 Total Ozone Mapping Spectrometer (TOMS) Absorbing Aerosol Product, Geophys. Mag., 40, 3, 2000.

Kerr J. B, and G. Seckmeyer, Surface Ultraviolet Radiation: Past and Future, Chapter 5. 2006.

Josefsson, W., and T. Landelius, Effect of Clouds on UV Irradiance: As estimated from cloud amount, cloud type, precipitation, global radiation and sundhine duration, J. Geophys. Res., 105, 4927-4935, 2000

Kinsell L.Coulson Solar and Terrestrial Radiation, Academic Press Inc. (London) LTD, New York (U.S.A), 1975.

Kirchhoff, V.W.J.H., A.A. Silva, C.A. Costa, N. Paes Leme, H.G. Pavao, and F. Zaratti, UV-B Optical *5.36* thickness observations of the atmosphere, *J.*Geophys. Res., *106*, 2963-2973, 2000

Lee Hai-Tien and Jeannette D. Wild, Ultraviolet Index, Research and Data systems,

Inc. U.S.A. 19 94.

Liou Nan Kuo, An Introduction to Atmospheric Physics, Academic Press Inc., 1983.

Lucas R., T. McMichael, W. Cmith, and B. Armstrong, Solar Ultraviolet Radiation, Global burden of diseases from solar ultraviolet radiation, Environmental Burden of Diseases Series, No. 13, World Health Organization, Public Health and the Environment, Geneva 2006.

McElroy, M.B., R. J. Salawitch, S.c. Wofsy, and J.A. Logan, Reductions of Antarctic ozone due to synergistic interactions of chlorine and bromine, Nature, 321, 759-762.

McKenzie R. L., G. Seckmeyer, A.F. Bais, J. B. Kerr, and S. Madronich, Satellite retrievals of erythemal UV dose compared with ground-based measurements at Northern and southern midlatitudes, J. Geophys. Res., 106, 24051-24062, 2001a.

Midgley G.F., S.J.E. Wand & C.F.Musil, Repeated exposure to enhanced UV-B Radiation in successive generations increases developmental instability (leaf Fluctuating asymmetry) in a desert annual, Ecology and conservation, National Botanical Institute, Private Bagx7 Claremont 7735, Cape Town, South Africa, 998.

Molina, L. T., and M. J. Molina, Production of Cl_2O_2 from the self-reaction of the ClO radical, J. Phys. Chem., 91, 433-436, 1987.

Ping-Shine Shaw, Rajeev Gupta, and Keith R. Lykke (2002), Characterization of an Ultraviolet and vacuum-ultraviolet irradiance meter with synchrotron radiation, Rev.Sci. Instrum. OCIS codes: 120.5630, 120.0280, 040.6070, 040.7190.

Renaud A., Staehelin J., Frohlich C., Philipona R. And Heimo A. :2000, Influence of Snow and clouds on erythemal UV radiation: Analysis of Swiss measurements and Comparison with models, J. Geophys. Res., 4961-4969.

Rozema J., B. Van Geel, L.O. Bjorn, J. Lean, and S. Madronich, Toward Solving the UV puzzle, Science, 296, 1621-1622, 2002.

Sabburg J. and J. Wong, The effect of clouds on enhancing UVB irradiance at the Earth's surface: A one year study, Geophys, Res. Lett., 27, 3337-3340, 2000.

Takao, T., M. Alonso, T. Kishi, K. Sakurai, O. Ijima, M. Takekawa, O. Narita, and M. Shitamichi, Ultraviolet spectral irradiance observations at Syowa Station,

Antarctica, Geophys. Mag., *3*, 95-107, 1999.

The Computer Desktop Encyclopedia, The Computer Language Company Inc. http://www.computerlanguage.com/tfd.html

The wikipedia encyclopedia online, Ultra Violet. http://en.wikipedia.org/wiki/UV_radiation

Zerefos C., A. Bais, C. Meleti, and I. Ziomas, A note of the recent increase of solar UV-B radiation over northern middle latitudes, Geophys. Res. Lett., 22, 1245 – 1247, 1995.

Zhiming Kuang, I. Remote Spectroscopic Measurement of Atmospheric HDO/H2O and Column CO2, II. Interannual Variations of the Earth's Reflectance, California, 2003